

MOLECULAR AND TEXTURAL SURFACE ENGINEERING FOR BIOLOGICAL SENSING

by

MOHAMMED ARIF IFTAKHER MAHMOOD

Presented to the Faculty of the Graduate School of
The University of Texas at Arlington in Partial Fulfillment
of the Requirements
for the Degree of

DOCTOR OF PHILOSOPHY

THE UNIVERSITY OF TEXAS AT ARLINGTON

May 2014

Copyright © by Mohammed Arif Iftakher Mahmood 2014

All Rights Reserved

Acknowledgements

I am grateful to my parents for their continuous support, patience and understanding. I will be forever indebted to my advisor Dr. Samir M. Iqbal for the opportunity to work with him, for his guidance, support and expertise. I believe I am not an easy person to deal with and I am thankful for bearing with me for all these years. My heartiest gratitude goes to Dr. Young-tae Kim, without whose support and advice I could never complete my research work. Dr. Ashfaq Adnan paved my way in molecular dynamics with his expertise and I am ever grateful for that. I also thank Dr. Donald Butler and Dr. Michael Manry for their kind consent to review my dissertation and for being in my PhD committee. I will take this opportunity to also extend my thankfulness to my co-workers Yuan Wan, Waseem Asghar, Mohammad Noor, Nabeel Shahid, Azhar Ilyas, Motasim Bellah, Waqas Ali, Raziul Hasan, Muhymin Islam, Madiha Hanif, Wenny, Umair Khan, Loan Bui, Samik Bhattari and many others for their advice, stimulating discussion and hands on help during my research. A special thank goes to the staff of the Department of Electrical Engineering and Nanotechnology Research Center for extending their helping hand throughout my way.

April 16, 2014

Abstract

MOLECULAR AND TEXTURAL SURFACE ENGINEERING FOR BIOLOGICAL SENSING

Mohammed Arif Iftakher Mahmood, PhD

The University of Texas at Arlington, 2014

Supervising Professor: Samir M. Iqbal

This research work was aimed at finding novel approaches for early cancer detection. In cancer diagnosis, the candidate molecules largely include free DNA, related proteins and tumor cells, listed in increasing order of size. The list is also commonly accepted as early precursor of the disease where DNA and proteins are available in patients' blood earlier and the cell starts to appear in relatively later stage. The ratio of these molecules to the background matter is extremely small. To make detection more difficult, these molecules, once dislodged from their primary location, get cleared fast. These factors call for extremely sensitive and efficient devices that won't let the trace amount of molecules pass without getting detected.

The first approach was focused on finding a novel method towards detecting the disease by analyzing the cell behavior on a functionalized surface. Cancer cells that remained calm with few to no movement on a generic surfaces were found to display elevated motility on a surface coated with specific RNA sequence. This RNA sequence bound complementarily to growth factor receptors that are commonly found in excess on the cancer cell surface. This behavior was analyzed using image processing techniques and it was found that there were distinguishing parameters between cancer and healthy cells.

In an attempt to increase the capture efficiency of the cancer cells, a platform inspired from the natural basement membrane was fabricated. The 3-D structure involved micro-nano

texturing using simple processing. The substrate was economical and took minimal time to prepare. It was found to capture cells from a mixture with superior efficiency.

Nanopore is a platform for detecting smaller molecules like DNA and proteins. The underlying mechanism when a molecule passes through the pore is very difficult to observe from outside but holds crucial information. As a result, molecular dynamics simulations that revealed the interaction between two molecules at atomic level were used to understand the protein-DNA interactions and the structural integrity of these molecules in experimental conditions. This parallel development of the technique is bound to pace up the nanopore research.

Table of Contents

Acknowledgements.....	iii
Abstract.....	iv
List of Illustrations.....	x
List of Tables.....	xviii
Chapter 1 Introduction.....	1
1.1 Overview of Research.....	2
1.1.1 Introduction (Chapter 1).....	2
1.1.2 Background and Review (Chapter 2).....	2
1.1.3 Cancer Cell Detection Based on their Dynamic morphological Behavior (Chapter 3).....	2
1.1.4 Micro+Nanotexturing of Substrates to Enhance Ligand-assisted Cancer Cell Isolation (Chapter 4).....	3
1.1.5 MD Simulation of Protein Translocation Through Functionalized Nanopore (Chapter 5).....	4
1.1.6 Future Works (Chapter 6).....	4
Chapter 2 Background and Review.....	5
2.1 Origin of Cancer.....	7
2.1.1 Oncovirus.....	8
2.1.2 Chemical Carcinogens.....	8
2.1.3 Physical Factors.....	9
2.2 Cancer Metastasis:.....	10
2.3 Basement Membrane and its Role in Metastasis.....	11
2.4 Cancer Biomolecules.....	13
2.4.1 Epidermal Growth Factor.....	13
2.4.2 Epidermal Growth Factor Receptor.....	14

2.4.2.1	EGFR Targeting.....	17
2.4.3	CTCs.....	18
2.4.4	Human Glioblastoma Cells	19
2.5	Possible Detection molecules.....	20
2.5.1	Antibody.....	20
2.5.2	DNA/RNA Aptamers:	23
2.5.3	Antibody versus Aptamer.....	27
2.6	Devices.....	28
2.6.1	Mechanical and Hydrodynamic Separation	28
2.6.2	Affinity based assays	31
2.6.3	Dielectrophoresis (DEP)	32
2.6.4	Magnetic Isolation	33
2.6.5	Density Gradient Centrifugation	35
2.6.6	Cytometric Methods.....	35
2.6.7	Microscale Optical Interactions	36
2.7	Review of Aptamer based Isolation Devices	37
2.8	Cell Migration.....	39
2.9	Nanopore and Molecular Dynamics Simulation.....	41
2.9.1	Computer Simulations	43
2.9.2	MD simulation	44
2.9.3	Simulation software :	45
2.9.3.1	VMD	45
2.9.3.2	NAMD.....	45
Chapter 3 Distinct Morphological Behavior of Tumor Cells on Aptamer		
Functionalized Chips.....		46
3.1	Introduction.....	46

3.2	Methods.....	47
3.2.1	Selection of Target: Specificity, Selectivity And Sensitivity	47
3.2.2	Aptamer Preparation	48
3.2.3	Preparation of anti-EGFR Aptamer Functionalized Substrates	49
3.2.4	Fluorescence Measurements.....	51
3.2.5	Isolation and Characterization of hGBM Cells	52
3.2.6	Image Processing.....	52
3.2.7	Image Segmentation	52
3.2.8	Contour Detection	53
3.2.9	Feature Extraction	53
3.3	Results	55
3.4	Conclusion.....	63
Chapter 4 Micro+Nanotexturing of Substrates to Enhance Ligand-assisted Cancer		
Cell Isolation		64
4.1	Introduction.....	64
4.2	Materials and Methods.....	66
4.2.1	Surface Preparation:.....	66
4.2.2	Surface Characterization	67
4.2.2.1	Profilometer:	67
4.2.2.2	SEM Imaging & Energy Dispersive Spectroscopy (EDS):	67
4.2.2.3	Contact Angle Measurement:.....	68
4.2.2.4	Atomic Force Microscopy (AFM):	68
4.2.3	Selection of Target Molecule:	68
4.2.4	Preparation of Anti-EGFR Antibody Functionalized Substrates	68
4.2.5	Acridine Orange (AO) Fluorescence Measurement:	69

4.3	Results	70
4.4	Conclusion.....	81
Chapter 5 Molecular Dynamics Simulation of 3-D Structural Integrity of DNA in a		
Functionalized Nanopore		
		82
5.1	Introduction.....	82
5.2	Methods.....	86
5.2.1	Molecular Dynamics Simulation Details	86
5.2.2	Molecular Models	87
5.2.3	Force Field	89
5.2.4	Simulation Details.....	90
5.2.5	Applied Forces and Electric Field.....	90
5.3	Results	91
5.3.1	Isolated DNA in Electric Field	91
5.3.2	Nanopore Protein Translocation	92
5.3.3	Deviation in 3-D DNA Structure during Protein Translocation.	98
5.4	Conclusions.....	100
Chapter 6 Future Work.....		
		101
6.1	Introduction.....	101
6.2	Integration and Automation of the System.	101
6.3	Optimization of Cell Response	102
6.4	Simulation of the System with EGFR-specific RNA aptamer	102
References		103
Biographical Information.....		112

List of Illustrations

Figure 2.1: Deaths from diseases other than cancer have declined significantly since 1950 [6]. This signifies the need for progress in cancer research and importance of finding alternative detection and therapeutic approaches.....	6
Figure 2.2: Two-Hit theory of carcinogenesis. Patients with hereditary onco-genome transferred from parents are more vulnerable to develop cancer..	9
Figure 2.3: Illustration showing cancer cells breaking through the basement membrane and using the blood circulation system. The cell penetrates into new organ and hence metatasizes..	10
Figure 2.4: SEM micrographs of basement membrane reveal its textured nature..	12
Figure 2.5: Amino acid sequence of EGF with disulfite bonds highlighted. Disulfite bonds help the protein keep its conformation.....	14
Figure 2.6: Schematic representation of the signal pathway for regulating tumor growth and metastasis.	15
Figure 2.7: Therapeutic approaches using EGFR targeting. Figure shows the interception methods of EGFR signaling pathway.....	18
Figure 2.8: Schematic representation of developing monoclonal antibodies through hybridization process.	21
Figure 2.9: Different fragments of an IgG molecule.	22
Figure 2.10: Use of DNA microarray in finding genetic abnormality. Receptor cDNA is amplified using PCR before printing them on the microarray. On the other hand, diseased cells along with control healthy cells are lysed and resulting cDNA is applied on the microarray to find out the difference in genetic expression.....	24

Figure 2.11: NMR-derived topology of the G-quartet and one of the deposited structures of the c-myc quadruplex.....	25
Figure 2.12: A simplified view of the SELEX process.....	26
Figure 2.13: Sieve based cell isolation approach.....	30
Figure 2.14: Schematics showing cancer cell isolation. Surface tethered probe DNA sequence is used to bind the RNA aptamer. RNA molecules fold into 3-D structures in the solvent. The specific RNA molecules have high affinity to EGFR. Cells with overexpressed receptor on the cell membrane bind strongly to the aptamer on the chip surface. Cells with low EGFR number (normal cells) are removed using gentle wash, leaving only cancer cells on the surface.....	32
Figure 2.15: Schematic representation of a cell structure, simplified to a sphere. The sphere represents the dielectric properties of the nucleated cell.....	33
Figure 2.16: Cell isolation using magnetic technique. Magnetic particles are attached to the target cells using affinity interaction. A permanent magnet is later used to attract and separate the cells with pre attached magnetic tag.....	34
Figure 2.17: Cell flow cytometry. Cancer cells are fluorescently pre tagged and detected using the laser before sorting out.....	36
Figure 2.18: Different forces in cell migration. It starts with protrusion of lamellipodia or filopodia by the force generated by actin polymerization. Once the membrane protrusion adheres to the substratum, translocation may occur by myosin interactions with actin filaments at the rear end. As a result cell detaches from the rear. The process involves disruption of cell–substratum adhesive interaction which is accelerated by myosin-mediated actin filament contraction pulling on adhesion complexes..	40
Figure 2.19: Flowchart of Nanopore fabrication.....	42

Figure 2.20: Protein detection using nanopore.....	43
Figure 3.1: Flow cytometry result showing affinity of the developed anti-EGFR aptamer to the tumor cell.	49
Figure 3.2 : Schematics of aptamer immobilization and cell capture.(a) Schematic depicting aptamer attachment chemistry starting with capture DNA immobilized on the surface through the PDITC linker (not to scale). The capture DNA provides larger radius of gyration and hence less steric hindrance to the aptamer. Aptamers make duplex with the capture DNA on one side and the other side is functional. The functional side binds to the target receptors on the cells. (b) Cells flatten out as these bind to the surface. (c) Microscopic image shows how surface-bound cells are flattened after attaching to the substrate.....	51
Figure 3.3: Contour detection from segmented image. After initial image processing "Level Set" method is used to detect cell contour. A binary image is obtained from the contour for feature extraction.	53
Figure 3.4 : Extracted cell radius superimposed on the original grayscale image. Total number of radial measurement is shown to be 10 for clarity. Higher resolution was used in actual feature extraction.	54
Figure 3.5 : Plot of astrocytes cell and substrate interaction for both bare glass surface and anti-EGFR RNA aptamer functionalized surface. The inset picture shows the variation of non-uniformity over time.....	56
Figure 3.6 : Fluorescence measurement of the functionalized surfaces. Acridine orange fluorescence is measured at different steps of surface functionalization to compare the presence of the surface bound oligonucleotides. Higher fluorescence intensity with RNA hybridized surface ensures the formation of RNA aptamer monolayer on the surface.	57

Figure 3.7 : Tumor cell activity on anti-EGFR aptamer modified surface. Five consecutive images with binary converted counterparts are shown. These images were taken after 30 second intervals for the same cell. 58

Figure 3.8 : Whole chip imaging. An approximately $\sim 5 \times 5 \text{ mm}^2$ glass chip was prepared for cell isolation. The mark on the right side was scratched to ensure that the aptamer functionalized side of the glass remains on top all the time. 59

Figure 3.9 : Comparison of hGBM cell activity on anti-EGFR and mutant aptamer substrates. EGFR over-expressing hGBM cells showed enhanced activity through shape variation and pseudopod formation when incubated on the anti-EGFR aptamer surface. Large error-bars indicate significant variations in cell shape in the pool of cells the data were collected from; since the formation and annihilation of the pseudopods, or changes in shape were not synchronized . In contrast, when these cells were incubated on the mutant aptamer coated control surface, the activity was negligible. The inset shows the variation of non-uniformity over time. 60

Figure 3.10 : Comparison of astrocyte cells' activity on both surfaces. Average nonuniformity for the astrocyte cells calculated over 15 minutes. the Cells remained calm and inactive on both the surface due to absence of any surface bound complementary moiety. The inset picture shows the variation of non-uniformity over time. 61

Figure 3.11 : Hausdorff distances between consecutive frames (averaged over 40 cells). Cancer cells show enhanced activity at the beginning and the activity reduces with time before finally settling to the surface. 62

Figure 4.1: Schematic of micro-pattern for enhanced cell capture. The top image shows a plain surface with nanotexture. The number of ligand-receptor

interaction is low compared to the bottom image. The textured pattern increases the odds for cell adhesion.	66
Figure 4.2 : AFM image of the nanomodified plane surface. (A) Shows plane surface Plane glass surface before RIE. The mean roughness remained below 1 nm. (B) Shows the roughened surface created using RIE. (C) A zoomed out micrograph showing uniformity of the modified surface.	70
Figure 4.3 : The hierarchical surface at 4 different magnification scales. The first image shows the micron scale roughness created using sandblasting. The (B), (C) and (D) shows the zoomed in images displaying the nano-texture created inside the micro grooves.	71
Figure 4.4 : EDS analysis. (A) and (B) shows the EDS obtained graph of the material composition from the surface. (A) represents the surface without any modification. (B) is obtained at least 24 hours after the RIE process and piranha cleaning. The graph shows no significant change in the surface material that can affect the immobilization of the RNA on the surface.	72
Figure 4.5 : Contact Angle Measurement. the \pm sign indicates the range around the mean.	73
Figure 4.6: Fluorescence Measurements. Acridine orange fluorescence is measured (n=10) at different steps of surface functionalization to compare the presence of the surface bound oligonucleotides. Higher fluorescence intensity with RNA hybridized surface ensures the higher number of RNA present on the surface.	75
Figure 4.7: Fluorscence micrographs of cells captured on the surfaces. (A) and (B) show the bright field and fluorescence micrographs of the cells captured on the simple nanotextured surfaces. (C) and (D) show the bright field and	

the fluorescence micrographs of of the cells captured on the hierarchical surfaces, respectively.	76
Figure 4.8: Cells captured on three surfaces functionalized with anti-EGFR antibody and anti-EGFR aptamer. Cells captured on the hierarchical micro+nanotextured surface are more than double than those captured on nanotextured surfaces, in both the cases.	77
Figure 4.9: SEM micrograph of cells bound on three different substrates (A) Plain glass surface, (B) Nanotextured Surface, (C) Hierarchical micro-nanotextured surface. The data reveals how cell attachment is increasingly stronger. On plain surface, cells are mostly globular whereas the cells show increased spreading from nanotextured to hierarchical surfaces. In hierarchical surface, cells show many pseudopods indicating better cell-surface interactions.....	80
Figure 5.1 : Typical nanopore experimental setup. (A) Analytes are allowed to pass from one side of the container to the other through the nanopore in the middle. Electrodes on both sides measure the ionic current indicating the translocation event. (B) Schematic of protein translocation through solid-state nanopore coated with ligand. The inset shows how protein target binds strongly to the DNA ligand once the binding sites from both molecules come in proximity to each other. The binding energy depends on the complementary manner of the position of the binding points.	84
Figure 5.2: The model of the protein translocation through silicon nitride nanopore. A single DNA strand with G-quartet structure is shown immobilized on the nanopore inside wall. The orange lines in the inset show the interaction between bases while forming the G-quartet structure.	88

Figure 5.3: Stability of the 3-D DNA structure under applied bias. (A) and (B) show the initial structure and the structure after the simulation was run with an applied field of 0.1 V/nm, respectively. The structure is stable indicating that the functionality or affinity due to the 3-D conformation remains active. (C) Shows the same structure under applied field of 1 V/nm. the DNA elongates and loses its 3-D conformation. (D) RMSD calculated from the initial equilibrated structure. The 3-D conformation can hold up to a moderate field of 0.6 V/nm whereas higher voltage disintegrates the structure. The inset shows the dramatic change in RMSD within the short range of voltage change from 0.6 to 1 (V/nm)..... 92

Figure 5.4: (A) Plot of interaction energy (VDW and electrostatic) between nanopore and the protein molecule while translocating through. Translocation times for all three scenarios are shown for comparison. (B) A comparison of the translocation times of three cases. The translocation times for the three cases were calculated from the interaction energies between protein and the nanopore wall. Due to the binding of the protein to the DNA, the translocation time is significantly higher compared to the translocation time through a bare nanopore. A protein-DNA complex shows the fastest translocation. 95

Figure 5.5: (A) Velocity comparison of three different scenarios of protein translocation inside the nanopore. (B) Shows the velocity of the protein when it passes through a bare nanopore. The magnified inset is presented to compare the entering velocity between three cases. 96

Figure 5.6 : Comparison of protein translocation time.(A) and (B) show the DNA inside the nanopore before and after translocation (arrows show the travel of protein). (C) Shows the RMSD deviation of the DNA while translocating.

(D) Shows a comparison of the protein translocation times through a nanopore coated with DNA holding its 3-D conformation, a nanopore with the same DNA that lost its structure and a bare nanopore. 99

Figure 6.1: Schematics showing multi chip based cartridge towards a generic device that targets multiple types of cancer 101

List of Tables

Table 2-1: Shows the protein over expressed in different cancer types. It can be noted that EGFR is present in all the mentioned carcinoma..... 16

Table 2-2: Shows the percentage of EGFR over expression in the different cancer types. 16

Table 2-3: Energies in Molecular Dynamics Simulation..... 45

Table 3-1: Differential change of pseudopod formation in the four combinations of cells and surfaces. 10 sets of random cells are taken from a pool of samples and presented in the table). The hGBM cells on anti-EGFR surface show significantly large number of changes when totaled over 25 frames that were captured 30 second apart..... 62

Table 4-1: Profilometer reading. Mean surface roughness with standard deviation (appended by \pm) measured for both micron scale and nanoscale features 73

Table 4-2: Comparison of cell capture efficiency on different surfaces. 78

Table 5-1: Comparison of protein translocation time in nanopores of 6 nm and 8 nm..... 97

Chapter 1

Introduction

Cancer is the second most dominant health problem in the world with death toll in millions every year. The disease imposes a heavy burden on the economy from personal level to the national scale. Billions of dollars are invested and spent every year towards cancer research, its diagnosis, prognosis and therapy. Till this day, early cancer detection is considered the most important player for positive outcomes of the treatment. Cancer dominantly stems from abnormal and uncontrolled cell proliferation, self-renewal potential and differentiation capacity of tumorous cells. The rate of spread of metastatic cancer inside host body can be rapid. Success of conventional therapeutics is somewhat limited once cancer spreads beyond the primary tumor. Hence, it is crucial to diagnose the disease as early as possible for its ultimate control and prevention. People diagnosed with cancer at early stages have as high as 90 percent survival rate. However, for patients diagnosed at later stages, this rate falls rapidly. This underwrites the significance of cancer diagnosis and treatment at early and possibly at premalignant stages.

One of the major obstacles in early detection is the unavailability of fast and economical methods that are easily performable without the need for expert supervision. Rarity and lack of phenotypic information is a major hindrance in the characterization and detection of cancer. An ideal detection device should be portable, user friendly and should require minimal and possibly non surgical sample drawing from the patients. Such Point-of-Care (POC) devices are major research objective and many methods engaging different engineering branches have been employed towards achieving this. Each method comes with its own shortcomings and till this date most of them remained confined within the research labs. However, every new direction

empower us with crucial stepping stone towards unraveling the mystery of ever-changing biological phenomenon behind the disease

The focus of this dissertation work is developing devices for early cancer detection. In this thesis work the main focus was on revealing the working mechanism of cancer biomolecules, developing new methods and improving the efficiency of the cancer detection and isolation approaches.

1.1 Overview of Research

In brief, behavior analysis of cancer cells was performed on a surface coated with a cell-specific RNA molecule. This was further extended to improve the surface towards better response using standard micromachining techniques. A Molecular Dynamics simulation of proteins passing through nanopore was performed to reveal the underlying dynamics of the translocation. A short overview of the chapters is presented below.

1.1.1 *Introduction (Chapter 1)*

This chapter provides a short summary of the research work done in this thesis and the drive and objective behind the research work.

1.1.2 *Background and Review (Chapter 2)*

Chapter 2 reviews origin of cancer and possible detection modalities. It gives an overview of the research works done in this field and the challenges that prevail. A short introduction to Molecular Dynamics is also provided at the end.

1.1.3 *Cancer Cell Detection Based on their Dynamic morphological Behavior (Chapter 3)*

Fabrication of bio-inspired surfaces and devices have been proven extremely important towards developing cancer detection devices. Tumors are precursor to cancer development.

Cancer prone cells are almost always associated with one or more oncogenes. These genes are translated to abnormal and over expression of many unwanted proteins on the cell surface. These overexpressed biomarkers are the main targets that enable the cell to react to the surface tethered molecules in a complete different way than a non-specific entity. Cancer cell behavior on a functionalized surface is analyzed in this chapter. Glass surface was coated/functionalized using RNA aptamer specific to the cell surface receptor. The overexpression of epidermal growth factor receptor (EGFR) on the human glioblastoma (hGBM) cell surface was used in experiments. An anti-EGFR aptamer molecule was used to functionalize the surface. The results showed that cancer cells behaved distinctively on the functionalized surfaces when compared to healthy cells. After initial image processing, some feature vectors were extracted to quantitatively distinguish the cancer cells.

1.1.4 Micro+Nanotexturing of Substrates to Enhance Ligand-assisted Cancer Cell Isolation (Chapter 4)

Bio-mimetic surface is crucial for increasing efficiency of any cell isolation method. Nanotextured basement membrane can anchor down the cancer cells to its loose underneath connective tissue through cell adhesion molecules. On the other hand, micro-scale structure can follow the 3-D contour of the cells and provide superior cell-surface contact. A surface with micro groove in combination with nanoscale texturing showed better cell isolation. The surfaces were created by sand gritting the glass followed by acid etch and reactive ion etch. Such textured substrates have more effective area and hence less steric hindrance thus facilitating higher number of molecule immobilization, which favors the cell isolation. The surface showed a high number of cell isolation compared to the plane or nanotextured surfaces alone. This chapter details these experiments.

1.1.5 MD Simulation of Protein Translocation Through Functionalized Nanopore (Chapter 5)

This work investigated the protein translocation through nanopores. Protein translocating through nanopore creates distinct ionic current signature when measured by external circuit. Such current depends on the interactions of protein with the pore or pore bound ligands. It is important for the ligands to maintain their structure for these interactions to take place. DNA structures can get deformed because of high electric field inside the pore and may lose their functionality. Again, any such translocation event will be affected by the size of the pore. This chapter focuses on the an all atom molecular dynamics (MD) simulation for investigating these phenomena.

1.1.6 Future Works (Chapter 6)

In this chapter, scopes of future works that can complement/supplement the current research are discussed

Chapter 2

Background and Review

As of January 1, 2012, approximately 13.7 million Americans were alive with a history of some sort of cancer and it is projected to reach to almost 18 million by 2022 [1]. Despite decades of extensive multidisciplinary research, reliable diagnosis methods and effective therapeutic approaches, let alone complete cancer cure, remain elusive to the physicians (Figure 2.1). Unlike other diseases, reasons attributed to the cancer cannot be singled out. Many factors starting from habitual practices to environmental exposures and hereditary genes are found liable for the disease. Finding roots of cancer, its diagnosis, appropriate prognosis and successful non-relapsing cure have been the most challenging tasks in human endeavor against diseases.

Cancer holds a unique position because of its genetic roots. Carcinogenic gene activation caused by internal or external factors that trigger cells to go outside regular activity arena and cause inappropriate cell signaling leading to abnormal growth and finally tumor progression [2, 3]. Such genetic disorder or deviance and its translation towards mutated, undesired and mostly uncontrolled protein synthesis lead to cancer. In advanced stages, cells dislodge from the primary tumor and travel through blood stream to distant organs eventually forming new tumors. The significance of these travelling cells, known as CTCs, in cancer spreading as well as potential biomarker for early diagnosis is well recognized [4]. Many other cancer specific biomarkers like proteins and cell-free DNA molecules also become available in the blood circulation as soon as metastasis starts. However, diagnosis through these cells and other biomolecules is a challenge due to their extremely small number and rarity compared to

the healthy counterparts [5]. Low selectivity and sensitivity of the techniques to discriminate between both types also is a major hindrance.

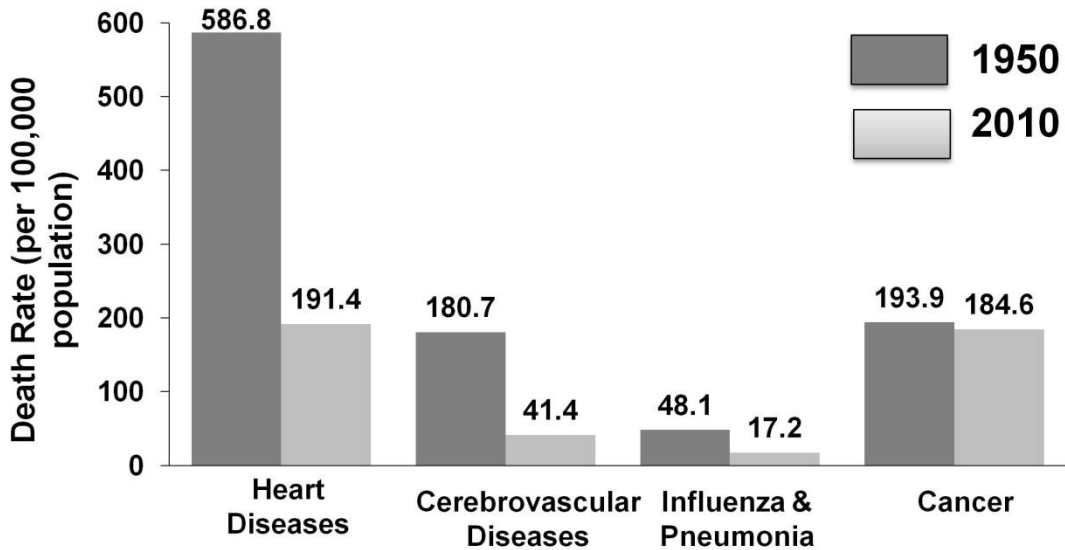


Figure 2.1: Deaths from diseases other than cancer have declined significantly since 1950 [6]. This signifies the need for progress in cancer research and importance of finding alternative detection and therapeutic approaches

In past two decades, a fairly comprehensive understanding of the cancer origin and progression steps has been achieved. The unfolding of the mystery is guided by the development of fast DNA sequencing techniques that led to completion of human genome project [7]. Detailed understanding of genetic regulation in human DNA and DNA functionality in protein synthesis has revealed the underlying process in cancer development steps. Advancement in computational power, techniques, algorithms and simulation software have assisted in parallel the development of the understandings. Modern characterization techniques and imaging methodologies have also contributed massively and continue to do so in such development.

Once the cancer root is recognized, it is imperative to develop fast and accurate techniques for diagnosis. Earlier symptoms are barely perceivable by the patients and in many cases, by the time patients report, the disease is already at its advanced stage. Regular

screening often fails to find the deep lying lesions that are at their preliminary stage. Again, these methods are very expensive and financially burdensome for the patients. A non invasive diagnostic approach through bodily fluid is promising yet has remained elusive. For example, the CTCs are extremely rare (~5 in a billion normal cells) in blood. As a result, any diagnostic approach through CTCs requires highly sensitive device. The blurry boundary between healthy cells and tumor cells, numerous expressions of cancer biomarkers, variation in expression level of these biomarkers in patients based on age, sex, race etc, make any such detection method increasingly complicated. A lot of work is yet to be done towards collecting the vast amount of reliable data for building a statistical backbone for devices employing these biomarkers for successful cancer detection.

To selectively isolate tumor cells from the blood, many methods have been previously introduced. Some of the methods will be discussed here later. Selectivity and sensitivity have always been a challenge in these devices. Advanced DNA manipulation techniques have created a field of opportunities to work on increasing performance of these devices. DNA/RNA sequence fragments or more specifically, aptamers, work as riboswitches inside cell nucleus to regulate genetic expressions and protein translation. These nucleic acid sequences can bind competitively to complementary portions of the DNA to turn OFF expression of certain genes. Aptamers have the property to fold into suitable 3-D structures to bind to specific proteins. This property qualifies these as superior candidates in isolation devices. However, before delving into devices, it is important to discuss briefly the causes that are established as cancer precursors.

2.1 Origin of Cancer

Evolution of cancer involves a process called carcinogenesis through which normal cells become cancerous in genetic and eventually in their phenotypic expressions. The reasons are attributed to many known and unknown physical factors. Several studies have reported

cancer to be caused by reasons starting from personal habits to the ever-changing environment people are exposed to. The sophisticated balance between cell proliferation and apoptosis (*programmed cell death*) is disturbed in the cancer cells. After series of mutations of genes, a transformed cancer cell goes into uncontrolled growth and differentiation state and becomes malignant [8]. The activation of proto-oncogenes and deactivation of cancer suppressor genes play important role in carcinogenesis. Mutation of these genes causes a loss or reduction in their functions and causes the cell to progress to cancer [9]. Inheriting one germline copy of a damaged gene increases the chance of developing cancer by many folds, as the two hit hypothesis by Dr. Alfred Knudson explains (Figure 2.2).

2.1.1 *Oncovirus*

Ellerman and Bang were the first to report an infectious virus for leukemia in 1908, and the disease was found to be transferred from one to another by cell-free tissue filtrates [10]. Numerous oncoviruses were discovered in later years [11-13]. These retroviruses contain cancer causing genome and infect through transferring and integrating viral nucleic acid (DNA or RNA) into host chromosome. These later get activated causing cell to go rogue or activate proto-oncogene in the genome [14].

2.1.2 *Chemical Carcinogens*

Chemical carcinogens can induce DNA-adduct formation by binding to the DNA either by covalent binding or some other bond and directly cause DNA fragmentation and sequence deletion. If a tumor suppressor gene is damaged this way, without proper DNA repair mechanism, the abnormal cells cannot be cleared and tumor cells start proliferating [15].

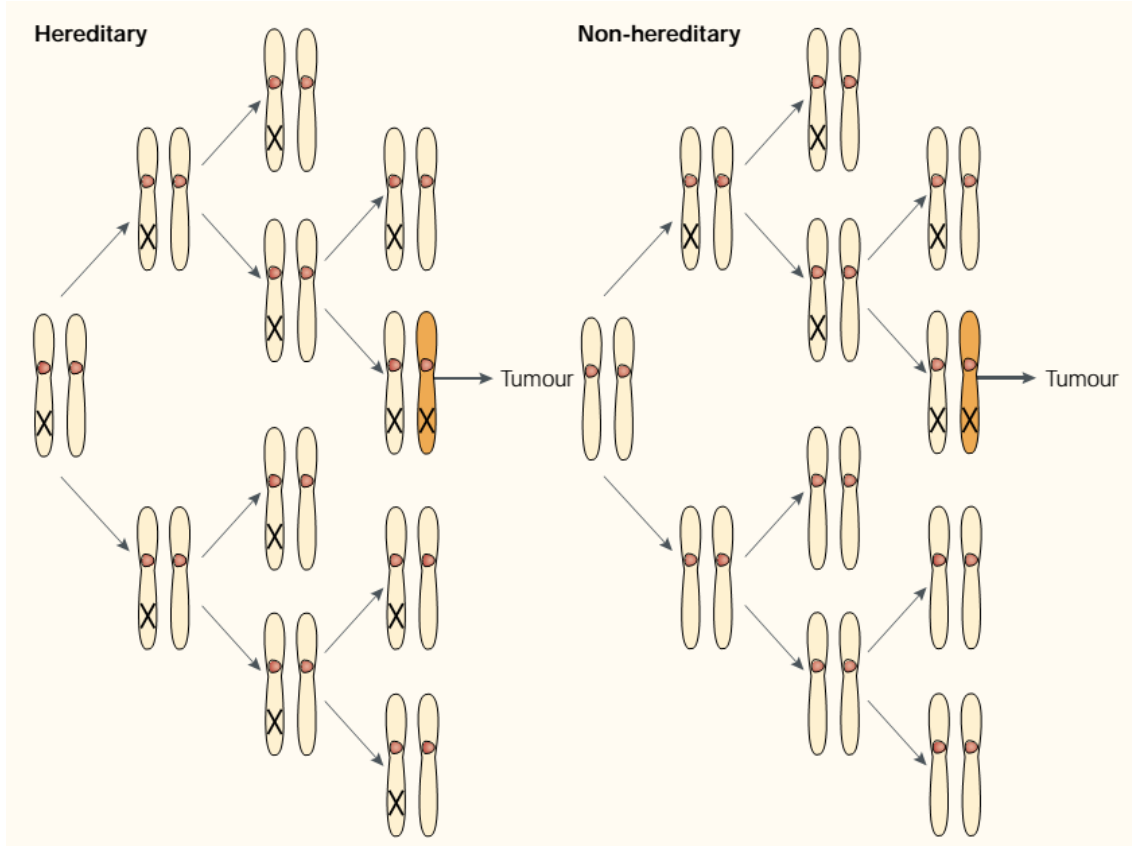


Figure 2.2: Two-Hit theory of carcinogenesis. Patients with hereditary onco-genome transferred from parents are more vulnerable to develop cancer. Reprinted with permission [16].

2.1.3 Physical Factors

Radiation sources like UV and also the radioactive materials are also primary reasons for cancer. Genetic change can happen when high energy particles hit chromosomes and cause the sequence to alter. Exposure to radiation may also trigger certain cell responses that can increase the likelihood of mutations [17].

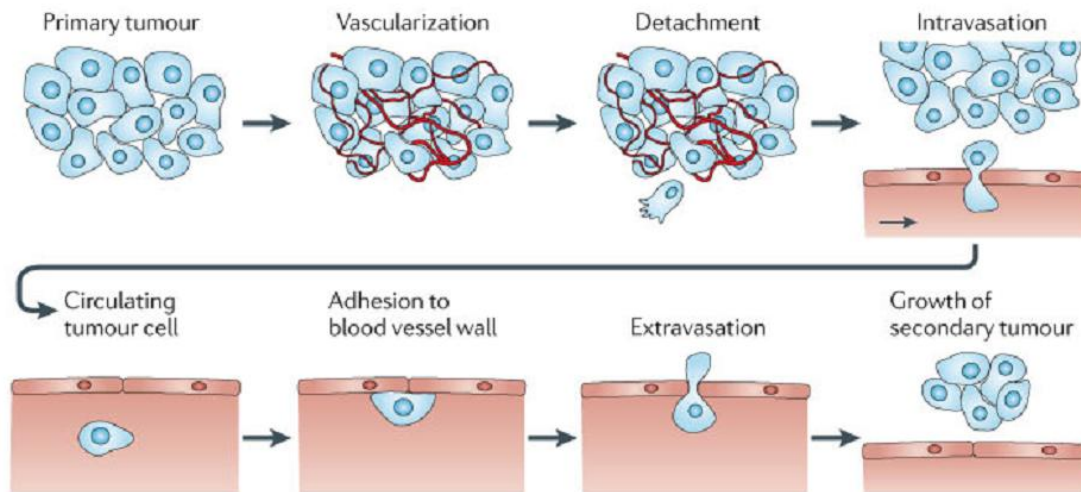


Figure 2.3: Illustration showing cancer cells breaking through the basement membrane and using the blood circulation system. The cell penetrates into new organ and hence metastasizes. Reprinted with permission [18].

2.2 Cancer Metastasis:

Cancer cells lose their ability of differentiation regulation and regress to a more embryonic unspecialized form showing malignant proliferation [19]. Integrins have important contribution to tumor growth and metastasis. These adhesion molecules promote tumor cell attachment, migration, and invasion and help arresting of metastatic cells within the vasculature of target organs. Mutation in integrin in the cancer cells collectively mediate transition of cancer cells from a stationary cell phenotype to an active invasive cell phenotype. Because of this transition, tumor cells behave in a very dynamic manner with the ECM and with host cells within the lymphatic system, the blood vascular system, and target organ tissue. To accelerate these processes, tumor cell integrins often cooperate with various other signaling molecules causing them to show enhanced activity [20].

It was also reported that abnormal gene expression (mutation, deletion or translocation) in human cancer and extrinsic factors in the tumor microenvironment can promote the motility of cancer cell [21]. With mutation of the adhesion molecules (such as E-cadherin and other

epithelial markers that mediate cell-cell adhesion, and cell-extracellular matrix adhesion), cancer cells become prone to detachment from their native tissue. The uncontrolled cell growth as well as the enhanced motility causes cell number to significantly increase and the native tumor to extend to the surrounding tissues. These rogue cells can easily migrate to the tissues and vasculature surrounding the tumor. Once these get into the blood circulation system, these travel to distant sites and form a secondary cellular colony (Figure 2.3).

This process is called metastasis and the process has two major steps. Cancer cells need to adhere to extracellular matrix which is essential for cells to survive and proliferate. After attaching, these cells have to penetrate basement membranes which form a barrier that most normal cells cannot break through. This is essential for the cell nutrition and survival [22].

2.3 Basement Membrane and its Role in Metastasis

Basement membrane is about 20-200 nm thick and its primary function is to anchor down the epithelium [23]. This provides the mechanical support and divides tissues into compartments. However, recent studies show that the basement membrane plays an important role in determining cell behavior, for example, in angiogenesis (*formation of new blood vessels to provide essential cell nutrition*) in cancer cells. The layer acts as a primary barrier against cancer by preventing the metastatic cells from penetrating into the deeper tissue region. Basement membrane consists of fibrous collagen, hyaluronic acid, proteoglycans, laminin, and fibronectin [23, 24].

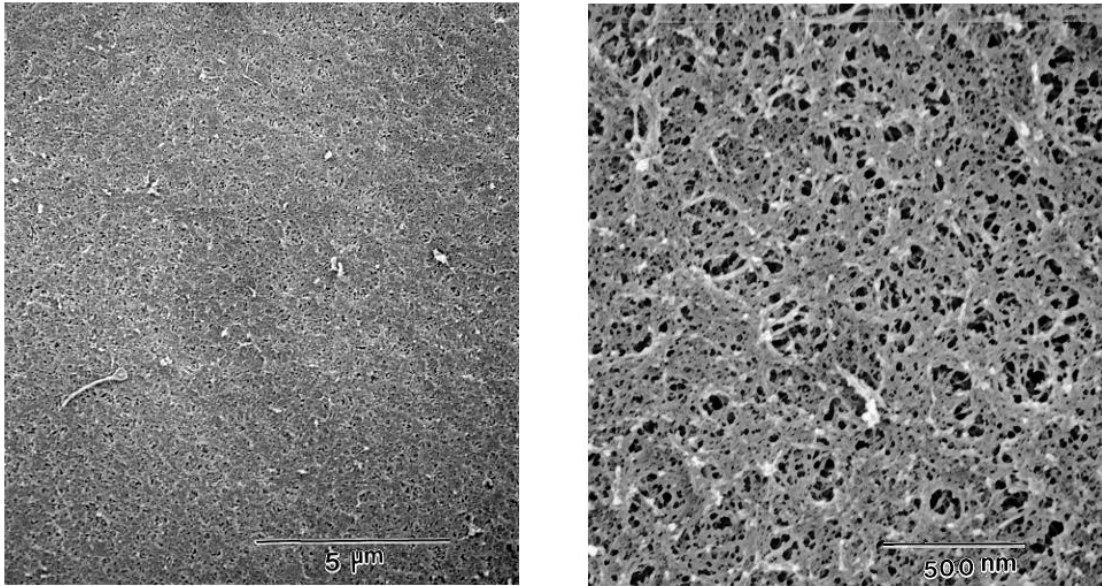


Figure 2.4: SEM micrographs of basement membrane reveal its textured nature. Reprinted with permission [25].

The integrin receptors along with the receptors on basement membrane can mediate cell attachment, their migration and differentiation [26]. At early stages, cancer cells are somewhat kept confined to the epithelial layer by the basement membrane. However, as the cell matures and proliferates, various metalloproteinases (*enzymes with catalytic functions*) activate which in turn enhances the activation potential that dissolves the basement membrane and other extracellular matrices and thus facilitate the invasion through. Change in phenotype and thus overexpression of integrins, and other adhesive molecules on the surface facilitate the cancer cell to escape from the membrane's structural constraints.

After penetrating the basement membrane, cancer cells can invade into surrounding tissue or spread to a distant site via bloodstream. Basement membranes possess a complex, 3-D topography consisting of micro and nanometer sized features [25]. SEM micrographs have shown that the basement membranes are comprised of micro and nanometer size pores, ridges, and fibers (Figure 2.4). The topography is essential for anchoring down the surrounding tissues and also for mediating several tissue functions.

The textured characteristics of the basement membrane that cancer cells exploit to migrate and penetrate through can also be utilized to improve cell adhesion and growth. Utilization of this property is important for efficient capturing of cancer cells from random samples. This was utilized in our experiments to show better cell adhesion.

2.4 Cancer Biomolecules

Cancer related proteins and growth factors like prostate specific membrane antigen (PSMA), vasoendothelial growth factor (VEGF) and epidermal growth factor receptor (EGFR) carries special interest in diagnosis. Over the last decade or so, numerous protein specific aptamers have been identified and isolated. Several membrane proteins have been utilized towards cancer cell isolation [27-29]. A comprehensive list of molecules that show increased presence in cancer cells can be found elsewhere [30]. In our experiments, we focused on EGFR for targeting cancer cells. This receptor is reported to be overexpressed in several cancer types.

2.4.1 *Epidermal Growth Factor*

As the name suggests, EGF is the biological signaling molecule for cell proliferation and differentiation (Figure 2.5). It is responsible for stimulation of transport, activation of glycolysis, activation of the synthesis of extracellular macromolecules, activation of DNA, RNA and protein synthesis resulting in increased cell multiplication [31-33]. Molecular weight of human EGF is 6045 kDa consisting 53 amino acid residues [34]. The molecule can specifically recognize EGF receptor on the cell surface. The dissociation constant of the pair is $\sim 2-4 \times 10^{-10}$ M [35]. Once the EGF reaches the cell surface, these are randomly distributed on EGFR sites, and bind very fast leading to saturation of EGFRs. Higher concentration of EGF naturally has faster binding speed. After EGF-EGFR complex formation, EGF is internalized via receptor mediated endocytosis and degraded in lysosomes. EGFRs are recycled in endosome and travel back to the cell surface [36].

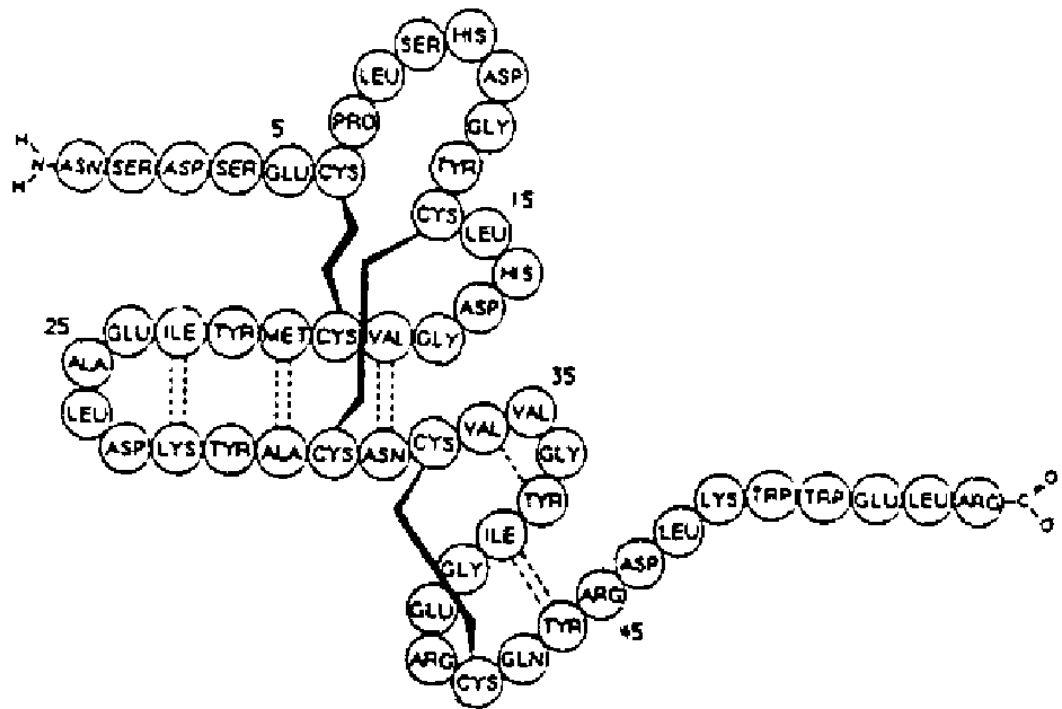


Figure 2.5: Amino acid sequence of EGF with disulfide bonds highlighted. Disulfide bonds help the protein keep its conformation. Reprinted with permission [33].

2.4.2 Epidermal Growth Factor Receptor

EGF receptor is a transmembrane glycoprotein that can recognize and bind to the protein members of the EGF-family (EGF, TGF- α , etc.). Molecular weight of this molecule is 170 kDa and the gene responsible for encoding it is identified as c-erbB1 [37]. Four functional domains of the molecule have been identified; an extracellular ligand-binding domain; a transmembrane domain; an intracellular tyrosine kinase domain, and a C-terminal regulatory domain [38]. The extracellular region is further divided into four sub domains, I, II, III, and IV. Homologous domain I and III are cysteine-poor and provide binding sites for the ligands. Cysteine-rich domain II and IV determine the conformation of the external domain. The intracellular domain contains the tyrosine kinase site and several autophosphorylation sites

clustered at the C-terminal tail. The receptor forms a dimer when ligands bind to the extracellular domain. This triggers receptor autophosphorylation through tyrosine kinase activity which in turn initiates the recruitment and phosphorylation of several intracellular components that promote cell proliferation and angiogenesis (Figure 2.6). Any mutation and hence modification in this complex chain of reaction pathway can cause abnormal cell proliferation leading to cancer formation with antiapoptosis and finally metastasis [39, 40].

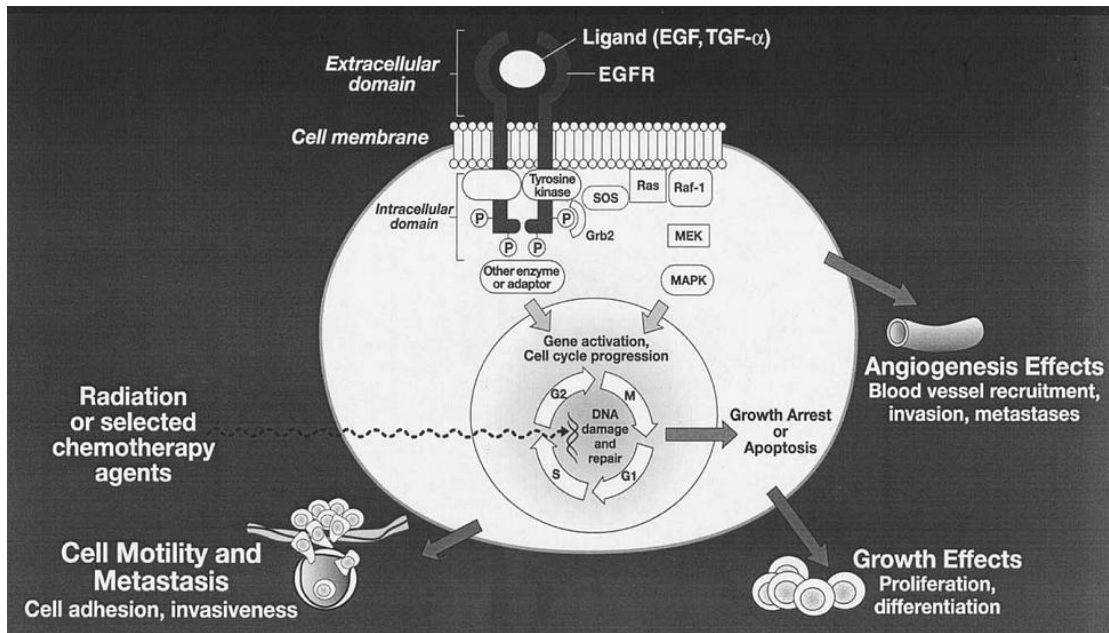


Figure 2.6: Schematic representation of the signal pathway for regulating tumor growth and metastasis. Reprinted with permission [36].

EGFR plays important role in cellular functions such as DNA synthesis, cell proliferation, migration, adhesion, and so on. In a healthy cell, 40,000 to 100,000 EGFR count has been reported on the membrane [32]. In tumorous cells, EGFR has been reported to be present in excessive amount. Many cancer cells such as breast cancer, cervical cancer, lung cancer, bladder cancer, ovarian cancer, and esophageal cancer are all reported to overexpress EGFR on cell surface (Table 2-1) [41]. For example, around 40 to 50% of glioblastoma and 80 to 100% of head and neck tumors overexpress EGFR (Table 2-2) [42, 43]. Naturally this

overexpression of EGFR is deemed to be an important indicating factor in cell malignancy. The number of EGFR in cancer cells can be 10 to 100 times higher than that in normal cells [44]. Therefore it is an attractive target for cancer detection and therapy [45].

Table 2-1: The protein overexpressed in different cancers. EGFR is common in all of these cancers

Disease	Biomarker
Breast Cancer	CEA, HER-2, EGFR
Cervical Cancer	Human Pappiloma Virus, EGFR
Lung Cancer	EGFR, KRAS, BRAF
Bladder Cancer	EGFR, HSP27, Annexin
Ovarian Cancer	EGFR, Haptoglobin α , CA-125
Esophageal Cancer	EGFR, Periplakin

EGFR-targeting therapies involve antibodies that bind to the extracellular domain or small-molecule tyrosine kinase inhibitors that can inhibit the kinase activity of EGFR [46]. However, mutant variations of EGFR have been reported in cancer cells that can restrict the use of the antibody in detection and therapeutic applications.

Table 2-2: Shows the percentage of EGFR over expression in the different cancer types.

Tumor Type	% of Tumors Overexpressing EGFR
Head & Neck	80-100
Kidney	50-90
Lung	40-80
Glioma	40-50
Ovarian	35-70
Bladder	31-48
Pancreatic	30-50
Colon	25-77
Breast	14-91

For cancer detection and therapy, it is important to recognize the mutant variants of the EGFR for their proper utilization in any isolation device [47]. Presently, nine mutations have been identified [48, 49]. Five of them are visible in extracellular region (EGFRvI, EGFRvII, EGFRvIII, EGFRvIII/ Δ 12-13, and EGFR.TDM/2-7), and the rest in intracellular region (EGFRvIV, EGFRvV, EGFR.TDM/18-25, and EGFR.TDM/18-26). In all these mutations, EGFRvIII (type III EGFR deletion-mutant receptor) is the most common. Its proto-gene lacks 801 base pairs, and as a result the amino acids from 6 to 273 in extracellular domain are deleted, which consists of exons 2 to 7 [50, 51]. Molecular weight decreases as a result from 170 kDa for EGFR wild type to 145 kDa in the mutant variation. In a normal cell, a pathway of ligand-receptor reactions is initiated by ligand binding. However, EGFRvIII causes continuous tyrosine kinase activation and receptor autophosphorylation. This stimulates cell proliferation at low level of ligand or even without ligand binding causing abnormal proliferation.

2.4.2.1 EGFR Targeting

EGFR and its overexpression have been studied and used before for cancer detection and treatment. Three methods are commonly pursued to achieve the goal: (i) Drugs binding to extracellular domain for inhibiting the binding of EGF to EGFR and to impede EGFR internalization, thereby interrupting the signaling; (ii) small-molecule tyrosine kinase inhibitors that inhibits the kinase activity of EGFR; (iii) Anti-EGFR ligand-bound cytotoxic agents which can specifically recognize cancer cells that internalize the agent into an endosome and translocate to the cytosol where they inhibit DNA amplification, protein synthesis and further cause cell death or apoptosis (Figure 2.7) [52]. Monoclonal antibodies, aptamers, enzyme inhibitors, small molecule drugs, immunotoxins, antisense oligonucleotides etc. have been applied in clinical therapy [53, 54].

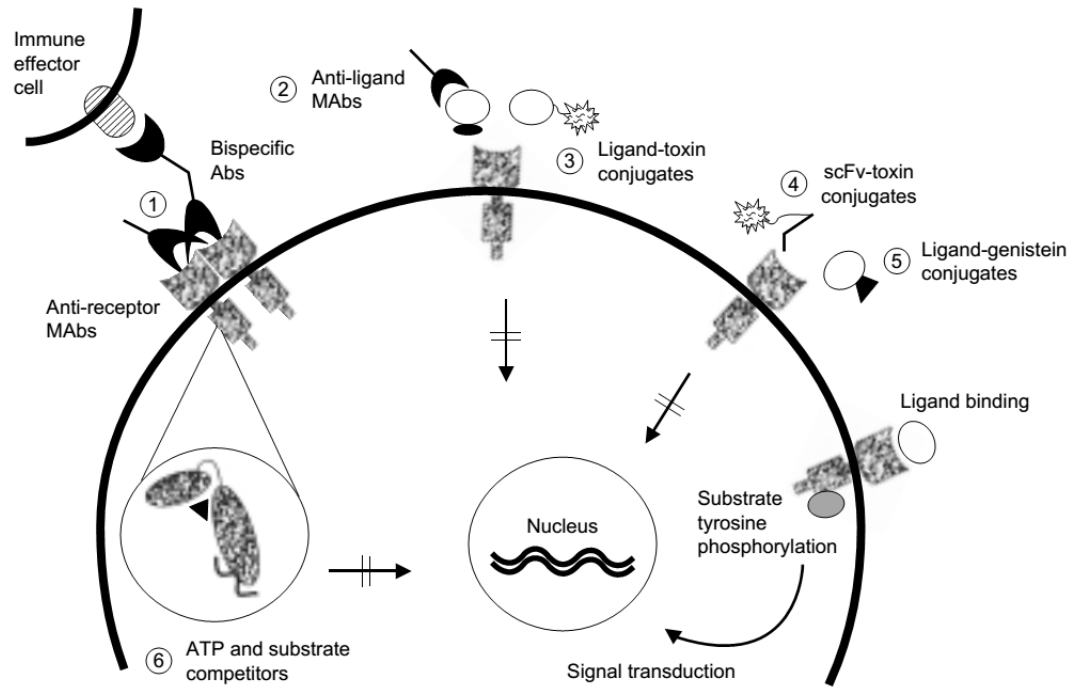


Figure 2.7: Therapeutic approaches using EGFR targeting. Figure shows the interception methods of EGFR signaling pathway. Reprinted with permission [55].

2.4.3 CTCs

Cancer cells enter into the blood circulation system via neighboring blood vessels, or through capillaries formed by angiogenesis. Once the basement membrane is breached the tumor cells detach from their native place and get into the surrounding blood vessels. Bloodstream can carry the cells to distant sites. These cancer cells in peripheral blood circulation system are called circulating tumor cells (CTCs). The presence of CTCs was found by Thomas Ashworth in 1869 and was identified immediately to be the origin of multiple tumors existing in the same person [56-58].

CTCs have high diagnostic potential in clinical oncology. These cells are important indicator of cancer progression and can reveal the genetic and phenotypic composition of the primary tumor. This information is valuable to predict patients' prognosis and to determine the

malignancy. Besides, it is also useful in designing personalized medicine, and to monitor the effectiveness of therapy [59]. In breast, prostate and colorectal cancer patients, studies have shown that number of CTCs in the peripheral blood is directly related to the survival rate of the patient. More number of CTCs indicate severity of the disease [60]. Number of CTCs is also an important monitoring parameter for post-treatment patient monitoring [61].

2.4.4 *Human Glioblastoma Cells*

Glioblastoma cells (hGBM) were used for experiments as these show overexpression of EGFR on cell membrane [62]. GBM is one of the most aggressive intracranial malignant tumors in humans and it accounts for 20% of all intracranial tumors. Average survival rate of patients with malignancy is only 12 to 15 months [63]. Malignant transformation in glioma stems from the sequential accumulation of genetic aberrations, such as various deletions, amplifications and point mutations, which can further lead to the deregulation of growth-factor signaling pathways [64]. The most common mutation in signal transduction pathways include EGFR and platelet derived growth factor receptor (PDGFR) [65]. Overexpression of EGFR on cell membrane has been reported in 40% to 90% of patients [66, 67]. At least three types of EGFR mutations have been found in high grade GBM: EGFRvI, EGFRvIII and EGFRvII [68]. As mentioned before, these mutant variants can autophosphorylate without external binding. EGFRvIII is the most commonly found mutant among gliomas. This leads to RAS/ERK and PI3 kinase/AKT pathway activation and hence cell survival, proliferation, invasion, angiogenesis, and inhibition of apoptosis. Currently, imaging is the major tool for diagnosis, and the definitive result requires a stereotactic biopsy or a craniotomy with tumor resection and pathologic confirmation. This is very tedious and painful for patients and often biopsy or subtotal tumor resection may result in incorrect tumor grading and intracranial spreading. Due to the aggressive nature of the tumor, a fast and economic approach of detection is important. Affinity based device promises such diagnosis success.

2.5 Possible Detection molecules

2.5.1 *Antibody*

Development of target specific molecules has been a goal for decades and immunologic approaches have been considered as a way to reach this goal. These efforts can be traced back to 19th century. With the progress of immunology, a solid knowledge was gained for use of antibodies towards imaging, detection and therapeutic applications. Radiolabeled antibodies were reported to be used to detect malignant tissues in mouse as early as 1940 [69]. One major milestone in this method was discovery of producing monoclonal antibodies (mAbs) by *in vitro* hybridization of immune cells and myeloma cells of the mouse (Figure 2.8) [70]. This method allowed for the isolation of large number of pure and specific antibodies for diagnosis. These mAbs are being used in isotropic and nonisotropic immunoassays, immunohistopathology, flow cytology, imaging and many others [71]. Modern immunotherapy uses antibodies alone as passive therapy or as toxic agents for drugs and isotopes [72].

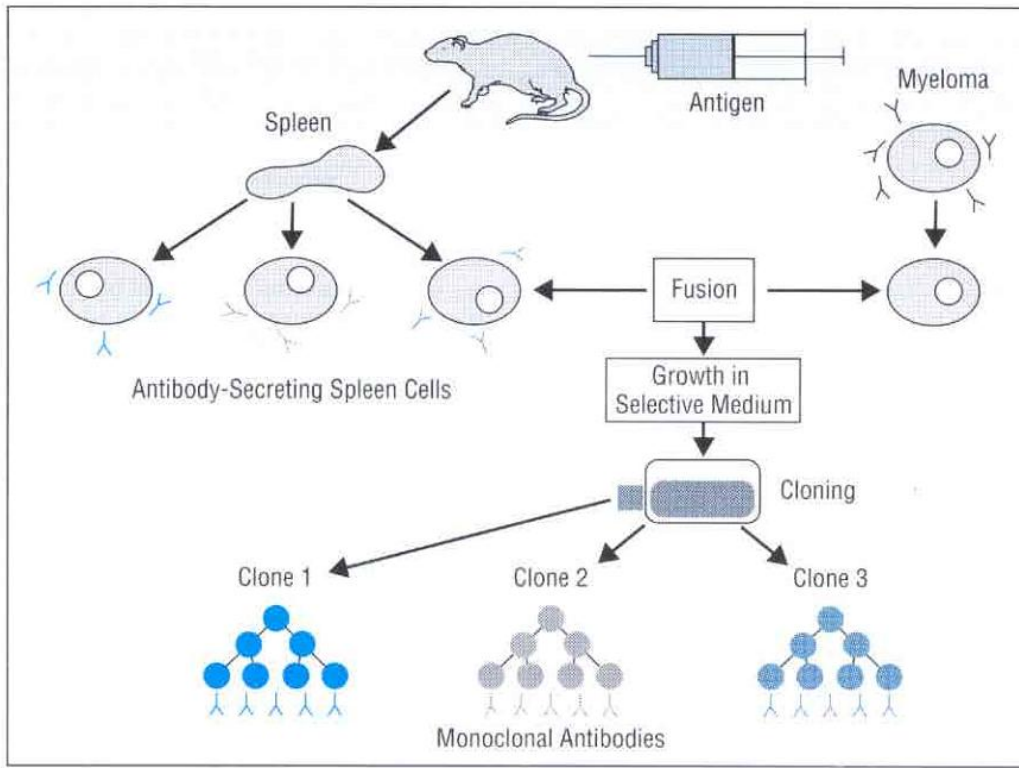


Figure 2.8: Schematic representation of developing monoclonal antibodies through hybridization process. Reprinted with permission [70].

Production of antibodies or immunoglobulins (Igs) is one of the major functions of the immune system. These antibodies bind to the foreign molecules and help eliminate them from the system. An individual Ig bind to one kind of epitope and these are produced by B cells. These antibody producing cells are isolated to create monoclonal mAbs population. B cells need to be hybridized with the mouse myeloma cell line to immortalize them. These hybrids can produce antibodies with desired specificity and in large scale.

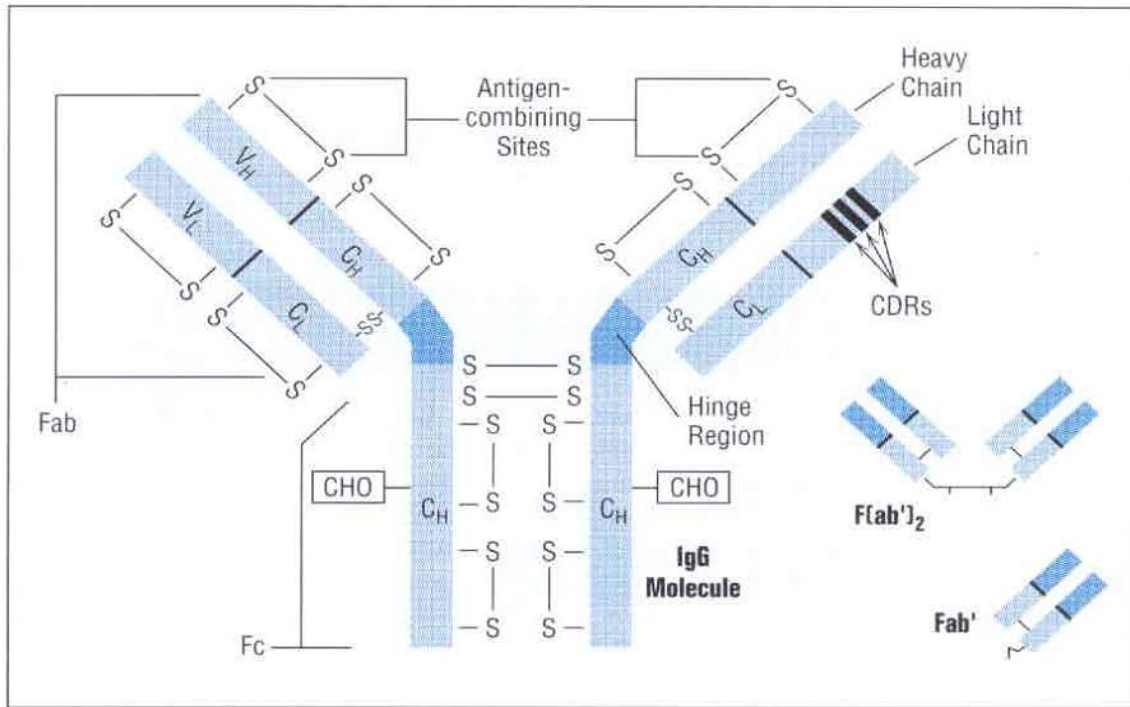


Figure 2.9: Different fragments of an IgG molecule. Reprinted with permission [70].

From the schematic representation of the IgG molecule given in Figure 2.9 it can be noted that it consists of two identical heavy chains. Also the molecule can be divided into two regions Fab (fragment antigen binding) and Fc (fragment crystallizable). The biological function is determined by the Fc region whereas the specificity is determined by the Fab region. Antibodies' variability comes from the change in sequence of a region called complementarity determining region (CDRs). When folded, CDRs create a complementary site for epitope binding. A plethora of murine MAbs against tumors have been developed and characterized using the hybridoma technology. Despite the large number, it is rare to find a mAb that is specific to a single cancer type. Most of the antigens recognized by the antibodies belong to a wide class of carcinomas [70, 73].

2.5.2 DNA/RNA Aptamers:

DNA microarray is a relatively recent and somewhat mature technology primarily used to detect genetic expressions in a sample. This has later been extended for detection of other biomolecules and proteins, specifically, cancer related biomarkers [74-76]. Microarray technology musters efforts of many fields such as molecular biology, micromachining, microfabrication technologies, microelectronics, robotics, surface chemistry etc. Arrays of DNA fragments (up to 10^6 test sites in 1-2 cm² area) are immobilized on suitable surfaces for selective hybridization with the reporter probes in the sample. Such binding, in later step, is positively detected using fluorescence [77], electrochemical [78], electronic [79], mass sensitive [80] as well as acoustic wave transducer methods [81]. The intensity of the fluorescence tag indicates the expression levels of the specific genes. These microarrays have found applications in lab, clinical and commercial setups such as in various diagnostic approaches, drug discovery, pharmacogenomic applications, genetic mapping and gene expression studies. In a typical application, both cancer cells and healthy cells are lysed to extract genomic sequences. These are amplified and tagged with different fluorescent materials before applying on the DNA coated microarray. A fluorescence imaging of the hybridized microarray indicates the presence/absence of certain genomic sequence in the diseased cells when compared to healthy ones (Figure 2.10). Recently, microarrays are getting a growing attention in fields like protein studies or proteomics and cellular analysis.

The ability of DNA strands to selectively bind to biomolecules made them suitable for using these oligonucleotides in cancer cell detection assays. The possibilities are endless and newer devices with novel applications are being reported frequently. Fully integrated biochips have been proposed to perform all the functions from sample preparation to detection in a microfluidic environment. This calls for development of a POC device setup [82]. However the technology doesn't come without challenges. Maintaining a low noise interpretation, stability of

the probe and the RNA, as well as reliability and reproducibility markers are still to be improved.

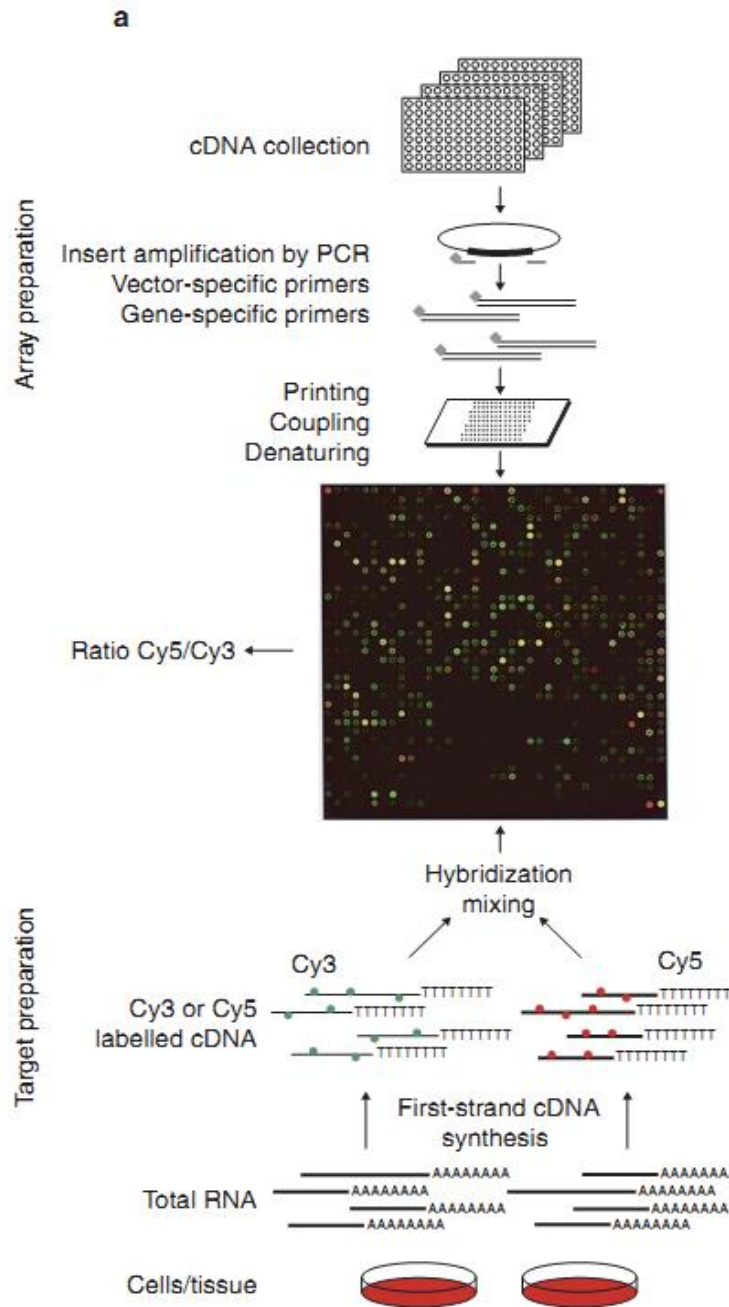


Figure 2.10: Use of DNA microarray in finding genetic abnormality. Receptor cDNA is amplified using PCR before printing them on the microarray. On the other hand, diseased cells along with control healthy cells are lysed and resulting cDNA is applied on the microarray to find out the difference in genetic expression. Reprinted with permission [83].

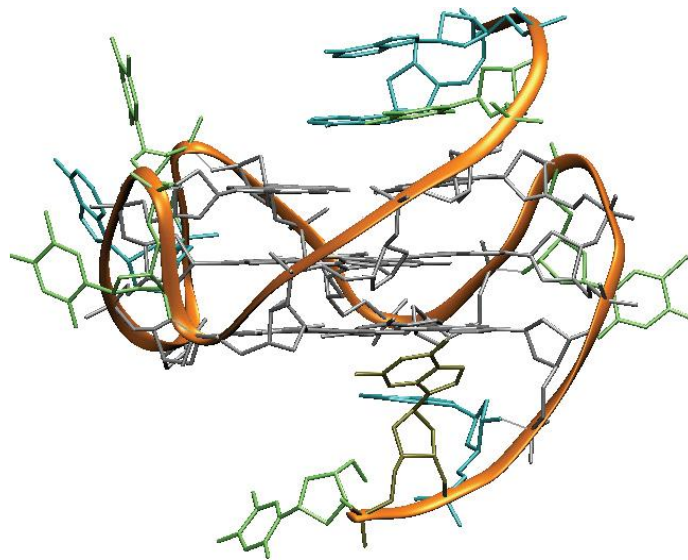


Figure 2.11: NMR-derived topology of the G-quartet and one of the deposited structures of the c-myc quadruplex. Reprinted with permission [84].

An important milestone of DNA technology is discovering the ability of DNA molecules to selectively bind to proteins. Single stranded nucleic acids have ability to form secondary and tertiary 3-D structures. These structures are formed due to folding back of the DNA/RNA by intramolecular base pairing leading to a loop conformation (Figure 2.11) [85]. The structures act as nucleation sites and play a critical role in RNA-protein recognition. A particularly interesting conformation is the G-quadruplexes formed due to the presence of short G-rich sequences also known as Tetrad or G-quartet structure [86, 87]. The fundamental unit of this quadruplex is the G tetrad which is formed by the association of four guanine residues [88]. Hydrogen bonding between nitrogen and oxygen atoms stabilize the tetrad [84, 89]. These can link together to form extended 3-D structures which have been reported to be further stabilized by metal ions present in the central region [89]. The ability of guanine residues to interact amongst each other via non-covalent bonding offers a novel opportunity for stable 2D and 3-D structural motifs that can be used for protein recognition and for the formation of chip-based sensors.

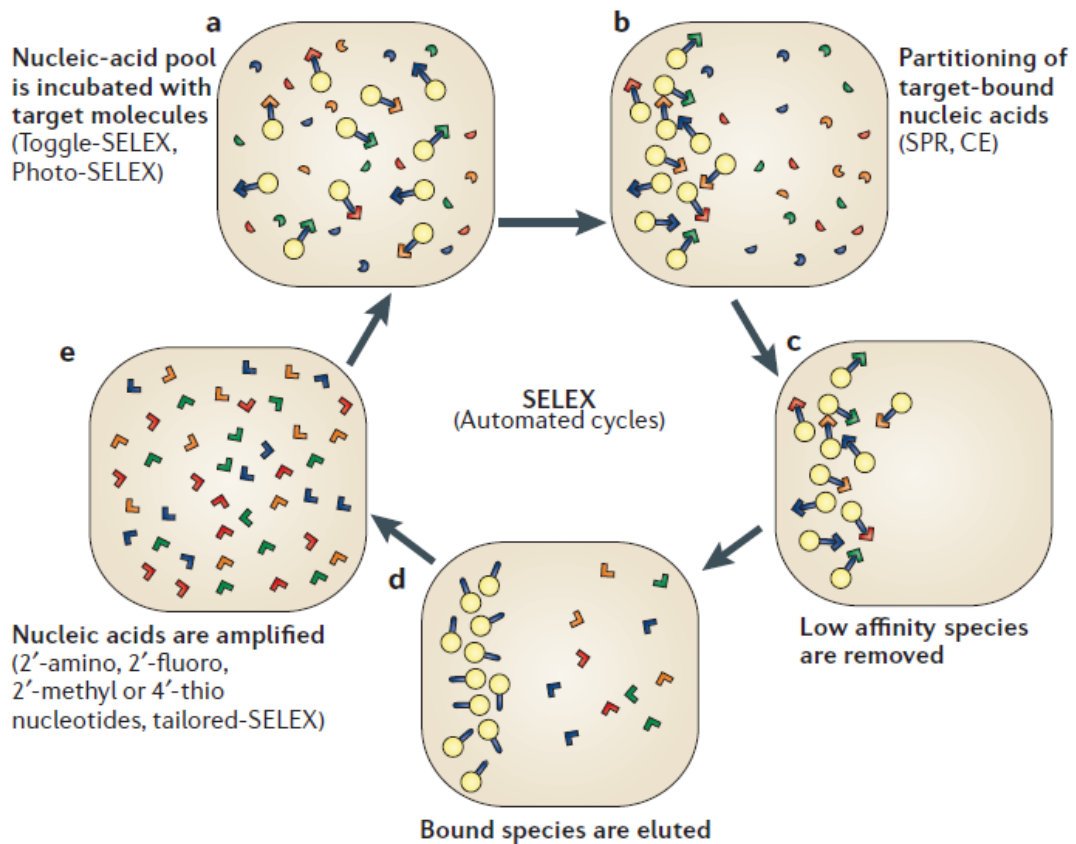


Figure 2.12: A simplified view of the SELEX process. Reprinted with permission [90].

The discovery of non-coding RNAs with specific catalytic properties or functions in gene regulation have led to re-evaluation of biological importance of these molecules [91]. The method called Systematic Evolution of Ligands by exponential enrichment (SELEX) has discovered many RNA molecules which have the capability to bind to specific molecular targets (Figure 2.12) [91]. These sequences can recognize a wide variety of molecules with high affinity and specificity and rely on the direct spatial contacts with its ligands. The binding induces structural changes, reorganization and stabilization which influences the folding and the functioning of the aptamer.

2.5.3 *Antibody versus Aptamer*

Aptamers can be used as primary structural units in biosensors developed to detect molecules ranging from proteins, metabolites, transcription factors and receptors etc [90, 92, 93]. They continue to show great potential in detecting disease biomarkers and are proven to be highly specific towards their targets. Specificity makes them suitable to be used as a tool for diagnostic purposes. Aptamers show some inherent advantages over respective antibodies when used in detection devices [94]. Synthesis of antibodies requires biological and physiological systems which makes them expensive. On the other hand, aptamer sequences can be prepared in lab. Aptamers are easier and more economical to produce with low batch-to-batch variations. In devices, antibodies require stringent physiological conditions when compared to aptamers, thus restricting range of application for antibodies. It should also be noted that kinetic parameters of antibody-antigen interactions cannot be altered. In some antibodies labeling or fluorescence tagging was previously shown to cause loss in their function. Many affinity-based approaches that rely on antibodies are also reported to be subjected to high levels of off-target cross-reactivity.

Aptamers can be manipulated to bind to a different region of the target molecule. Moreover, they are chemically stable at wide range of pH, temperature, and ionic conditions and can be reversibly denatured [95, 96]. Aptamers are getting growing attention in cancer diagnosis and therapeutics [97]. These molecules demonstrate comparable affinity and specificity of antibody but show added advantages. Aptamers don't have the large hydrophobic cores of antibodies and as a result they don't aggregate. Aptamers can be site-specifically labeled with functional groups or dyes. Selection conditions of aptamer can be manipulated to desirable properties for in vitro assays. The hydrophilic nature of aptamer can provide surface passivation against nonspecific binding.

Aptamer uses have been reported before in cell labeling studies [98], in activating cell signaling pathways [99], and in cell isolation and detection [100]. In this research work, both

antibody and aptamer based isolation devices are designed and implemented with emphasis on aptamer based isolation due to its superior performance.

2.6 Devices

As hinted before, the major challenges in cancer diagnosis through CTC are the faithful isolation of the cells and their post-isolation viability. Number of CTCs in the bloodstream is extremely rare, usually 1 to 10 in 1 ml of blood, whereas the number of red blood cells is in the billions. To make things worse, the survival time of CTCs in bloodstream is relatively short and 85% of them get cleared in 5 minutes [101]. Once isolated, CTCs must be kept viable for subsequent molecular analysis. CTCs also have large variability in their molecular functional characteristics [102]. The kind of biomolecule expression and their number on the cell surface are subjected to many factors. As a result, targeting a single biomolecule is not enough. Targeting of combination of few selected molecules is essential. The isolation specificity of device is another important factor. Many approaches, relying on either the physical properties or immunochemical characteristics of CTCs, have been studied before for detection and isolation; however, the reported efficiency is not yet sufficient for definitive clinical application.

2.6.1 *Mechanical and Hydrodynamic Separation*

Mutated cells show distinguishing physical characteristics compared to healthy cells in terms of deformation, increased nuclear size as well as changes in other internal organizations. It was previously reported that tumor cell lines derived from liver, prostate, breast, and cervical human carcinomas had significantly larger cell sizes compared to peripheral blood leukocytes [73, 103]. A number of separation techniques were studied based on measuring the effects of mechanical and/or hydrodynamic forces on the cells, usually in microfluidic environments. Methods of such separation have evolved from a simple porous sieve. Power of such techniques lie in their simplicity since cells don't need any pre- or post-treatment. For example,

a technique named "Isolation by Size of Epithelial Tumor cells (ISET)", developed by ScreenCell, allows direct enrichment of epithelial cells using a "sieve" for filtration. The filter-based micro-devices exploit the cell size differences between cancer cells and the smaller normal cells for efficient isolation and further on-chip analysis (Figure 2.13). The captured cells were reported to remain viable for further manipulation such as electrolysis or immunofluorescence. However, in many cases the physical difference between cells are not so obvious and mechanical methods alone are not sufficient for faithful isolation [104].

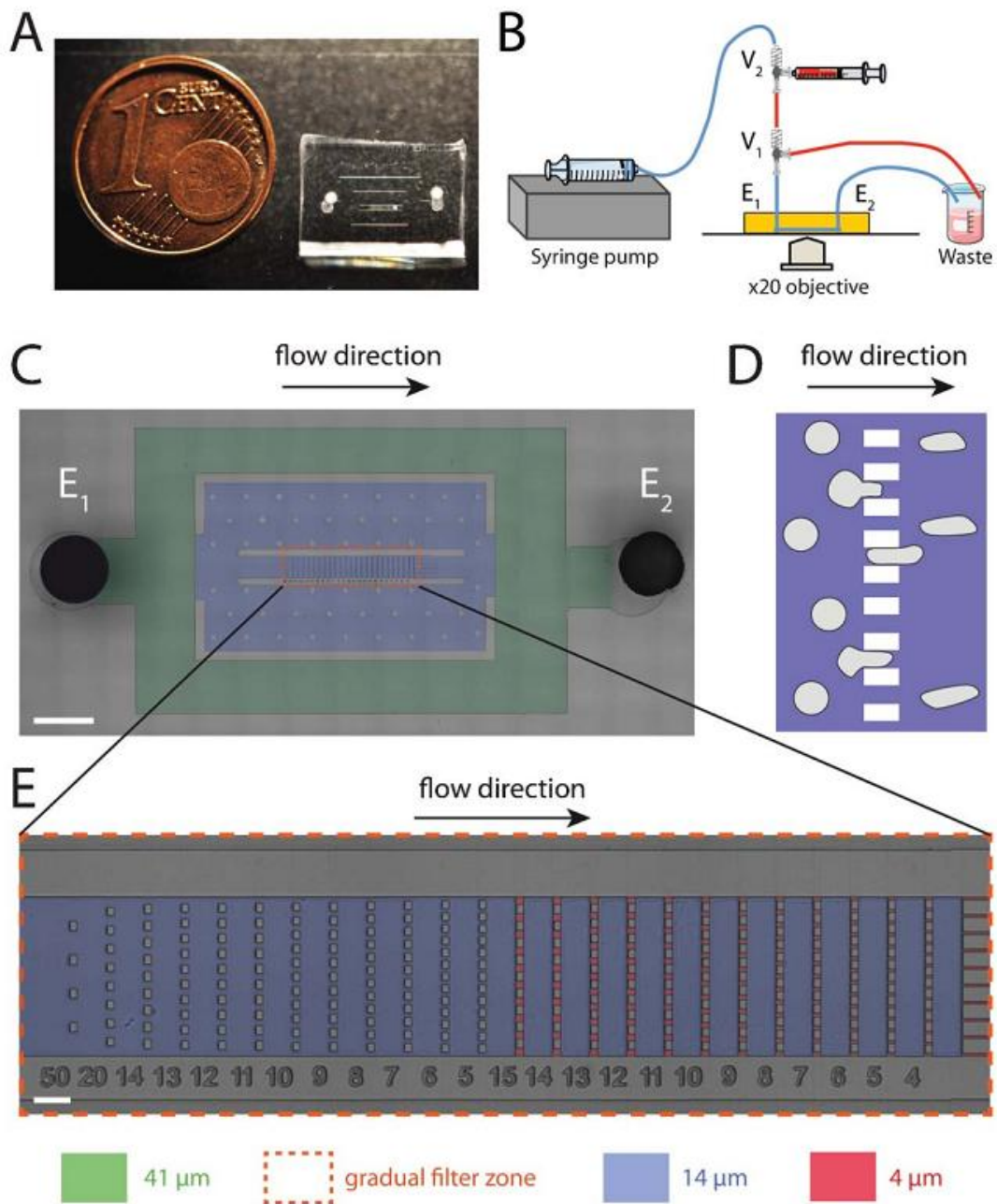


Figure 2.13: Sieve based cell isolation approach. Reprinted with permission [105].

2.6.2 Affinity based assays

In many cases, cells don't show distinguishing physical and mechanical attributes. This results in poor selectivity in capture and isolation in the devices employing only physical or hydrodynamic separation. This necessitates the need for other modes for effective detection. Cancerous cells demonstrate abnormal growth of several proteins and receptors on the cell surface, when compared to healthy cells. This deviation is statistical in nature and can be both in the protein count as well the extent of their mutation from the original forms.

Devices were reported to employ target specific molecules, especially the membrane proteins recognizable on the cells of interest, immobilized onto the surface in microfluidic environments. These molecules specifically recognized the proteins on the target cells and subsequently isolated them (Figure 2.14). On the contrary, normal cells that have low or normal expression of the target protein can pass without getting bound to the surface. The affinity between specific molecules and corresponding cell membrane proteins is usually constant. The major challenge in these devices is to increase the contact between the capture molecules and cells in microfluidic devices.

Many devices with appropriate surface modifications have been developed for cell isolation in the last two decades. With optimized flow rate, minimized steric hindrance, controlled shear stress, and suitable topography, cells of interest were reported to be isolated with promising efficiency. Iqbal and coworkers have reported work with anti-EGFR aptamer with capture efficiency (*ratio of the number of captured cells to the total number of tumor cells*) of 62% [106].

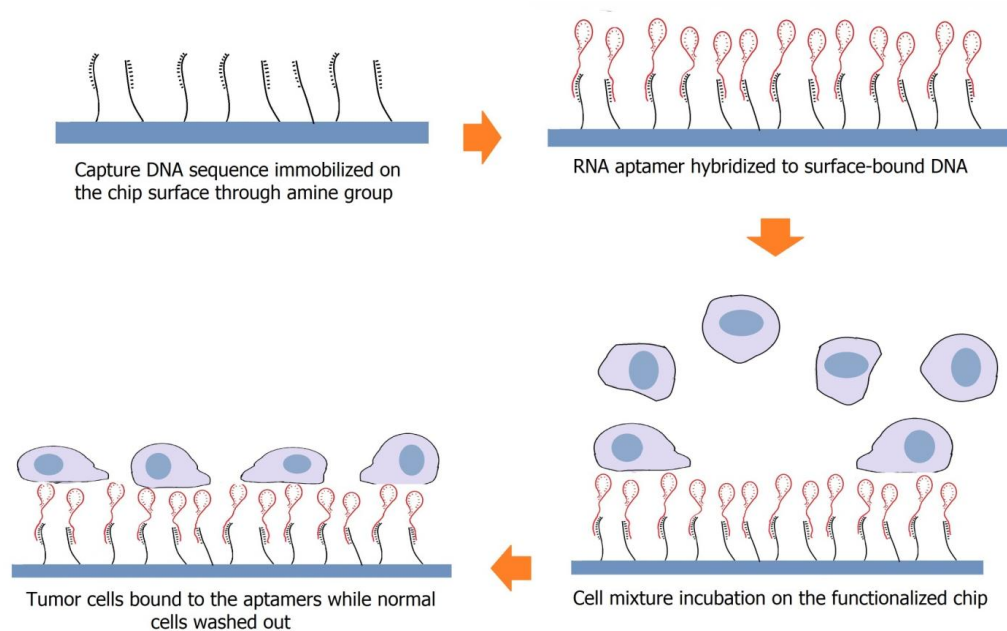


Figure 2.14: Schematics showing cancer cell isolation. Surface tethered probe DNA sequence is used to bind the RNA aptamer. RNA molecules fold into 3-D structures in the solvent. The specific RNA molecules have high affinity to EGFR. Cells with overexpressed receptor on the cell membrane bind strongly to the aptamer on the chip surface. Cells with low EGFR number (normal cells) are removed using gentle wash, leaving only cancer cells on the surface.

Microfluidic devices have been employed for CTC isolation utilizing these capture molecules. Devices with microposts and herringbone structures have been reported to show increased efficiency in cell isolation [107]. Microfluidic devices employing anti-PSMA aptamers have also been used for isolating prostate cancer cells[108].

2.6.3 Dielectrophoresis (DEP)

DEP promises tag-less cell separation. Separation of cells occurs when a dipole of significantly varying magnitude is created on cells in a non-uniform AC electric field. This property has been used for separation and transportation of cells based on their size, shape and dielectric property of the cell structure. There are measurable differences in the membrane capacitance of cells. A cell structure can act as a capacitor where two conducting (electrolyte) layers are separated by a thin dielectric one (membrane) as shown in Figure 2.15. Dielectric

property varies depending on the water content of the cell, presence of ions in the cytoplasm and the containing medium. Cell capacitance also depends on the effective area of the plasma membrane and internal folds and microvillis. These properties vary with physiological states of the cells, thus measurement of capacitance promises to be a good indication of diseased stage of a cell.

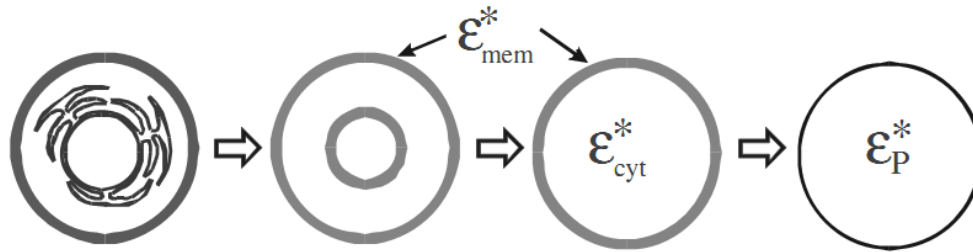


Figure 2.15: Schematic representation of a cell structure, simplified to a sphere. The sphere represents the dielectric properties of the nucleated cell. Reprinted with permission [46].

DEP has been reported for spatial manipulation, sorting and enrichment of target cells in biosensors and immunoassays. This has been used as tweezers in artificial engineering of three-dimensional cell constructs [109, 110]. However, it is plagued by the drawbacks like poor cell viability due to high electric field requirement, complex device design, fouling of the medium. Also, at early stages of cancer, cells don't demonstrate significant difference in their dielectric properties, thus challenging the isolation.

2.6.4 Magnetic Isolation

Magnetic cell isolation techniques offer simplicity in terms of device design. As the name suggests, cells with magnetic property or magnetic tags attached to the cells prior to isolation are subjected to external magnetic field to isolate the target cells (Figure 2.16). Some cells like RBCs show inherent paramagnetism because of their iron content [111] and these can demonstrate sufficient pull to magnetic field without any external tag. Some bacteria also show similar property. However, cancer cells lack any inherent magnetism and hence to separate

these, it is important to selectively tag the tumor cells with magnetic labels. Once a magnetic contrast between the healthy and tumor cells is created, conventional magnetic isolation are applied for isolation and sorting.

Magnetic isolation technique promises certain advantages. Compared to vigorous force applied in centrifuging or even filtering, this is milder and thus prevents any damage to cells during the isolation process [112]. At slower flow rate, ions present in the solution are not affected by the applied magnetic field and remain mostly static. This prevent cells from accumulation on the surface because of the membrane charge and hence providing a better selectivity. However, tagging the cells with magnetic labels and un-tagging after isolation introduce added complexity. Complete release of magnetic tags is difficult and the membrane protein can be easily dislodged while removing the magnetic tag. This raises a question of cell viability and reliability of post isolation analysis.

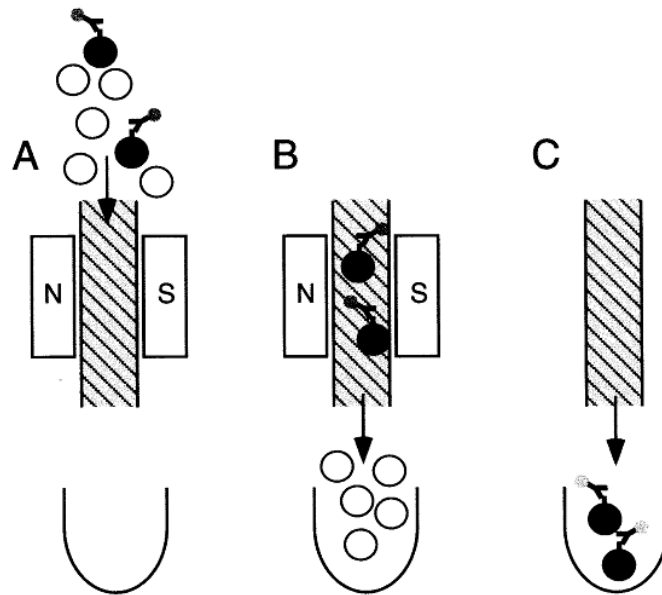


Figure 2.16: Cell isolation using magnetic technique. Magnetic particles are attached to the target cells using affinity interaction. A permanent magnet is later used to attract and separate the cells with pre attached magnetic tag. Reprinted with permission [113].

2.6.5 *Density Gradient Centrifugation*

Normal cells and mutated cancer cells have been shown to have varying density and this property is used to separate these from whole blood [114, 115]. Density gradients can be created by placing layers of gradient media resulting in the movement of the heaviest cells to go to the bottom and the floating of the lightest cells to the top. The sensitivity and specificity of this method were not satisfactory especially due to the very small number of CTCs in the circulation.

2.6.6 *Cytometric Methods*

These methods are based on cell counting based on prior selective tagging of the cells. Laser-scanning cytometry and multiphoton intravital flow cytometry are commonly used [116]. In laser scanning cytometry, blood samples are pretreated with labeled antibodies targeting cancer cells. These cells are detected from the flow using laser detector and separated out, followed by cell lysis (Figure 2.17). This is a serial process and sample processing time is extremely high. Also, these cytometric methods require expensive flow cytometry and professional facilities.

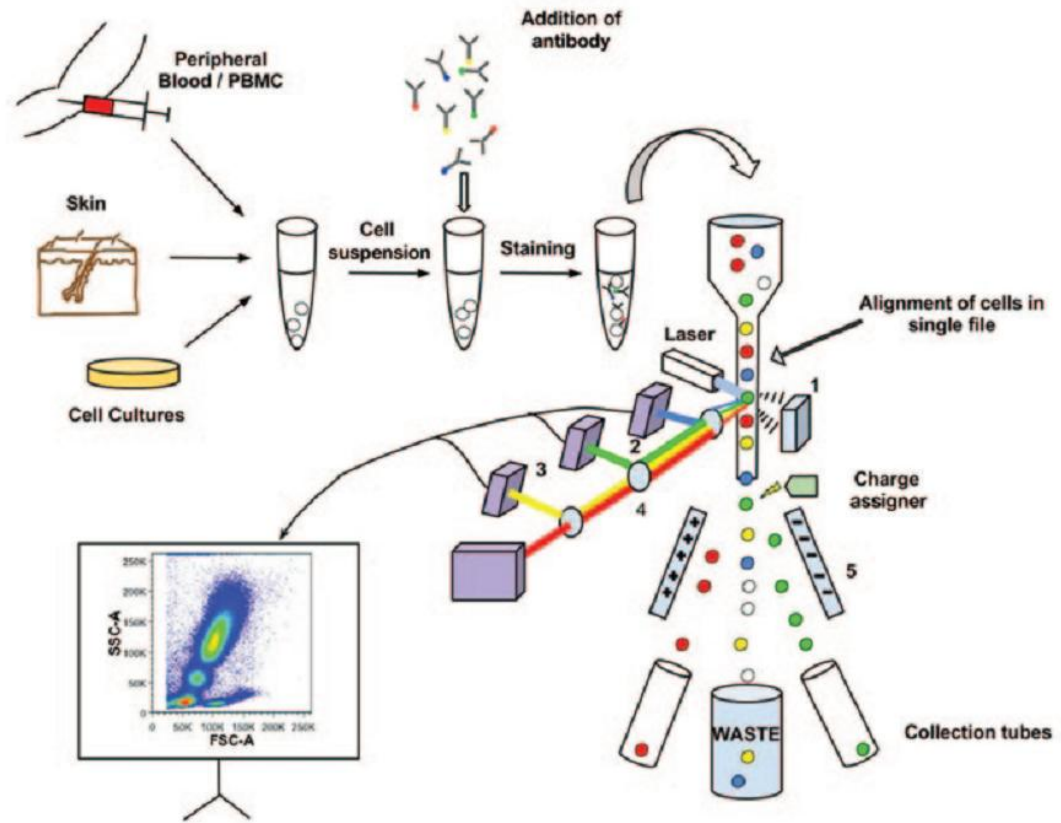


Figure 2.17: Cell flow cytometry. Cancer cells are fluorescently pre tagged and detected using the laser before sorting out. Reprinted with permission [117].

2.6.7 Microscale Optical Interactions

In this method, highly focused laser beam is used to apply an attractive force to physically hold and move cells [118]. It is capable of handling nanometer and micrometer sized dielectric objects. Cells can be moved through the gradient from weak electric field region to the stronger region. Although high-throughput cell manipulation has been claimed, whole blood analysis remains a challenge. The isolation efficiency has also been unsatisfactory .

2.7 Review of Aptamer based Isolation Devices

One mode of cancer detection approaches is to use aptamers as probes to recognize and bind to cancer specific and/or overexpressed biomarkers. This is usually followed by direct or indirect identification of cancer cells with appropriate biosensing techniques. A number of aptamer based techniques such as nucleic acid amplification [119], magnetic relaxation switching sensing [120], electrochemical detection [121], chemiluminescence or colorimetric determination [122] and others have been tested for cancer cell detection and quantitative analysis of receptors at a single cell level. Limit of detection (LOD) has been narrowed down to single cancer cell level and some of them have already claimed successful detection with real biological samples. LOD of aptamer based biosensors for onco-protein is reported to be in picomolar, femtomolar and even in some cases down to attomolar range [123]. Many comprehensive reviews of aptamer based cancer cell detection with different mechanisms are readily available. Aptamers based cancer cells isolation approaches can be generalized into two broad categories: (i) Devices where free floating cancer cell are isolated on the surface grafted aptamer and (ii) Devices where cells pre-treated with a suitable molecule and aptamer complex to facilitate isolation or detection at a later stage.

This dissertation research has mostly focused on the first method, where cancer cells were enriched onto aptamer grafted substrates. Challenges in this method remain in isolating cells from fluids drawn from the patients drawn fluid with high specificity and sensitivity. The ratio of target to the non-specific cells is billion to one. This require supreme sensitivity in the designed devices.

One effective way for efficient cell attachment is to increase the odd for more cells to come in contact with the surface. Higher interactions between cancer cell surface molecules and aptamer can competitively resist external dislodging forces. Increasing the aptamer grafting density, reducing the distance when cells deviate from the fluid flow toward the substrate, and decreasing the flow rate can effectively capture cancer cells [124].

Natural substrates are seldom plane and usually textured in nature. In tissue culture, substrate mimicking the ECM matrix have been proven to facilitate superior growth and proliferation [125]. This ECM matrix, as shown before (Figure 2.4), has micro and nanoscale pores and roughness to better interact to the cells. Inspired from this, nanotextured substrates, ranging from a few nm to hundreds of nm, have lately emerged as a promising cancer cell detection and isolation platforms. These provide more surface area for aptamer immobilization and also lower the rolling velocity of cells in microchannels [126]. This ensures firm attachment and hence better isolation of the target. Cancer cells can dynamically arrange focal adhesions on these as well [127]. Cancer cell isolation efficiency on these surfaces was reported to reach 80-95% with the trade-off of decreased specificity.

It is noteworthy that “mean capture yield” using anti-EpCAM antibodies in CTC-microchip has been shown to be around 65% [27]. In addition, the false-negative results in CTC isolation and detection are very much possible. The combination of affinity interactions and biomimetic nanostructured surfaces may further improve isolation and detection efficiency; therefore nanostructured surfaces have been introduced into this field.

Despite the promising results, challenges prevail. Very few of aptamer based biosensors have shown clinical validity or utility, and most of these methods still remain in laboratory settings. For example, when diagnosing with blood or urine sample drawn from patients, large amount of blood proteins produce significant noise signals and interfere with the detection and isolation of the relatively low amount of target cells or proteins [128]. As mentioned before, cell heterogeneity and/or associated protein diversity remains a major challenge. Continuing mutation of the target proteins (splice variants, post-translational modification, and rare events) poses a significant obstacle. Careful selection of target protein and the binding aptamer is necessary for accurate diagnosis. Finally, understanding the biochemistry of aptamer and protein interaction at molecular level is fundamental for the detection method.

These research directions bolster the idea that textured surfaces can increase cell isolation efficiency and require deeper attention. However, jury is still out on the best topography for optimum capture. Cell isolation is a complicated mechanism which involves many factors like cell toughness, density and quantity of adhesive elements, immunoaffinity interactions, substrate material, surface topography, flow rate, channel dimensions, various flow conditions, and so on. Scope for more work is still there to explore best conditions for all the various factors.

2.8 Cell Migration

Cell migration is an important biological phenomenon. It is an essential process for development and functioning of nervous system, inflammatory response, wound healing and many others. In many cells this property remains suppressed but can be triggered by wounding or oncogenic transformation [129, 130]. In fact, this plays a central role in cancer metastasis where tumor cells migrate from the initial tumor mass to the blood circulatory system and later attaches to a distant organ and proliferate. Cell migration is an integrated process where different element like chemical and physical properties of the cell structures, their kinetic and mechanical characteristics and their co-ordination with the external stimuli play in synergy. A comprehensive understanding is required before any claim in alteration of such behavior can be made [131].

Cell migration has been previously shown to be modulated by change in concentration of the adhesion receptors, cytoskeletal linking proteins and extra cellular ligands. It was shown that changing physiochemical properties like receptor-ligand binding affinity and strength of receptor-cytoskeleton interactions also affect cell motility. Migration starts with microscopic nonuniformities in receptor-ligand binding and the gradient in stimulus caused by that. Cells thus acquire a spatial assymetry which enables them to turn the intracellularly generated forces into net cell body translocation. Molecular rearrangements in the filamentous and F-actin

distribution, spatial asymmetries in integrin adhesion receptors and integrin-cytoskeleton linkages facilitate migration (Figure 2.18) [132].

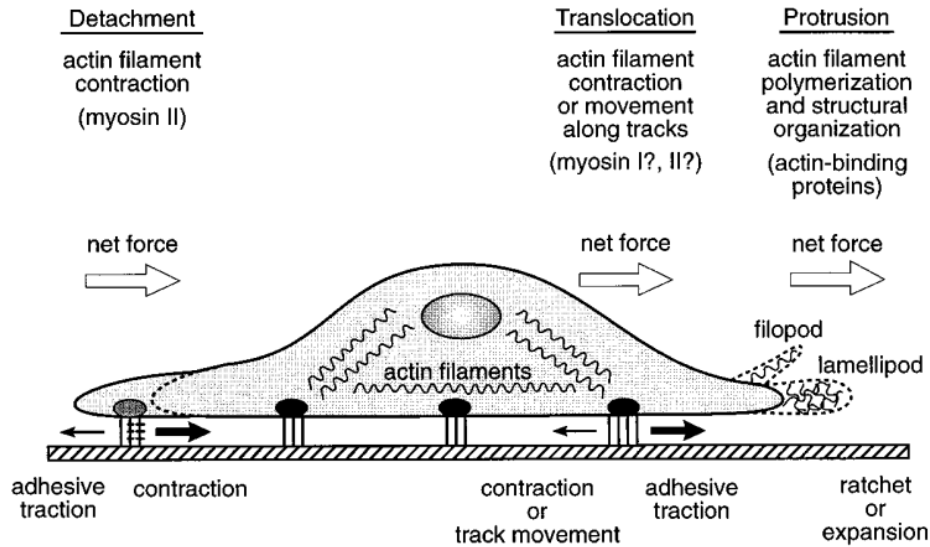


Figure 2.18: Different forces in cell migration. It starts with protrusion of lamellipodia or filopodia by the force generated by actin polymerization. Once the membrane protrusion adheres to the substratum, translocation may occur by myosin interactions with actin filaments at the rear end. As a result cell detaches from the rear. The process involves disruption of cell– substratum adhesive interaction which is accelerated by myosin-mediated actin filament contraction pulling on adhesion complexes. Reprinted with permission [131].

Lamellipodia and filopodia are extensions of the cell when cell is crawling in two dimensional substrate. These can protrude tens of microns from the main cell cortex. It is universally accepted that this extension occurs in response to local actin polymerization and structural organization by means of cross-linking into lattices or bundles. A contractive force is needed for cell to migrate which depend on the active myosin based motors and happen within the anterior and posterior region of the cell. Myosins belong to a family of ATP-dependent motor proteins and are responsible for muscle contraction in cell motility processes.

Cell behavior on bio modified chips can play important role in motility stimulation. This is especially important in cancer cells. In fact, the turning ON or OFF motility on functionalized

chip can be an important prognostic tool and holds big promise. This phenomenon has been investigated in our work.

2.9 Nanopore and Molecular Dynamics Simulation

Nanopore is a novel platform to electrically visualize the binding event of a single molecule inside the pore [133]. Any such binding inside causes a change in the ionic current setup through the pore and the disturbance record can be analyzed to detect binding affinity, molecular dimensions and few other parameters. The use of nanopore includes but not limited to rapid sequencing of DNA, detection of proteins and metal ions and it is utilized to discover the underlying methods of the polymer dynamics and transportation [134-136]. The idea of detecting protein through nanopore is that any binding event will cause change in the conformation of the molecule which in turn affect the molecular occupancy inside the channel thereby altering the conductance of the channel. One of the advantage of using nanopore is that it requires no molecular tag with minimal preparation. Rise of synthetic nanopore technology circumvented the issue of vulnerability of biological nanopore and thus making it feasible to use them in detecting bigger molecules like proteins (Figure 2.19) [137]. As learned before, proteins play crucial roles in carrier transport, molecular motors, cellular structural support etc. To perform such functions, they possess wide range of size, shape, weight and surface charge distribution etc. Solid-state nanopores are specially suitable to detect the differences in different protein parameters (Figure 2.20). Again enzyme mediated unfolded proteins can also be potentially sequenced using a nanopore setup [138]. Possibilities are hence endless. Nanopore is drilled, usually in silicon nitride membrane using lithography. Pore diameter of only few nanometers have been reported and studied for molecular detection.

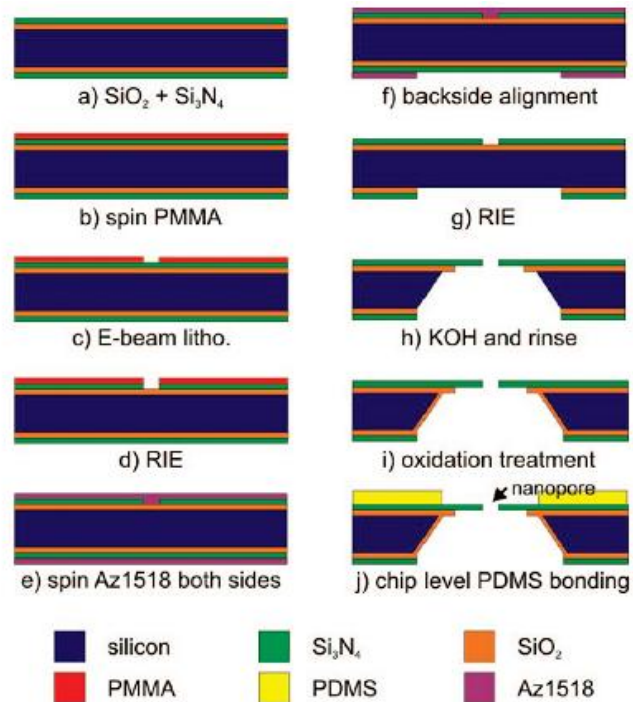


Figure 2.19: Flowchart of Nanopore fabrication. Reprinted with permission [139].

In addition, capture molecules can be tethered to the inside wall of the pore that can bind specifically to a target biomolecule and thus creating a force specific detection. The challenges that presently exists in this method is in functionalization of the pore as well as high cost of fabricating nanopore. Also, distinguishing features due to binding to the target molecule are yet to be uncovered.

By the time these problems are circumvented, molecular dynamic simulation can predict the events that take place inside a nanopore. Several challenges exist for protein translocation. For disease diagnosis, it is important to be able to detect protein in its native form. Alternatively a precise track of any transformation of the protein shape need to be determined. This is challenged by several factors. A protein molecule may not enter the pore due to its inability to find a sterically compatible geometry when it encounters the pore opening. Protein in its native form has charge distribution on its surface and hence may show selectivity during the

insertion event. The 3-D structure of protein may become unfolded (mostly depending on the disulfide bonds they have at their native state) under the electric field inside the nanopore which might result in losing the selectivity. Unlike nucleic acid sequence, the charge density of protein depends on the sequence of the protein. Again, the change in conformation may change the net force and hence the direction of the protein movement inside the pore [140].

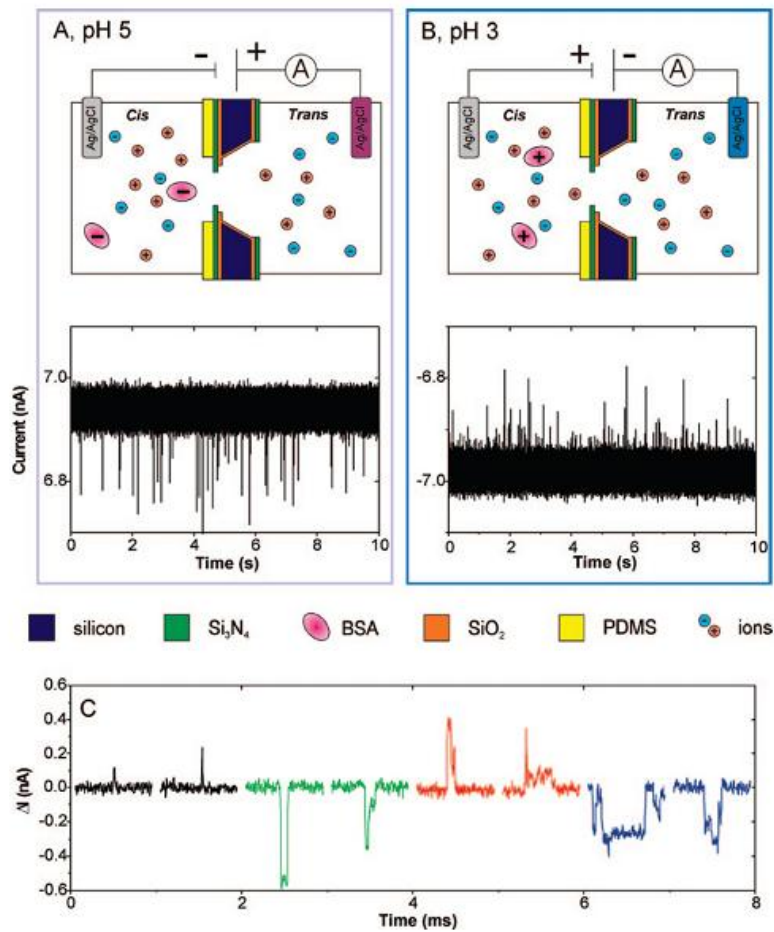


Figure 2.20: Protein detection using nanopore. Reprinted with permission [139].

2.9.1 Computer Simulations

Computer simulations are carried out for better understanding the properties of molecular assemblies in terms of their structure and the microscopic interactions between them.

This can run in parallel and serves as a complement to the laboratory experiments. The two mainstream class of simulation techniques are molecular dynamics (MD) and Monte Carlo (MC). Hybrid techniques are available that combine features from both. The advantage of MD over MC is that it enlightens the dynamical properties like transport coefficients of the system, time-dependent responses to perturbations, rheological properties and spectra. Simulations are also carried out for experiments that are difficult or impossible to perform in the laboratory [141].

Computer simulations provides a bridge between microscopic length and time scales and the macroscopic world in the laboratory. Information obtained at molecular level through MD simulations can reveal the secret behind the macroscopic measurements and can give exact predictions only to be limited by the computational budget. The advancement of the theoretical background of this simulation promises to uncover great amount of detail in the biomolecular systems.

2.9.2 MD simulation

MD simulations calculate the energy of each molecule separately in an ensemble (a *group of adjacent molecules inside the body in consideration*) for a given time. The program uses Newtonian or quantum mechanical calculations to determine the state of a molecule based on the state of all the molecules in the ensemble at previous time step [141].

The effective molecular energy can be expressed as a sum of potentials derived from simple physical forces (Table 2-3).

$$Energy = E_{bonded} + E_{nonbonded}$$

$$E_{bonded} = E_{bond-length} + E_{angle} + E_{rotation}$$

$$E_{nonbonded} = E_{van-der-Waals} + E_{electrostatic}$$

Table 2-3: Energies in Molecular Dynamics Simulation.

Bonded	Bond length potentials	$E_{\text{bond-length}} = \sum k_b (b - b_0)^2$	This represents the vibrational motion of the bonded molecules and modeled as harmonic potential Here K_b is the spring constant.
	Bond angle potentials	$E_{\text{bond-angle}} = \sum k_\theta (\theta - \theta_0)^2$	This terms takes care of the steric barrier between atoms separated by 3 covalent bonds
	Rotation potential	$E_{\text{rotation}} = \sum k_\phi \left(1 + \cos(n(\phi - \delta)) \right)$	This models the steric barrier between atoms separated by 3 covalent bonds
Non-bonded	Coulomb potential	$E_{\text{coulomb}} = \sum \frac{q_i q_j}{4\pi\epsilon_0 r_{ij}}$	This represents the electrical interactions.
	Van der Waals	$E_{\text{Van-der-Waals}} = \sum_{i < j} \epsilon \left(\left(\frac{r_m}{r} \right)^{12} - 2 \left(\frac{r_m}{r} \right)^6 \right)$	Commonly known as Lennard-Jones potential

2.9.3 Simulation software :

2.9.3.1 VMD

VMD is a molecular dynamics program designed for modeling, visualization and analysis of biological systems like protein, nucleic acids etc. This program acts as a graphical front end of the MD simulation program [142].

2.9.3.2 NAMD

NAMD is a parallel molecular dynamics program suitable for high performance simulations of large biomolecular systems. The program is based on Charm++ parallel objects, which was developed with primary focus on proteins, peptides, nucleic acids carbohydrates and small molecule ligands etc. NAMD can handle beyond 200,000 cores for larger simulation [143].

Chapter 3

Distinct Morphological Behavior of Tumor Cells on Aptamer Functionalized Chips

3.1 Introduction

Tumor cells overexpress multiple signaling proteins on their membranes. While incubated on aptamer functionalized surfaces, it was found that cancer cells showed dynamic morphological changes in their membranes. The balancing forces between the membrane molecules and the surface entities, together with the flexibility of the membranes caused these cells to show distinct activities and variations in their dynamic morphologies. These behaviors, once quantified, can distinguish cancer cells from normal ones on the surfaces grafted with binding molecules. When compared to their healthy counterparts, cancer cells demonstrate distinguishing behavior in terms of their shape changes with time, non-uniformity, and formation of pseudopods etc.

Many types of cancer cells show overexpression of EGFR. Anti EGFR antibody and anti-EGFR aptamers both have been reported to selectively isolate cancer cells. The capture and analysis of human glioblastoma (hGBM) cells were done on glass chips functionalized with EGFR specific RNA aptamer molecules. A mutant aptamer coated surface was used as control. The hGBM cells are known to overexpress EGFR and these were specifically distinguished and isolated using anti-EGFR RNA aptamers.

During the capture of hGBM cells by the surface-bound aptamers, the cells showed distinct morphological attributes, which were absent in normal cells. Several feature vectors were extracted based on transient morphological changes from the acquired images during incubation. The comparison of the vectors from healthy and diseased cells showed distinctions between tumor and normal cells on the surface. These distinguishing features have the potential to be used as fast and effective means to detect cancer, possibly in point-of-care

device setup. The method can serve as an additional modality to support histological findings and to identify tumor cells based on their physical behavior.

3.2 Methods

The hGBM cells and astrocytes were obtained from consenting patients at the University of Texas Southwestern Medical Center at Dallas, Texas as per the approved Institutional Review Board (IRB) protocols. Astrocytes are glial cells from the same lineage as hGBM cells. Therefore, comparing hGBM with astrocyte for differentiating between tumor and normal or healthy cells gives an accurate and precise comparison, while minimizing other factors that may affect results. Silicon dioxide (microscope glass slides) surface was functionalized with RNA aptamer. This aptamer was known to selectively bind to EGFR. The cells were incubated (Figure 3.2). Time lapsed images were taken using optical microscope and recorded images were analyzed using software developed and reported here. Conventional image processing along with contour detection were used to follow cell behavior. Quantitative data was extracted to compare between control and cancer cells.

3.2.1 *Selection of Target: Specificity, Selectivity And Sensitivity*

EGFRs are overexpressed on tumor cells and were chosen for the experiment. In fluorescence experiment for verifying the binding ability of the aptamer to EGFR and its variant, mouse glioma cells bound to anti-EGFR aptamers showed increased fluorescent activity (60 a.u.) when compared to fibroblast cells (5 a.u.). This difference was due to the low number of EGFR on normal cell surfaces.

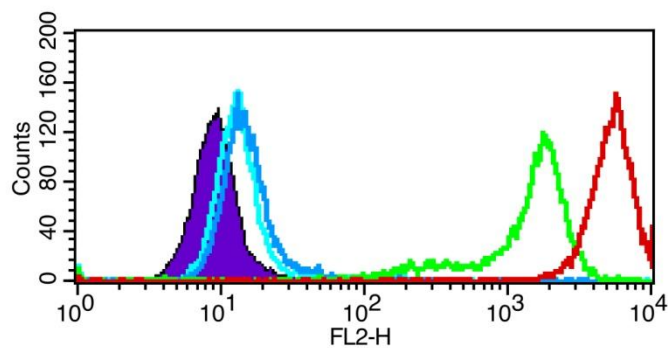
A large amount of mouse-derived tumor cells were captured while using anti-EGFR aptamer modified surface as capture substrate (Figure 3.1). The anti-EGFR aptamer had capturing efficiency (ratio of the number of captured cells to the total number of tumor cells) of 62%. When aptamer and antibody based tumor cell isolations were compared, it was observed






that aptamers had higher specificity to tumor cells compared to the antibodies. The capture efficiency of 94.82% has been reported in comparison to antibody's 68.81% [144]. This specificity of the aptamer can be attributed to its ability to bind to the extracellular ligand-binding domain III of the receptor which is present in both wild type and mutant EGFR. The specific binding of the aptamers to the domain minimizes any chances of non-specific adsorption. Tumor cells have high density of sialylation on their surface compared to surfaces of normal cells. Increased sialylation gives the tumor cells a net negative charge which is then intuitively repelled by the negative charge of the aptamer, further minimizing non-specific adsorption.

Aptamer's selectivity and sensitivity was further improved by using capture oligonucleotide. The capture DNA was covalently immobilized on the surface (functionalization). This DNA captured the aptamer, increased the distance between the aptamer and the substrate surface and minimized any steric and electrostatic hindrance that may have arisen due to surface tethering. This also increased the radius of gyration, allowing for increased reactivity.

3.2.2 Aptamer Preparation

Anti-EGFR RNA aptamer selection and sequence has been reported before (Figure 3.1) [144]. Anti-EGFR aptamer sequence was: 5'-GGC GCU CCG ACC UUA GUC UCU GUG CCG CUA UAA UGC ACG GAU UUA AUC GCC GUA GAA AAG CAU GUC AAA GCC GGA ACC GUG UAG CAC AGC AGA GAA *UUA AAU GCC CGC CAU GAC CAG*-3'. The sequence for mutant aptamer was 5'-GGC GCU CCG ACC UUA GUC UCU GUU CCC ACA UCA UGC ACA AGG ACA AUU CUG UGC AUC CAA GGA GGA GUU CUC GGA ACC GUG UAG CAC AGC AGA GAA *UUA AAU GCC CGC CAU GAC CAG*-3'; (the extended sequence used to bind to capture DNA is shown in italics). Substrate-anchored DNA probe had the sequence: 5'-amine-CTG GTC ATG GCG GGC ATT TAA TTC-3'



Key	Name	Parameter	Gate
	cell_sample.002	FL2-H	No Gate
	cell_sample.003	FL2-H	No Gate
	cell_sample.005	FL2-H	No Gate
	cell_sample.001	FL2-H	No Gate
	cell_sample.004	FL2-H	No Gate

Cells
 Cells+biotin control
 Cells+Mut
 Cells+E07, control
 Cells+E07, new

Figure 3.1: Flow cytometry result showing affinity of the developed anti-EGFR aptamer to the tumor cell.

3.2.3 Preparation of anti-EGFR Aptamer Functionalized Substrates

The aptamer binding protocol was adapted from literature [145, 146]. Glass slides were used as substrates and were cut into $\sim 5 \times 5 \text{ mm}^2$ pieces. Piranha solution ($\text{H}_2\text{O}_2:\text{H}_2\text{SO}_4$, 1:3) was used to clean the slides for 10 minutes. The slides were then rinsed with deionized (DI) water and dried in gentle nitrogen gas blow. After drying, the slides were placed for 30 minutes in a methanol/DI water (19:1) and 3% APTMS solution. The glass substrates were then washed with DI water and methanol and incubated for 30 minutes at 120°C . A dimethylformamide (DMF) solution was then prepared using 10% pyridine and 1 mmol/l *p*-Phenylene diisothiocyanate (PDITC). The substrates were then immersed in the DMF solution for 5 hours at 45°C . The substrates were successively rinsed with DMF and 1,2-dichloroethane. After rinsing, the slides were dried with nitrogen gas. A $30 \mu\text{mol/l}$ of modified DNA solution with a 5' amine group was prepared using DI water with 1% *N,N*-Diisopropylethylamine (DIPEA). The $15 \mu\text{l}$ of the DNA

solution was then placed on each glass substrate. The substrate was incubated overnight in a humid chamber at 37 °C. After incubation these were successively washed with methanol and diethylpyrocarbonate (DEPC) treated DI water. Unreacted PDITC moieties were then capped onto the functionalized devices to deactivate the surfaces. This was done by immersing the glass slides for 5 hours in 150 mmol/l DIPEA in DMF and 50 mmol/l 6-amino-1-hexanol. Again, each substrate was sequentially washed with ethanol, DMF, and DEPC-treated DI water. RNase free and DEPC treated DI water was then used to properly wash the incubator. A 5 µl of 1 µmol/l anti-EGFR RNA aptamer was placed on each substrate in the presence of 1X annealing buffer [10 mmol/l Tris (pH 8.0), 1 mmol/l EDTA (pH 8.0), 1 mmol/l NaCl]. After being subjected to 2 hours of hybridization at 37°C, substrates were then washed with 1X annealing buffer and DEPC-treated DI water for 5 minutes. A mutant aptamer using the same protocol was hybridized onto control substrates and used as a negative control device. 1X PBS (pH 7.5) with 5 mmol/l magnesium chloride solution was prepared and the substrates were then placed in it for 1 week or used immediately.

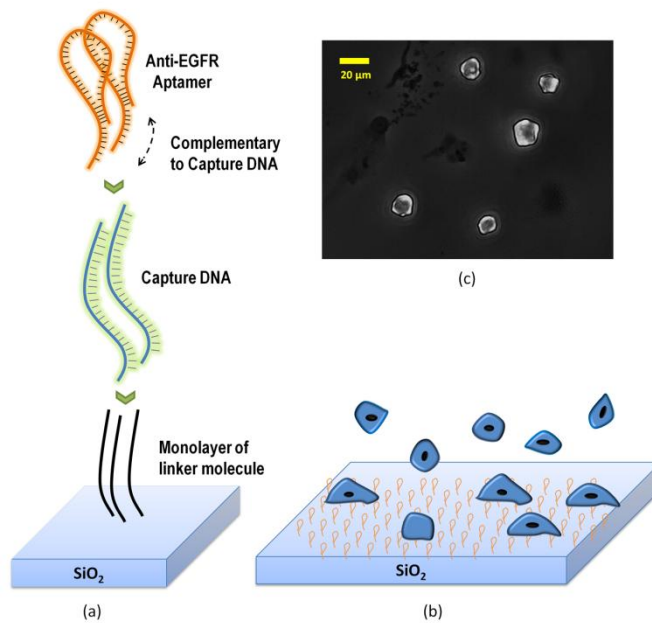


Figure 3.2 : Schematics of aptamer immobilization and cell capture.(a) Schematic depicting aptamer attachment chemistry starting with capture DNA immobilized on the surface through the PDITC linker (not to scale). The capture DNA provides larger radius of gyration and hence less steric hindrance to the aptamer. Aptamers make duplex with the capture DNA on one side and the other side is functional. The functional side binds to the target receptors on the cells. (b) Cells flatten out as these bind to the surface. (c) Microscopic image shows how surface-bound cells are flattened after attaching to the substrate

3.2.4 Fluorescence Measurements

Immobilization of ssDNA and RNA aptamers on the glass surface was verified by fluorescence measurements of Acridine Orange (AO) stain at an excitation wavelength of 460 nm and an emission wavelength of 650 nm. The chip surfaces were prepared as mentioned before and were stained at different immobilization steps. In short, AO solution of concentration 2 mg/ml was prepared in sterilized DI water and the samples were completely immersed into it and kept on the shaker for 30 minutes. It was later washed thoroughly with DEPC water before fluorescence measurement. The fluorescence intensity was analyzed with ImageJ software.

3.2.5 *Isolation and Characterization of hGBM Cells*

The hGBM cells were readily placed in ice cold HBSS solution after being taken from the patient's brain. The specimens were on average larger than 50 μm^3 . Lymphocyte-M (Cedarlane labs) was used to remove the red blood cells from the specimen. A solution of 2% papain and dispase was used to gently dissociate the intact hGBM cells, followed by gentle grinding (trituration). FACSCalibur machine (BD Biosciences) was then used to sort out the cells. Clonal expansion and formation of orthotopic tumors was observed in both CD133+ and CD133- fractions. Cells from the CD133+ fraction were then used in the experiments.

3.2.6 *Image Processing*

Time lapsed optical micrographs were acquired at 30 second intervals using Leica microscope with DFC295 camera at 20X magnification. A moving stage microscope was used to image the entire chip. Cell density was measured using hemocytometer and was optimized at 100,000 cells per ml to avoid cells attaching to each other. The images were saved at 4096x3072 resolutions in tiff format.

3.2.7 *Image Segmentation*

Each cell was cropped out using image segmentation algorithm. The algorithm provided an approximation of the center of the cell body. Based on the image magnification of the microscope, a 200x200 pixel cropping was performed around the estimated center. This cropping kept a typical cell completely inside the frame. Images where two or more cells were seen clumped together were discarded. Less than 5% images showed such clumping behavior of cells. The number of pixels were optimized to increase the speed as well as to retain the required information.

3.2.8 Contour Detection

After initial Wiener filtering, contrast enhancement and smoothing, separated cell image contours were detected using “level set” algorithm [147]. Energy parameters were defined for each image and an initial contour was estimated. A recursive algorithm was developed to minimize the total energy in the equation. Minimum energy occurred at the cell membrane of the image where change in contrast from pixel to pixel became the largest. Contour image plot was then converted to binary format for further analysis. Binary morphological image processing functions ‘erode’ and ‘dilate’ were used to eliminate spurious pixels. The cellular region in the binary image was represented as white and the rest of the frame was represented as black (Figure 3.3). This conversion made it suitable to statistically analyze the extracted data, without losing any important morphological information.

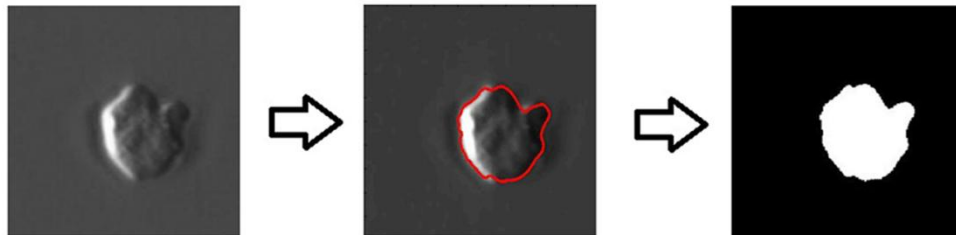


Figure 3.3: Contour detection from segmented image. After initial image processing "Level Set" method is used to detect cell contour. A binary image is obtained from the contour for feature extraction.

3.2.9 Feature Extraction

Centroids for all cells were determined by taking average pixel count in both horizontal and vertical directions. Cell membrane distances from the center were calculated at a resolution of 24 degrees (Figure 3.4). Total of 15 radii were calculated for each cell. Resolution was optimized to maximize the differences in the radii. Too low a number would have missed important data, whereas large number of radii would have failed to amplify the differences between successive radii.

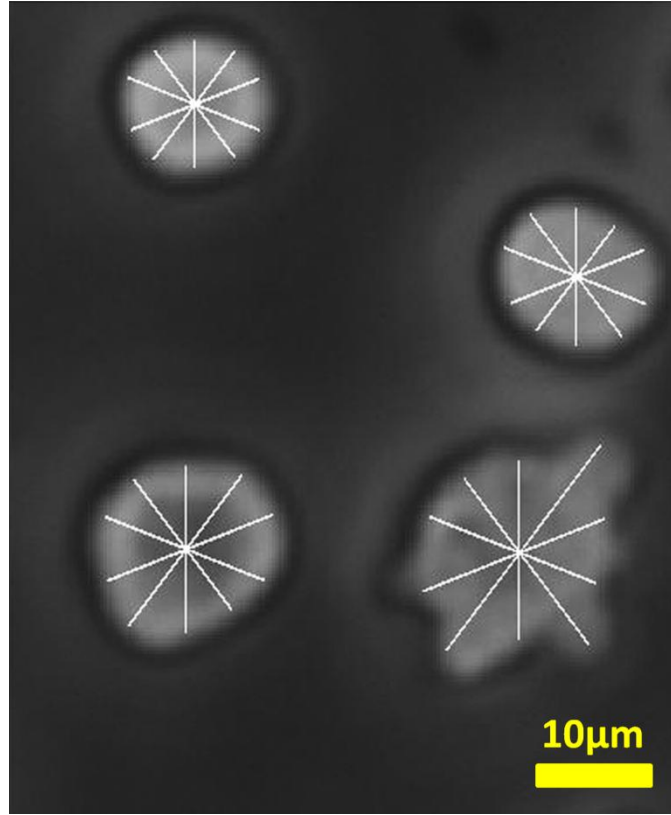


Figure 3.4 : Extracted cell radius superimposed on the original grayscale image. Total number of radial measurement is shown to be 10 for clarity. Higher resolution was used in actual feature extraction.

Cancer cells showed random shape changes during incubation on the surface. Shapes changed from oval to elliptical and highly non-uniform shapes with multiple pseudopods emerged. The shape randomness was tracked from frame to frame for each cell. Non-uniformity of cells was calculated from the differential of two successive radii. For two successive radii, r_n and r_{n+1} , the differential was $\Delta r = r_{n+1} - r_n$. An empirical threshold was determined to amplify the difference and a non-uniformity parameter was calculated as:

$$\Delta r_n = r_{n+1} - r_n$$

$$\Delta r' = \begin{cases} 0 & \text{if } (\Delta r) < 9 \text{ pixels} \\ (\Delta r)^2 & \text{if } (\Delta r) > 9 \text{ pixels} \end{cases}$$

$$\text{non-uniformity (N.U)} = \sum_{n=1}^{N-1} (\Delta r')$$

“Hausdorff distance” is a standard metric to determine the variation from one image to another by calculating and comparing point-to-point distance between contours. Hausdorff distances between cells in two consecutive frames were thus measured based on pixel level information [148]. This calculated the maximum value among all minimum distances between any two possible point sets on the two cell membranes. A comparison was made frame by frame for healthy and cancerous cells.

Pseudopods were defined as an extension of the membrane over a threshold multiplier of the average radius. Such extensions were calculated and tracked for a 360 degree rotation of radius for every frame. Cancer cells showed random extension and contraction of pseudopods, whereas normal cells remained still and did not show much activity. Hence change in number of pseudopods over time was an important discriminating factor in this context. The rate of change in number of pseudopods from frame to frame was thus calculated. An extension was considered a positive change and its contraction was counted as negative. Formation of pseudopods at different angles was measured and recorded to keep track of the cell wall changes.

3.3 Results

As mentioned before, the RNA aptamers on the surface create a passive monolayer that inhibits regular cell-surface interaction through adhesion molecules. On bare glass, astrocytes indeed interact with the surface, though at a much reduced pace. A comparison of astrocytes cell-surface interaction on a piranha cleaned bare glass and an aptamer functionalized glass substrate is presented in Figure 3.5.

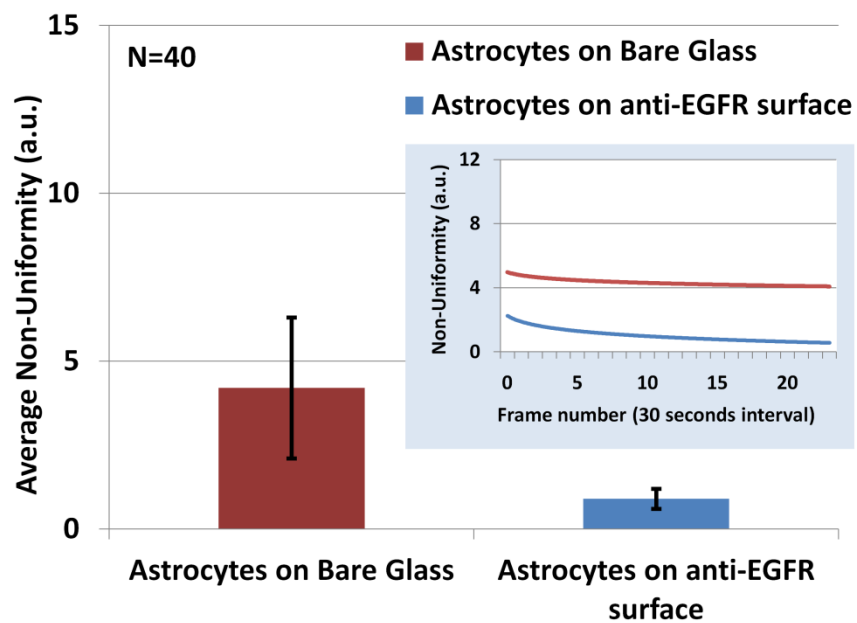


Figure 3.5 : Plot of astrocytes cell and substrate interaction for both bare glass surface and anti-EGFR RNA aptamer functionalized surface. The inset picture shows the variation of non-uniformity over time.

However, such surfaces may introduce non-specific cell activity and false detection. Because of the RNA monolayer, while the other modes of cell-surface interaction are disabled, only the complementary molecules on the cell membrane can possibly interact with the surface. Hence it is important to ensure a uniform and dense monolayer to inhibit non-specific interaction. Binding of probe DNA and RNA to the substrate was verified through staining by acridine orange (Figure 3.6).

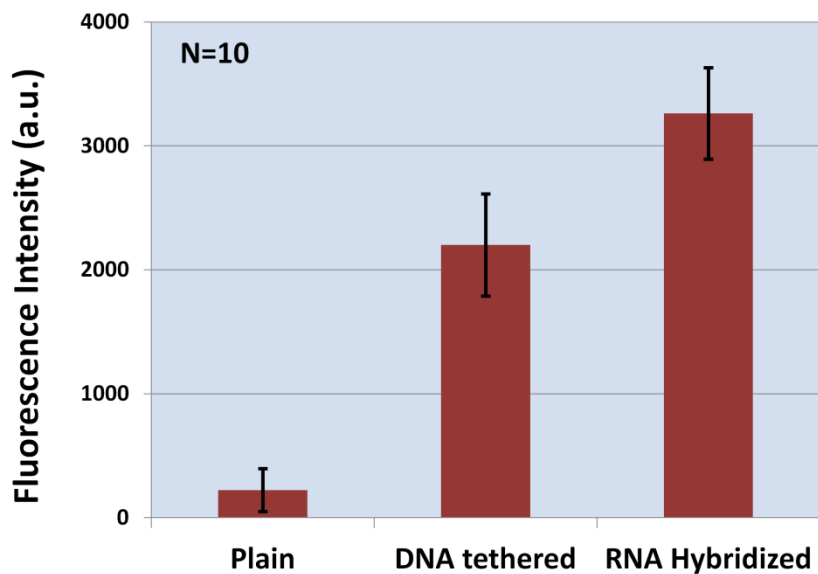


Figure 3.6 : Fluorescence measurement of the functionalized surfaces. Acridine orange fluorescence is measured at different steps of surface functionalization to compare the presence of the surface bound oligonucleotides. Higher fluorescence intensity with RNA hybridized surface ensures the formation of RNA aptamer monolayer on the surface.

In all cases, before incubating on the substrates, cells were centrifuged and the supernatants were removed. Sterilized 1X PBS solution (with 5 mmol/L MgCl₂) was added to dilute the cells. The functionalized slides were placed in PDMS wells and 0.5 ml cell solution was placed on each substrate to make sure it was completely submerged. After 3-4 minutes of settling, images were captured at 30 seconds interval. The period was optimized to capture maximum activity and to minimize processing overhead. Tumor cells on the aptamer modified surfaces showed enhanced activities (shape changes with time, non-uniformity, and formation of pseudopods etc.) while attaching to the surface. All four kind of samples (two anti-EGFR modified surfaces and two surfaces modified with mutant aptamers) were measured on the same day. The cells were taken out of the incubator and kept at 37 °C. The experiment was done both in and outside an incubation chamber and negligible differences were observed

during the short time of imaging. However, complete data acquisition process was done within 20 minutes to minimize artifacts from unwanted cell death.

After Image acquisition, each cell image was separated out and contours were detected. On average, the time for such contour detection depended on a number of factors like the microscope light, aperture size, etc. These were optimized to enhance the edge contrast of the cells which resulted in more efficient and faster processing speed as low number of computational iterations were needed. The algorithm could be tuned for computing either smoother surfaces of the binary images or faster processing speed. For rapid processing, the edges were kept slightly rough. The roughness eventually averaged out over the whole membrane and minimally affected the extracted data (Figure 3.7).

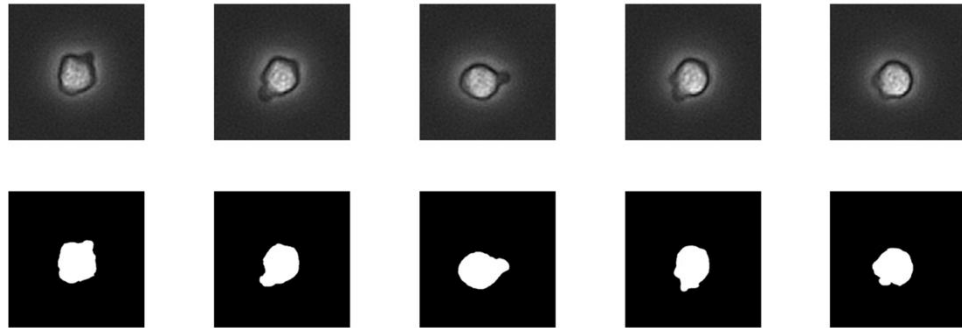


Figure 3.7 : Tumor cell activity on anti-EGFR aptamer modified surface. Five consecutive images with binary converted counterparts are shown. These images were taken after 30 second intervals for the same cell.

During the processing, most errors occurred due to limitations on the depth of field of the imaging microscope. When a pseudopod extended, the boundary of the pseudopod region went slightly out of focus and this created some distortions. Sequential images of 100 regions, each measuring the changes in the cell contours over time, were taken on a moving-stage microscope to ensure cell activity was recorded across the whole surface of the chip (Figure 3.8). The analysis of the 100 regions showed statistically different behavior between cancer and normal cells.

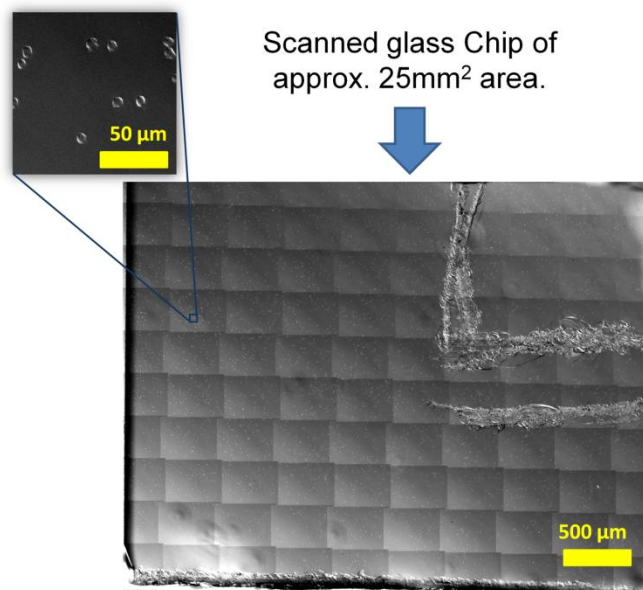


Figure 3.8 : Whole chip imaging. An approximately $\sim 5 \times 5$ mm² glass chip was prepared for cell isolation. The mark on the right side was scratched to ensure that the aptamer functionalized side of the glass remains on top all the time.

There were four combinations of cells and functionalized surfaces: (i) hGBM cells + anti-EGFR aptamer surface, (ii) Astrocytes + anti-EGFR aptamer surface, (iii) hGBM cells + mutant aptamer surface and (iv) Astrocytes + mutant aptamer surface. The last three combinations were controls for the experiments. Every cell in a frame was tracked and underwent image processing and data analysis. Nonuniformities and Hausdorff distances for the four combinations were calculated.

The hGBM cells on anti-EGFR aptamer surfaces showed much higher nonuniformity in their surface contours over the period of image acquisition. The same cells remained calm and inactive on a non EGFR-specific mutant aptamer coated surface (Figure 3.9). As shown before (Figure 3.5), the control cells (astrocyte) also did not show such activity or morphological changes on the EGFR-specific surface. Enhanced activity of the cancer cells on the surface resulted in higher cell nonuniformity. Over 25 frames, tumor cells showed non-uniformity ranging from 8-10 a.u. on average, whereas in the controls, this remained below 1 a.u..

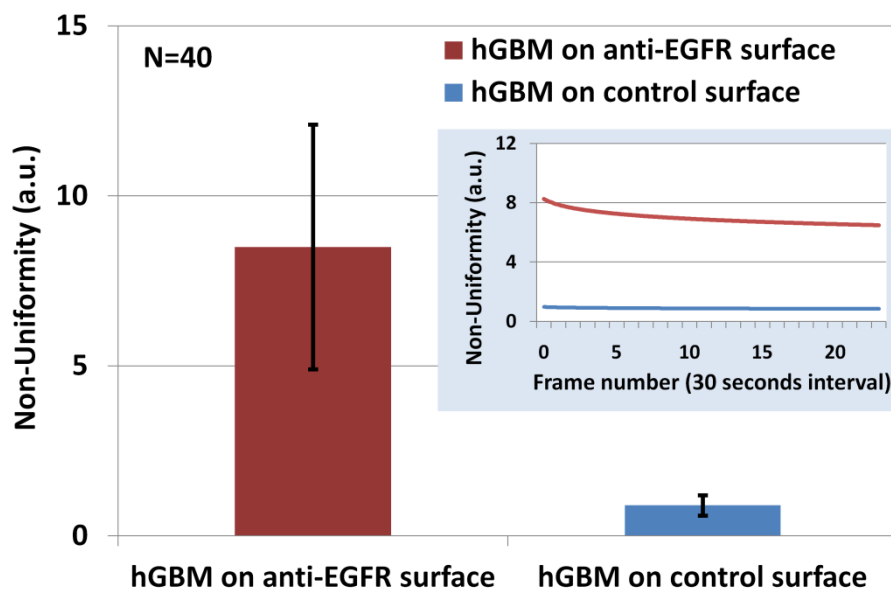


Figure 3.9 : Comparison of hGBM cell activity on anti-EGFR and mutant aptamer substrates. EGFR over-expressing hGBM cells showed enhanced activity through shape variation and pseudopod formation when incubated on the anti-EGFR aptamer surface. Large error-bars indicate significant variations in cell shape in the pool of cells the data were collected from; since the formation and annihilation of the pseudopods, or changes in shape were not synchronized. In contrast, when these cells were incubated on the mutant aptamer coated control surface, the activity was negligible. The inset shows the variation of non-uniformity over time.

To verify whether such activity was EGFR specific, in a separate experiment, astrocytes cells were incubated on both the anti-EGFR and the mutant aptamer coated control surfaces. As expected, these cells showed negligible activity on these surfaces (Figure 3.10). This results indicates that the surface was indeed passivated by the RNA layer and a complementary ligand on the surface can activate the cell towards shape changes. Such activity might also be triggered by a complementary antibody layer on the surface.

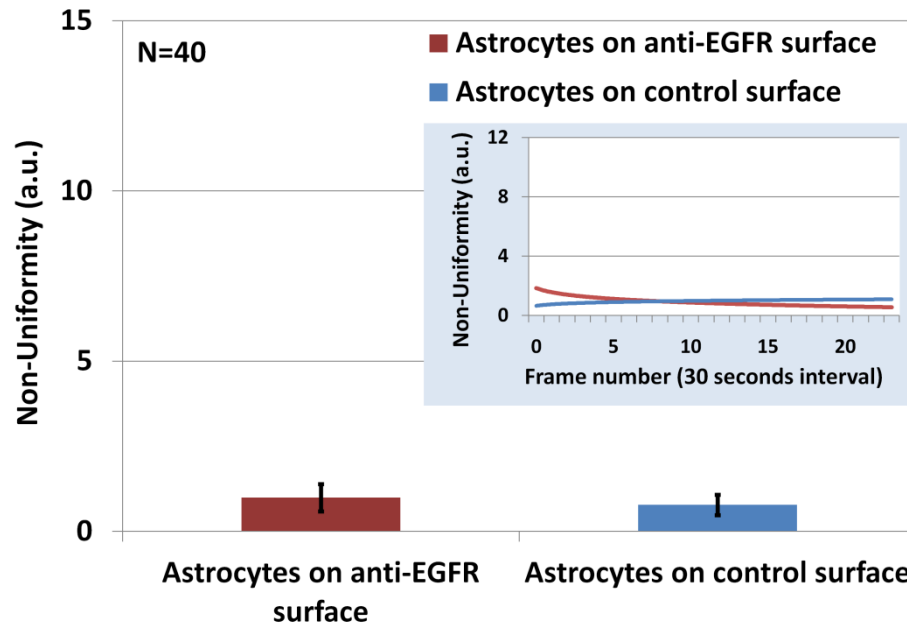


Figure 3.10 : Comparison of astrocyte cells' activity on both surfaces. Average nonuniformity for the astrocyte cells calculated over 15 minutes. the Cells remained calm and inactive on both the surface due to absence of any surface bound complementary moiety. The inset picture shows the variation of non-uniformity over time.

The Hausdorff distances between the contours of cells also showed distinguishing behavior as shown in Figure 3.11. The tumor cells on the anti-EGFR aptamer surfaces consistently showed higher Hausdorff distances compared to the controls. On average, the Hausdorff distances were calculated to be 4500 (a.u.) for tumor cells whereas for controls these stayed around 200 a.u..

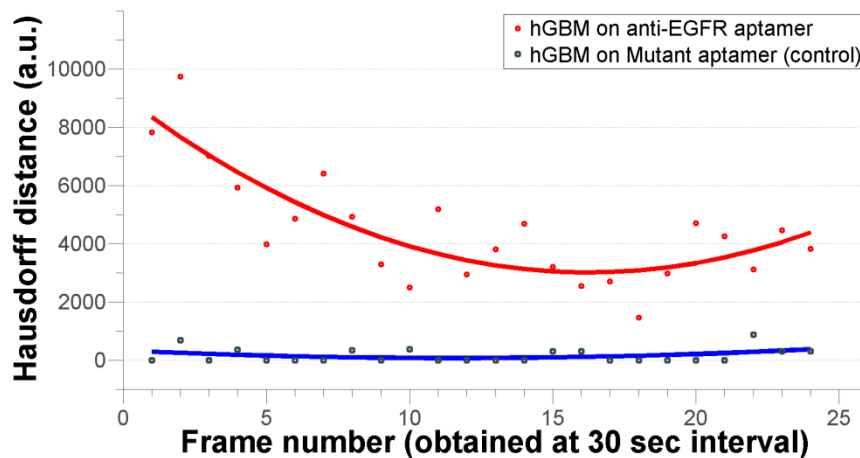


Figure 3.11 : Hausdorff distances between consecutive frames (averaged over 40 cells). Cancer cells show enhanced activity at the beginning and the activity reduces with time before finally settling to the surface.

The rate of change of pseudopods between frames are shown in Table 3-1. On average, the tumor cells on anti-EGFR aptamer surface showed pseudopods forming at different locations on the wall of the same cell as seen in consecutive frames. There was constant formation and contraction of pseudopods. Each contraction was considered as a change of -1 while formation of a new pseudopod was counted as +1. On the other hand, control combinations showed minimal changes in cell contour. Even if there were pseudopods at start, these stayed at the same orientation in all subsequent frames.

Table 3-1: Differential change of pseudopod formation in the four combinations of cells and surfaces. 10 sets of random cells are taken from a pool of samples and presented in the table). The hGBM cells on anti-EGFR surface show significantly large number of changes when totaled over 25 frames captured 30 second apart.

Cell and surface combination	Cell									
	1	2	3	4	5	6	7	8	9	10
Astrocytes on anti-EGFR aptamer	0	0	0	0	5	3	2	5	0	1
Astrocytes on mutant aptamer	0	0	3	0	0	4	0	0	1	0
hGBM on anti-EGFR aptamer	20	7	28	12	6	11	9	7	5	14
hGBM on mutant aptamer	0	0	1	0	0	0	0	0	1	0

3.4 Conclusion

It was shown that there are quantitative differences in the interactions of normal and tumor cells on functionalized surfaces. This can be used as a quick cytological indicator of cancer cells. By using appropriate image processing techniques in combination with suitable surface preparation, a detection method for tumor cells can be implemented. It has the potential to serve as an additional modality to support histological findings and to identify tumor cells based on their physical behavior from blood samples or biopsy specimens directly drawn from patients.

Chapter 4

Micro+Nanotexturing of Substrates to Enhance Ligand-assisted Cancer Cell Isolation

Comprehensive understanding of the impacts of surface texture and functionalization chemistry is important for chip based cell isolation. This work presents bio-inspired textured surface that can guide cellular activities such as proliferation, differentiation, and migration. The texture mimics the extracellular matrix and basement membrane for superior target cell adhesion. The larger surface area of nanotextured surface assists cell's attachment through surface-anchored ligands. The flatter morphology of captured cell was associated with higher binding force that prevented cells from being eluted under high shear stress. Taking it a step further, ligand functionalized hierarchical micro-nano textured surfaces were employed for improved sensitivity of cancer cell isolation over simple nanotexturing. The isolation efficiency was over 84%. The hierarchical surfaces were compatible with previously reported nanotextured devices used for cancer cell isolation.

4.1 Introduction

Making "cell-friendly" surfaces is an important first step in isolation and behavioral characterization of cells from similar origins but with different phenotypes [149]. Cell monitoring is crucial for accurate cancer diagnosis. Circulating tumor cells (CTCs) have shown potential to reveal the biology of metastasis and provide understanding of cancer prognosis. Comprehensive characterization of cell-surface interactions and the influence of surface parameters (surface area, texture, wettability, surface bound ligands and charges) on cell responses can lead to engineering surfaces with better sensitivity for cell isolation [150].

In tissue engineering, several works have shown that micron and submicron scale roughness on the surfaces lead to enhanced differentiation and cell proliferation [151]. The morphology of the cells adhered to the surface have been reported to be guided by the surface topography [152-154]. Micro and/or nanostructured surfaces have been developed for cancer

cell isolation purposes as well. In case of CTC isolation, because of their rarity in patients at early stages of cancer (as few as 1 CTC per ml in peripheral blood), devices demand highest level of sensitivity to maximize cell capture from the available samples. Nano textured surfaces have been reported previously to provide improved cell isolation efficiency [155]. In these devices, overexpressed receptors on cancerous cells were targeted to bind to the tethered complementary ligands on the substrates [156]. The effective step towards binding more ligands was to increase the surface area through creating texture on the surface [157]. Higher number of ligands on the surface improves the binding odds for cell surface receptors and ultimately the cells to bind to the ligands. Recently, nano textured surfaces have also been reported to isolate and enrich cancer cells without any ligands. The isolation was attributed to dynamic arrangement of integrin-mediated focal adhesions [158].

Numerous tools and processes are available to fabricate textured surfaces of various pore sizes, dimensions and lengths. Chemical etching [127], nano-embossing [159], chemical vapor deposition [160], electrospinning [161] etc. are used for textured surface preparation. These can fabricate different dimensions of nanostructure, ranging from few nm to hundreds of nm. Geometries and patterns are tunable; both repetitive and random structures can be achieved. The processes, however, are tedious. For example, surface coatings, plasma etching, metal deposition, lift-off and wet chemical etching are common to many [162].

A biomimetic hierarchical topology of glass surface was created with two step etching process. This enhanced the availability of the surface to the cells (Figure 4.1). The micro-patterns on the surface cused well with the cell contour whereas the nanotexture mimicked the basement membrane feel for better adhesion and isolation. Glass slides were sandblasted to create micro grooves on the surface followed by reactive ion etching (RIE) to create nano-pattern inside the grooves. Cell capture yields were 208% and 225%, respectively, in antibody and RNA aptamer functionalized surfaces. This result is comparable to that obtained from nanopillars, carbon nanotubes or nanowires surfaces. This simple method and competitive

capture efficiency enabled our hierarchical topology of glass substrate to be an economic but highly sensitive cell isolation platform.

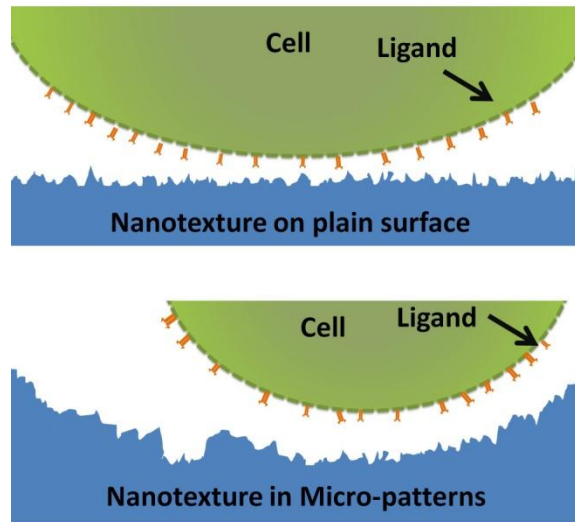


Figure 4.1: Schematic of micro-pattern for enhanced cell capture. The top image shows a plain surface with nanotexture. The number of ligand-receptor interaction is low compared to the bottom image. The textured pattern increases the odds for cell adhesion.

4.2 Materials and Methods

Chemicals used for the experiments were obtained from Sigma-Aldrich (St. Louis, MO) unless mentioned otherwise.

4.2.1 *Surface Preparation:*

Fisherbrand microscope slides (soda lime glass) were used as standard surface. To create microgrooves, glass slides were sand gritted using standard 3M™ aluminium oxide sandpaper (100-grit with average grit size of 141 μm). To remove any residue particles, the surfaces were then cleaned with 3 cycles of 10 minutes of ultrasonication, isopropanol and ultrapure deionized(DI) water. To further smoothen the surfaces, these were immersed in

diluted (50:1) hydrofluoric acid for 10 minutes followed by Piranha solution (H_2SO_4 : H_2O_2 , 3:1) cleaning for another 10 minutes. To create nanotexture, a plain glass surface was initially subjected to RIE using TECHNICS MICRO-RIE 800 (10 SCCM O_2 , 3 SCCM CF_4 , 250 Watt, 220 mTorr) for 30 minutes. The glass surfaces were cleaned using Piranha solution and DI water and inspected using Atomic Force Microscope (AFM) and Scanning Electron Microscope (SEM). The microscopy characterized both topography and surface chemistry. After confirming the formation of nanoscale topography on plain surfaces, specimens with microgrooves were subjected to the same treatment to create the hierarchical structure. The sand gritting process was skipped in the control samples. The control slides were subjected to RIE as mentioned earlier after piranha cleaning.

4.2.2 *Surface Characterization*

4.2.2.1 Profilometer:

To evaluate the micron scale changes in surface topography, the substrates were characterized using "KLA Tencor Alpha Step IQ" profilometer with scanning stylus of 5 μm radius and 60° angle. Six samples were measured for each surface conditions and average measurements were recorded for each specimen.

4.2.2.2 SEM Imaging & Energy Dispersive Spectroscopy (EDS):

Surface topography was examined in SEM/EDS Leo Supra 55 VP. Before imaging, the glass surfaces were coated with 3 nm of gold to avoid surface charging. Images were taken at 12 kV accelerating voltage and 30 μm of aperture. For imaging cells, a 6 nm gold coating was done on the fixed cells and the imaging was done at 5 kV.

To identify and quantify the surface elements of RIE-processed samples, the Energy Dispersive X-ray Spectroscopy (EDAX, Genesis) was done at low vacuum setting at an applied voltage of 30 kV.

4.2.2.3 Contact Angle Measurement:

Contact angle measurements were done using a Rame-Hart contact angle goniometer with ultra-pure water as the sessile drop fluid. On each sample a ~10 μ l water drop was placed at three places and the contact angle of water-substrate interface was noted down by visually observing through a microscope.

4.2.2.4 Atomic Force Microscopy (AFM):

Surface topography was qualitatively evaluated using AFM (Park XE 70 AFM) in non-contact mode with NANOSENSORS™ PPP-NCHR probes. Maximum tip diameter was less than 10 nm with nominal force constant 42 N/m and resonance frequency of 330 KHz. Several samples were scanned and were plain-leveled before measuring the roughness.

4.2.3 Selection of Target Molecule:

Human glioblastoma (hGBM) is a malignant brain tumor [163]. EGFR overexpressed hGBM cells were used in experiments as the tumor cell model. EGFR overexpression have been previously reported on tumor cell surfaces with density ranging from 40,000 to 100,000 per cell [32]. Anti-EGFR RNA aptamer has been previously reported to bind with both mouse derived wild-type EGFR and mutant EGFRvIII with superior specificity[164]. Fluorescent tagging of glioma cells was previously shown to verify the overexpression of the EGFR on the cell surfaces [165].

Isolation and culture of human glioblastoma (hGBM) cells were done as described in Section 3.2.5.

Aptamers were prepared as previously described in section 3.2.2.

4.2.4 Preparation of Anti-EGFR Antibody Functionalized Substrates

The antibody and aptamer, to capture EGFR were functionalized on substrates as per protocol adapted from literature [145, 146]. In brief: glass surfaces were sized into ~5x5 mm²

pieces. To create hydroxyl group (-OH) on the surfaces, these were cleaned with Piranha solution for 10 minutes, followed by O₂ plasma exposure. The slides were then rinsed with DI water followed by nitrogen drying. To create free amine groups on the surfaces, the substrates were immersed for 30 minutes in methanol/DI water (19:1) and 3% APTMS solution. These substrates were then washed again with DI water and methanol and later incubated for 30 minutes at 120 °C. A dimethylformamide (DMF) solution was prepared using 10% pyridine and 1 mmol/l *p*-Phenylene diisothiocyanate (PDITC) and the substrates were immersed into the solution for 5 hours at 45 °C. Later, these were rinsed with DMF and 1,2-dichloroethane and dried with gentle blow of nitrogen. Monoclonal anti-EGFR antibody produced in mouse (2 µg/ml) was diluted in PBS and applied on the surface. Surface was immersed in the antibody solution at 37 °C for 1 hour. To deactivate the unreacted PDITC moieties the substrates were immersed for 5 hours in 150 mmol/l DIPEA in DMF and 50 mmol/l 6-amino-1-hexanol. This step was done instead of any BSA blocking procedure to prevent non-specific protein adsorption. Again, each substrate was sequentially washed with ethanol, DMF, and DEPC-treated DI water. These were then rinsed and stored in PBS, dried in a stream of nitrogen and were used immediately.

Anti-EGFR RNA aptamer functionalized substrates were prepared in the same method as described in section 3.2.3.

4.2.5 *Acridine Orange (AO) Fluorescence Measurement:*

AO solution was prepared in sterilized DI water (2 mg/ml) and the substrates were completely immersed into it and kept on the shaker for 30 minutes. The substrates were later washed thoroughly with DI water before fluorescence measurements.

4.3 Results

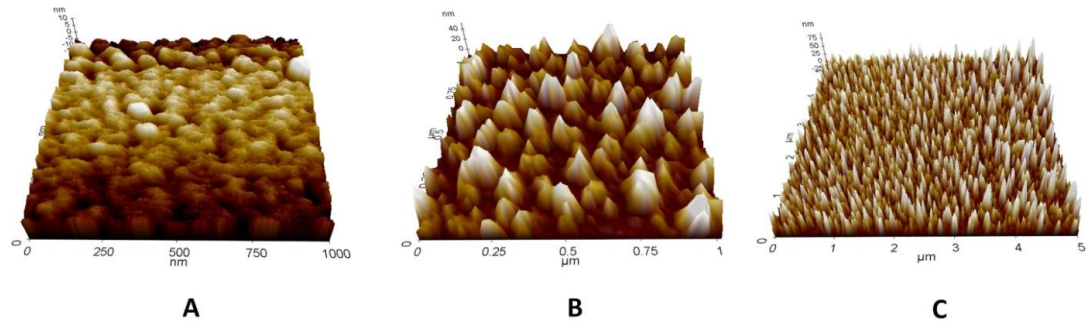


Figure 4.2 : AFM image of the nanomodified plane surface. (A) Shows plane surface Plane glass surface before RIE. The mean roughness remained below 1 nm. (B) Shows the roughened surface created using RIE. (C) A zoomed out micrograph showing uniformity of the modified surface.

After initial cleaning with piranha solution the substrates were subjected to the RIE process. The process was tuned through variation of gas composition and flow rate to create roughness of high density. The surface was found homogenously covered with nanoscale structures as can be seen in Figure 4.2. The sand gritted surface, after piranha cleaning and diluted (50:1) Hydrofluoric Acid treatment to remove any remaining residue, were subjected to the same RIE process to create the hiererchical structure that has nano patterns in micro grooves. SEM image revealed the nanostructure inside the microgrooves (Figure 4.3).

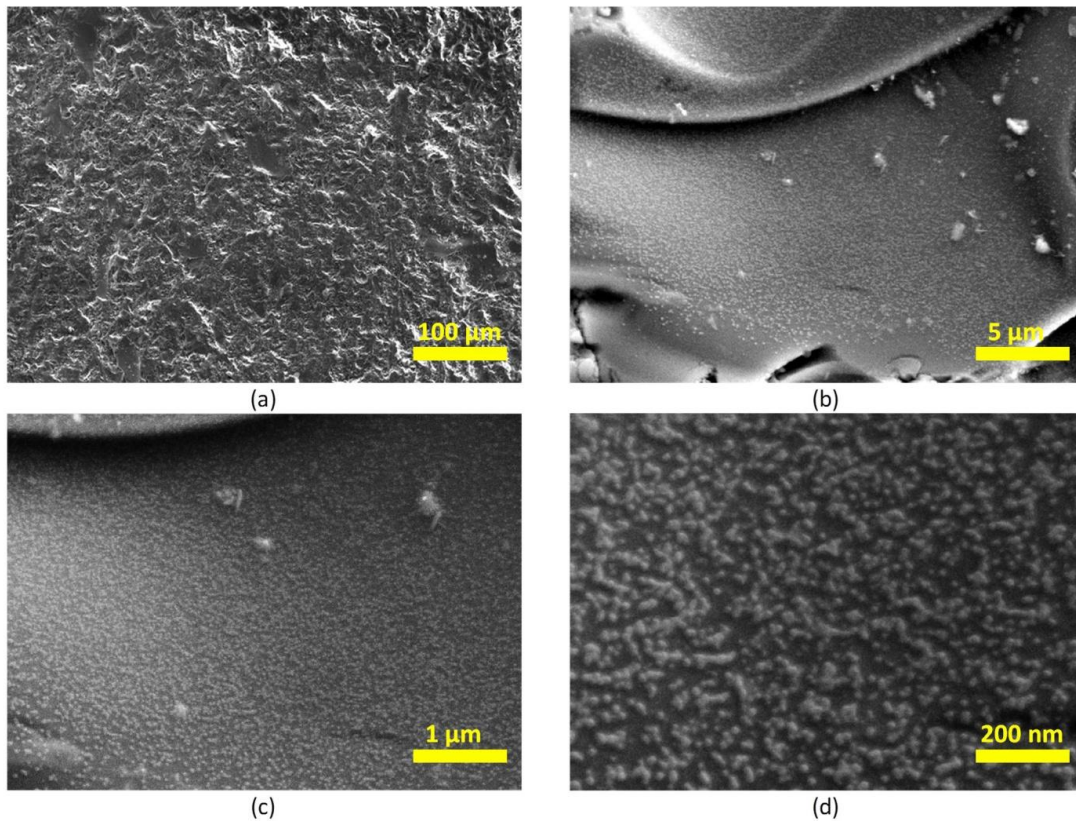
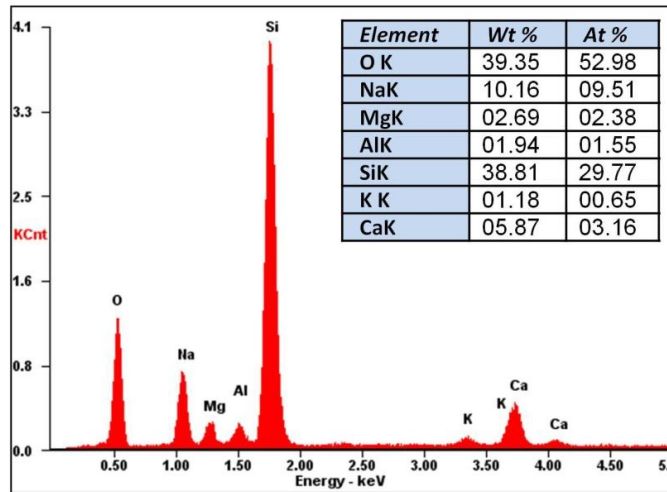
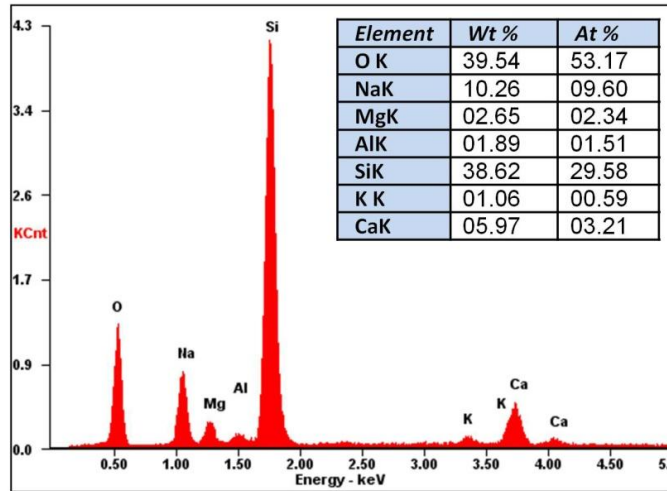


Figure 4.3 : The hierarchical surface at 4 different magnification scales. The first image shows the micron scale roughness created using sandblasting. The (B), (C) and (D) shows the zoomed in images displaying the nano-texture created inside the micro grooves.

To ensure no compositional change have taken place on the surface, energy - dispersive X-ray spectroscopy (EDS) was performed. EDS elemental analysis of a plane glass and final hierarchical surface showed no change in the surface bound material ensuring no new material introduction to the surface that can potentially alter the cell surface interaction (Figure 4.4).



A



B

Figure 4.4 : EDS analysis. (A) and (B) shows the EDS obtained graph of the material composition from the surface. (A) represents the surface without any modification. (B) is obtained at least 24 hours after the RIE process and piranha cleaning. The graph shows no significant change in the surface material that can affect the immobilization of the RNA on the surface.

Surface roughness measured by profilometer and AFM is shown in Table 4-1. The profilometer reading reveals the micron scale roughness whereas AFM reading was used to measure the nanoscale roughness.

Table 4-1: Profilometer reading. Mean surface roughness with standard deviation (appended by \pm) measured for both micron scale and nanoscale features

	Profilometer reading (in μm) Scan Area (2000 μm x 2000 μm)	AFM reading (in nm) Scan Area (5 μm x 5 μm)
Average Roughness	0.575 ± 0.3	21.6 ± 1.9
Average RMS	0.7 ± 0.8	26.27 ± 2.0
Maximum Depth	3.5 ± 1.2	27.53 ± 3.9

Hydrophilic property of material changes with the surface texture and hydrophobic surface become more hydrophobic with introduction of surface texture and vice versa [166]. Water contact angle measured on the prepared surface with goniometer showed the change in hydrophilic property due to the texturing. Surfaces with nanotexture (13.9°) and the hierarchical texture (11.2°) was found to exhibit increasing hydrophilic property than the plane surface (25.1°).

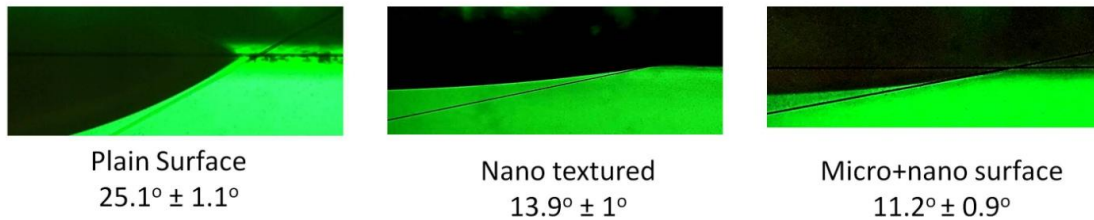


Figure 4.5 : Contact Angle Measurement. the \pm sign indicates the range around the mean.

Six samples from each group was used for the experiment. PDITC creates a diisothiocyanate layer on the glass surface, one end of which attaches to the surface tethered APTES and the other end can bind to any amine-bearing capture molecules like single strand oligonucleotide probes or proteins. The amine group of antibody binds directly to the PDITC terminal. Unreacted PDITC end groups are capped to prevent any nonspecific adsorption. To

immobilize aptamer on the surface, a probe DNA was amine modified at one end to bind to the surface tethered PDITC. This DNA molecule hybridizes to the extended region of the protein capturing aptamer. The probe DNA along with the hybridized aptamer was previously reported to render advantages like lessening steric and electrostatic hindrances, increased reactivity for the aptamer through increasing the radiation of gyration etc [144].

Immobilization of ssDNA and RNA aptamers on the glass surface was verified by fluorescence measurements of Acridine Orange (AO) stain at an excitation wavelength of 460 nm and an emission wavelength of 650 nm. The chip surfaces were prepared as mentioned before and stained at different immobilization steps. In short, AO solution of concentration 2 mg/ml was prepared in sterilized DI water and the samples were completely immersed into it and kept on the shaker for 30 minutes. It was later washed thoroughly with DEPC water before fluorescence measurement. The fluorescence intensity was analyzed with ImageJ software (Figure 4.6).

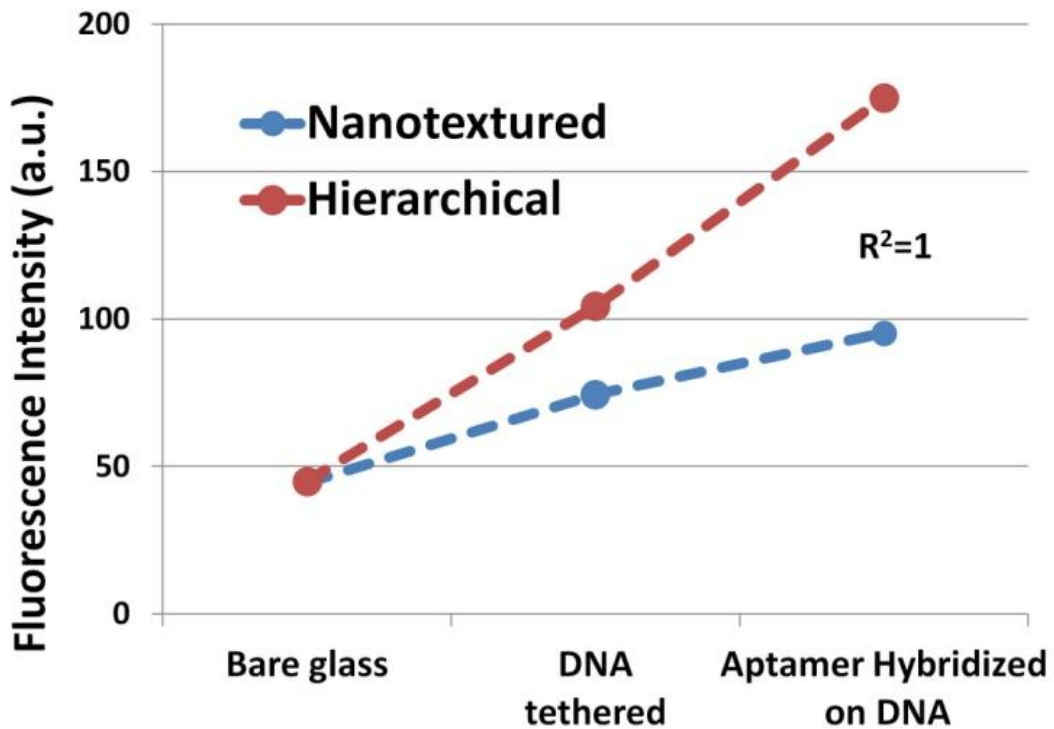


Figure 4.6: Fluorescence Measurements. Acridine orange fluorescence is measured (n=10) at different steps of surface functionalization to compare the presence of the surface bound oligonucleotides. Higher fluorescence intensity with RNA hybridized surface ensures the higher number of RNA present on the surface.

In all experiments, the cells were centrifuged first to remove supernatants and then diluted with sterilized and warm 1× PBS solution (with 5 mmol/L MgCl₂). Each substrate was completely covered with the cell suspension (typically 70 µl). Cell concentration of 150,000/ml was used. The average cell density on the substrates before washing was roughly 800 per mm². The substrates were then incubated for 30 minutes at 37°C and washed gently with PBS solution on a shaker (Boekel Scientific) at 90 rpm for roughly 5 minutes in orbital and reciprocal movements.

EGFR overexpressing hGBM cells were previously reported to bind preferentially to the surface bound complementary ligands such as aptamers or antibody. As fluorescence analysis indicates, the textured surface contains amino groups (from APTES and PDITC modification), which helps in binding more antibody or RNA aptamer on the surface. Thus, the increased density of immobilized ligands facilitates cell capture. Increased surface area of the textured surface enables higher protein adsorption as well as focal contact adhesion sites. This makes the surfaces better suited for overall cell isolation. It was found that the number of hGBM cells bound to the hierarchical surface was significantly higher than the plain surface bound cells. Nanotexturing of the plane surface increased the capturing efficiency as reported before [167]. However, the cells showed significantly higher preference to the hierarchical glass surface modified with the ligands.

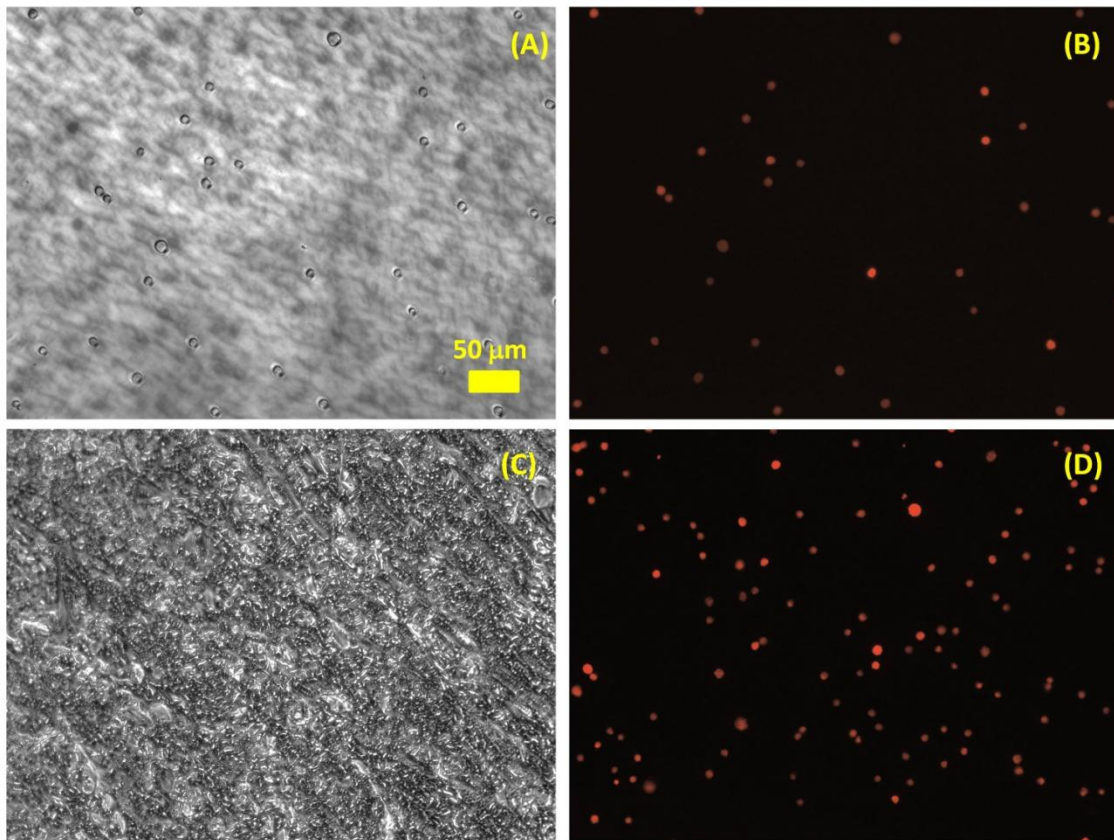


Figure 4.7: Fluorescence micrographs of cells captured on the surfaces. (A) and (B) show the bright field and fluorescence micrographs of the cells captured on the simple nanotextured surfaces. (C) and (D) show the bright field and the fluorescence micrographs of the cells captured on the hierarchical surfaces, respectively.

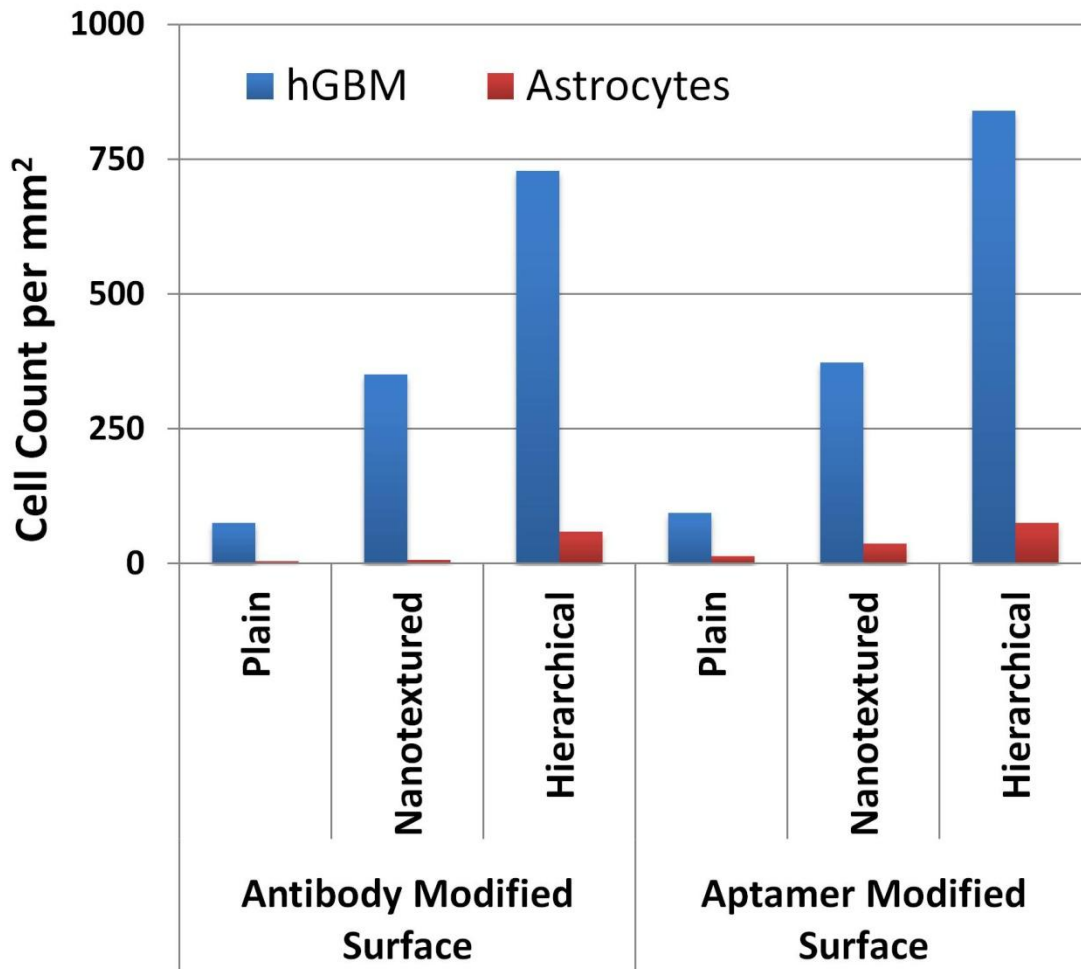


Figure 4.8: Cells captured on three surfaces functionalized with anti-EGFR antibody and anti-EGFR aptamer. Cells captured on the hierarchical micro+nanotextured surface are more than double than those captured on nanotextured surfaces, in both the cases.

For antibody modified surface, 208% of increased cell isolation was observed compared to nanotextured surface (Figure 4.8). On average, there were 75 hGBM cells captured on plane surface (SD, 16.45; max of 96 and min 64 cells per mm², respectively). The average number of cells captured on the nano textured surface was 350 per mm² (SD, 37.43; max and min of 392 and 304 cells per mm², respectively) and number of cells on the hierarchical surface was 728 per mm² (SD, 36.715; max and min of 792 and 660 cells per mm², respectively).

For RNA aptamer modified surface, 339% of increased cell isolation was obtained relative to nanotextured surface (Figure 4.8). On average, there were 62 hGBM cells captured on plane surface (SD, 13; max of 96 and min 64 cells per mm², respectively). The average number of cells captured on the nano textured surface was 165 per mm² (SD, 36.23; max and min of 194 and 123 cells per mm², respectively) and number of cells on the hierarchical surface was 560 per mm² (SD, 90; max and min of 653 and 502 cells per mm², respectively).

It is possible that cells can be trapped mechanically in the larger groove, resulting in higher physical absorption and lowered isolation specificity. To verify such non-specific binding, similar experiment with control astrocytes cells were performed on the same set of surfaces. Although number of astrocytes cells captured increased in the hierarchical structured surface, as can be seen in Figure 4.8, the number of hGBM cell isolation was so high that total specificity of the device increased too.

Aptamers provide a homogeneous layer on the surface when compared to the antibody. Although the binding force of antibody is slightly stronger than the aptamer (K_d=1 nM in antibody vs 2.4 nM in aptamer), the homogeneity of aptamer on hierarchical surface ensures a denser aptamer film on the surface. This creates an overall stronger bond to the cell surface receptors. The capture efficiency of each group is summarized in Table 4-2. It can be noted that aptamer functionalized hierarchical surfaces can capture 84% of cancer cells, compared to 72.8% obtained from antibody grafted surface. This further proves homogeneous functionalization and hierarchical structure make up very well for the smaller binding affinity of aptamers.

Table 4-2: Comparison of cell capture efficiency on different surfaces.

Cell Type	Anti-EGFR molecule	Plain	Nanotextured	Hierarchical
hGBM	Antibody	7.5%	35%	72.8%

	RNA Aptamer	9.4%	37.2%	84%
Astrocytes	Antibody	0.4%	0.64%	5.9%
	RNA Aptamer	1.3%	3.6%	7.5%

It is possible that cells can be trapped mechanically in the larger groove; resulting in higher physical adsorption and lowered isolation specificity. The number of captured astrocyte cells increased for the hierarchical structured surface, from 0.64% to 5.9%; in contrast, the capture yield of hGBM cell increased from 9.4% to 84%. Such significant increase of capture efficiency cannot be simply totally attributed to physical adsorption. Increase in cancer cell isolation efficiency on nanotextured PDMS was previously reported with the trade-off of decreased specificity [167]. In the hierarchical surface the superior efficiency could be attributed to the increased binding area and better hydrophilic environment. These factors would be present while the homogeneous aptamer layer on the substrate created a negatively charged surface area. These negative charges should have repelled negatively charged cancer cells as the cancer cells are known to have higher sialylation on the surface compared to the normal cells.

The higher number of surface-grafted RNA aptamer on hierarchical surface although generate stronger repulsion between cell and substrate surface but specific binding energy landscape overcome this. Cell morphology also dictated the isolation efficiency of the surface. Morphology of captured cells has been reported to be flatter on nanotextured substrates with increased number of pseudopods. This indicated that more receptors on the cell membrane may have come in contact with the capturing aptamers. Flatter orientation also caused decreased cell height that further assisted cells from being eluted. SEM micrographs of cell attached on different surfaces revealed that cell were bound strongly on the hierarchical surfaces with increased number of pseudopods and much flatter surface area (Figure 4.9). This

can be attributed to the increased surface area as well as increased number of ligands on the surfaces for cells to interact with. On plain surface, the cells remained spherical.

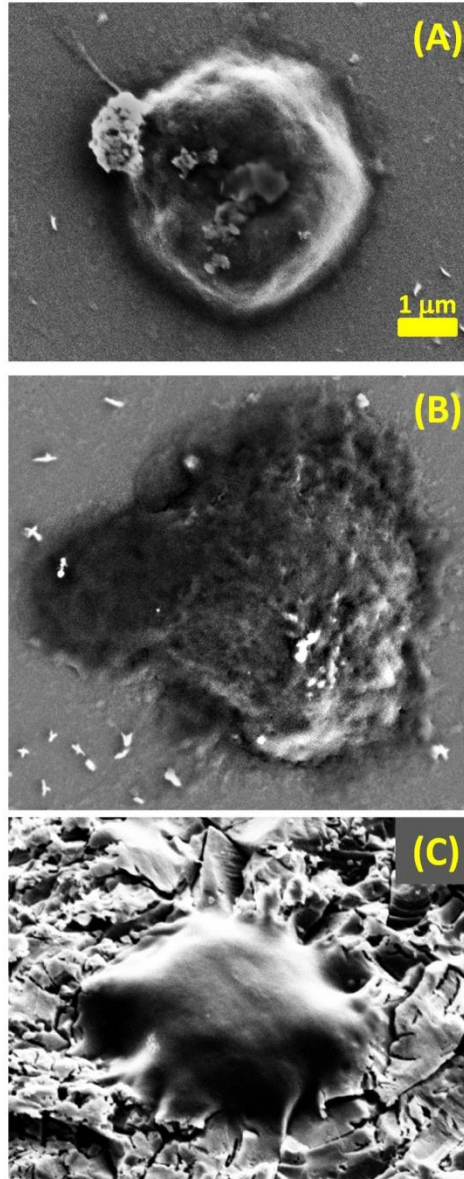


Figure 4.9: SEM micrograph of cells bound on three different substrates (A) Plain glass surface, (B) Nanotextured Surface, (C) Hierarchical micro-nanotextured surface. The data reveals how cell attachment is increasingly stronger. On plain surface, cells are mostly globular whereas the cells show increased spreading from nanotextured to hierarchical surfaces. In hierarchical surface, cells show many pseudopods indicating better cell-surface interactions.

Previously, 80-95% of capture yield was reported to be achieved with nanopillar, nanowires and other nanostructured surfaces. Our hierarchical surface can achieve 84% of isolation efficiency that is very competitive to these reported literatures. However, our preparation method is two-step, simple, and very straight-forward. Typical sample size prepared through other complex processes is small, and normally these devices can only process 0.5 ml blood sample analysis. The approach shown here can easily prepare hierarchical surfaces on common glass slide (75x50 mm²), that can meet the need to process large volume of samples.

4.4 Conclusion

Targeted cell isolation techniques with superior efficiencies hold utmost importance for early cancer detection. This paper has shown a device platform for maximum cancer cell isolation. The optimization of surface with micro and nanotexturing reliably isolates 84% of tumor cells from a sample. With simplified fabrication technique and reusability, this provides an excellent path toward developing economic point of care (POC) devices. Although capturing of non-specific cells increased slightly with the surface texturing, however, due to high number of cancer cell isolation, sensitivity of the device significantly increased. The microtexture showed better fit with the cell contour whereas nanotexture stimulated better cell adhesion.

Chapter 5

Molecular Dynamics Simulation of 3-D Structural Integrity of DNA in a Functionalized Nanopore

5.1 Introduction

Biomarker-specific nucleotide sequences, called aptamers, have gained attention in cancer cell isolation and detection techniques due to its superiority in terms of structural stability, target-specificity and easy reproducibility. Self-assembly and 3-D conformation of these DNA/RNA structures, that can complement the target biomarkers' binding sites, have given them the edge towards capturing proteins and cells. On the other hand, synthetic nanopores have gathered momentum towards single molecular detection due to their robustness and simplicity. Researchers have reported several nanopore-based protein and DNA detection methods such as residue tracking, conformation mapping, and translocation speeds etc. Among these methods, detecting and identifying protein/DNA based on the translocation through nanopore has received more attention because of their simplicity, efficacy and ability to detect rare biomarkers. In this method, the inside wall of the nanopores are typically coated/functionalized with protein specific ligands. If electric field is applied across the nanopore inner wall, then an ionic current flows through the nanopore. When the target protein passes through the pore, it interacts with DNA-ligand coated in the nanopore and the process alters overall potential energy profile which is essentially specific to the protein to be detected. The fundamental challenge in this process is to ensure whether these detection motifs can hold their functionality under applied electric field. For aptamers to hold their functionality, it is important that they don't denature or don't lose their structure. As described later, DNA can be elongated due the high electric field inside the pore and thus may lose its functionality. An all atom Molecular Dynamics (MD) simulation was done here to examine the effect of external electric field on the 3-D conformation of such ligand-DNA structures. It was found that G-Quartet DNA structure could hold its 3-D conformation below a critical voltage determined by the sequence.

The simulations also demonstrated how the grafted molecules and the pore size affected the translocation time.

Many diseases can be diagnosed using one or multiple biomarkers. These biomarkers may consist of alien entities inside host body, or disease-induced proteins overexpressed or downregulated by the host body itself as part of its defense mechanism. These proteins become available in the circulatory bloodstream at early stages of the disease progression and work as disease precursors. Detection and identification of such proteins is an effective method for diagnosis and monitoring of the prognosis henceforth.

Over the past several years, significant progress has been made on nanopore-based DNA detection technologies [146]. These approaches are transferrable towards detection of protein biomarkers [168]. DNA and protein are two intertwined moieties by virtue of their functions in cellular mechanism. Proteins are synthesized by DNA transcription; on the other hand, certain proteins play significant roles in regulation of such transcriptions. This regulation is accomplished by selectivity between the DNA segments and the regulatory protein. This selectivity is a useful property that can be used in vitro for detection of certain proteins. Nanopore is a highly suitable but simple platform for utilizing this extraordinary property. Present protein detection modes like gel electrophoresis require strict lab environments. A nanopore based method promises easy and quick detection without need of expert supervision. Synthetic nanopores have gathered recent momentum towards single molecule detection due to their robustness and measurement simplicity. Detection and identification of protein can also be done from the translocation behavior. In this method, protein or DNA is allowed to pass through a nanopore of comparable size in an ionic solution and under applied electric bias (Figure 5.1). The ionic current is measured and parameters like translocation time, velocity, and current dip are measured as electronic signatures. This detection scheme is comparatively simpler and possesses smaller footprint. Specific proteins when passing through the nanopore create statistically significant ionic current dips. DNA coating of the nanopore inside wall creates

selective functionality and adds new dimension to this technique. The same can be approached by coating with complementary antibodies as well. However, in case of antibodies, higher control is required since they need stricter conditions to produce and also are more vulnerable (i.e. easily degradable) in in vitro conditions. DNA/RNA based devices hence give broader usability. Much focus has recently been given to detection of proteins using nanopores. Unraveling the mystery of how protein transport takes place in cellular environment opened up new windows towards such methodologies. Enzyme assisted protein translocation through nanopore has indicated promise of protein sequencing through nanopore. However, many biophysical phenomena are yet to be discovered for complete understanding of working at such small dimensions.

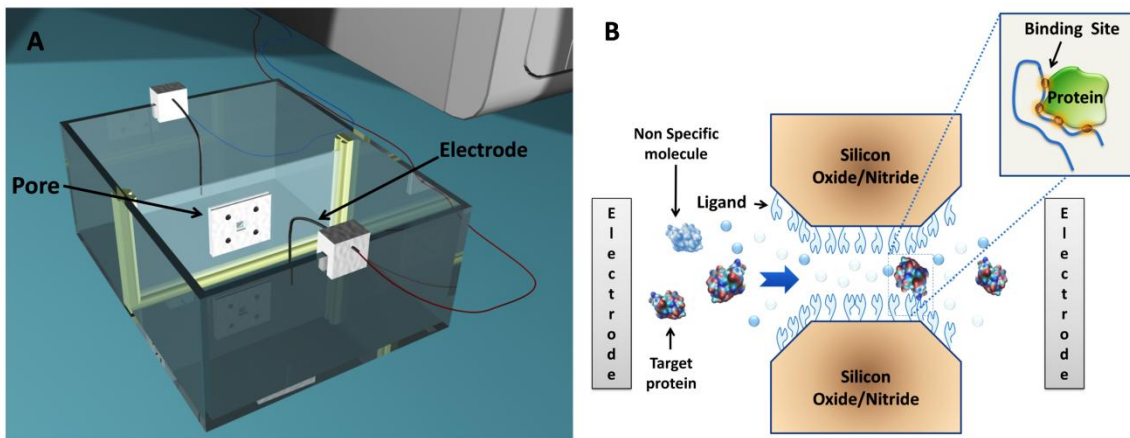


Figure 5.1 : Typical nanopore experimental setup. (A) Analytes are allowed to pass from one side of the container to the other through the nanopore in the middle. Electrodes on both sides measure the ionic current indicating the translocation event. (B) Schematic of protein translocation through solid-state nanopore coated with ligand. The inset shows how protein target binds strongly to the DNA ligand once the binding sites from both molecules come in proximity to each other. The binding energy depends on the complementary manner of the position of the binding points.

Nanopore based measurement comes with certain challenges, especially in experimental conditions. In their native state, DNA or nucleic acid sequences can fold into various secondary and tertiary 3-D structures (hairpin loop, G-quartet, etc.), creating binding

sites for certain biomolecules [169, 170]. For example, G-quartet is a naturally occurring DNA structure involved in regulating genetic expressions in cellular machinery. These act as translational repressors of specific target mRNAs [171]. On the other hand, these 3-D DNA structures have also been employed, in vitro, to screen and isolate target biomolecules from a random population. In their native physiological states, biomarkers such as proteins fold into 3-D structures determined mostly by their amino acid sequences. This property gives them the specific biological functionality. Both of these 3-D entities, when in proximity, can create strong binding, even though complementarity is not clearly evident. Target specific DNA sequences or aptamers have been reported to successfully isolate cancerous biomarkers and even tumor cells from the samples with high selectivity [144]. These aptamers show superiority in terms of structural stability, target-specificity and easy reproducibility.

Suitable chip-substrates or microfluidics devices have been functionalized with specific aptamer sequences with samples passed over/through. Target molecules come in the vicinity of the aptamers, land on them and get loosely attached due to non-specific electrostatic attraction. However, as determined by the disassociation constant, these get detached from the binding site within a short period and through a process called "facilitated diffusion" these finally reach the target segment of the nucleotide sequence where multiple binding sites from both molecules can complement each other hence creating a much stronger bond (Figure 5.1(B)) [172]. If the bond is strong enough against thermal and mechanical perturbations, the target molecule gets immobilized. For example, epidermal growth factor receptor (EGFR) overexpression has been reported to be associated with several cancers [173, 174]. Anti-EGFR aptamer has been developed that binds strongly to the either dimeric or monomeric EGFR. The aptamer binds competitively to the EGFR and thus inhibits the downstream signaling for cell growth, proliferation and tumor growth. However, any such binding is dependent on the external force competitively applied over the protein-DNA complex. A simple mechanical force can dislodge the protein bound to the DNA. Shear stress applied by fluid flow has been shown to release

cells that were bound through this protein-DNA interactions [175]. The perturbation of the DNA structure has also been reported by joule heating with micro-heaters fabricated beneath the surface [176]. An electric field applied to the free DNA has been shown to elongate DNA bound to a surface [177]. Dependence of these structures on so many variables calls for an investigation in MD environment with various forces applied.

Again, DNA travelling through coated nanopore has been shown to slow down due to ligand specific affinity [146]. A protein passing through a nanopore coated with that protein-specific DNA would face the same effects. Protein would slow down or even chemically bind to the surface of the nanopore depending on the force applied by the electric field and any other mechanical forces inside the nanopore. The protein may bind to the target DNA and stay immobilized for a while before getting finally dislodged. Another modality for such protein detection is to pre-treat the sample with protein-specific DNA. The free-floating protein-DNA complex should result into distinctive translocation features. Characterization of the surface properties is important for all these scenarios.

Single molecule level protein-DNA interactions were characterized inside nanopore using classical MD simulations. The stability of the DNA structure under different applied electric fields was quantified and the effect of the DNA structure on the translocation of protein through nanopores was measured.

5.2 Methods

5.2.1 *Molecular Dynamics Simulation Details*

The stability of DNA structure under applied electric field, the mechanism of protein translocation through DNA functionalized nanopore and travel of protein-DNA complex through a bare nanopore were studied using all-atom MD simulations. The freely available massively parallel MD simulation package known as Nanoscale Molecular Dynamics (NAMD) was used to perform the simulations. Visual Molecular Dynamics (VMD) was used to analyze and visualize

the outputs. All simulations were performed on the Lonestar supercomputer cluster at Texas Advanced Computing Center (TACC). Two cases were studied; first, investigation was carried out for the stability of the DNA structure in a typical experimental condition i.e. in ionic solution and under applied bias; and second, the translocation events of the protein through the nanopore were simulated for three different cases to investigate the respective translocation times.

5.2.2 *Molecular Models*

To examine the stability of the 3-D DNA structure, a protein databank (PDB) file of an x-ray resolved nucleotide sequence was obtained from the Research Collaboratory for Structural Bioinformatics (RCSB) PDB. It is known that the quadruplex topology of DNA depends on both the number and nature of the nucleotides participating in the construction of the motif. we chose a 11-mer single-stranded DNA (ssDNA) (PDB id 2AVJ) for our study [178]. The x-ray resolved crystal structure of the DNA showed that it formed G-quartet. The residue sequence of this DNA was: 5'-G-G-G-G-T-T-T-G-G-G-G-3'. It should be noted that this DNA has a TTT linker which is responsible for forming the folds. It also provides the DNA its signature preferred loop conformation. This sequence is known to bind to thrombin protein.

For nanopore translocation model, the human alpha-thrombin was modeled after the structure defined in 1HAP PDB, reported first in 1996 [179]. In the crystallographically resolved structure, this is a complex of thrombin protein and a 15-mer DNA. The nucleotide sequence was shown to have two stacked G-quartets, linked by two T-T loops and T-G-T loop at the opposite ends. This specific structure was chosen for the known binding affinity of the DNA sequence to the specific thrombin protein. Thrombin in humans play important role in the coagulation cascade thus preventing blood loss.

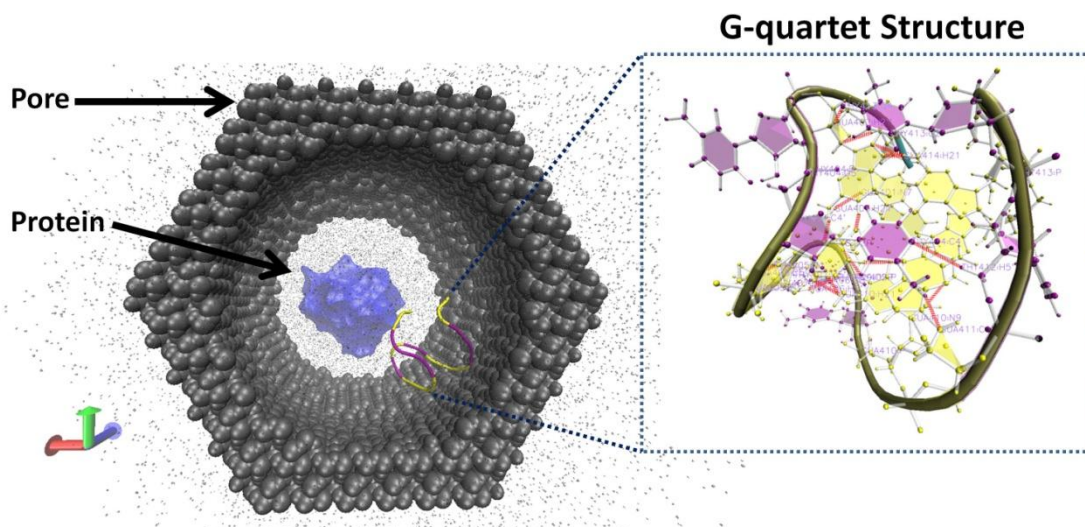


Figure 5.2: The model of the protein translocation through silicon nitride nanopore. A single DNA strand with G-quartet structure is shown immobilized on the nanopore inside wall. The orange lines in the inset show the interaction between bases while forming the G-quartet structure.

The snapshot of the initial model is shown in Figure 5.2. The DNA structure was first solvated by KCl enriched water molecules. The water molecules were represented by TIP3P model and K^+ and Cl^- ions were added at 1 M concentration. Salt concentration was chosen roughly close to standard experimental solutions [180]. This system had an atom count of 1240 (with 872 water molecules). The system was taken to be large enough to be free from any force from a self image in periodic model. For nanopore segment, the simulation super cell consisted of rigid nanopore and solvated DNA protein complex. Modeling of the nanopore was done by freely available crystal scripting software [142]. It was constructed using silicon nitride (Si_3N_4) with a constricted nanopore diameter at the center. The smallest diameter of the nanopore was 6 nm. Total atom count was 103,204 after addition of water and ions. In experiments, 3' or the 5' end of the DNA is usually modified with certain chemical groups and immobilized to the surface through other linkers. In our model, the 3' end guanine base was fixed on the nanopore

wall. The surface tethered probe was positioned inside the nanopore so that it came in contact with the thrombin protein when it passed through.

5.2.3 Force Field

The inter atomic and intermolecular interactions between different species were modeled using CMAP corrected CHARMM force field [181-183]. Repulsive and attractive dispersion for short-range interactions were described by Lennard-Jones potential with a cut-off distance of 1.1 nm and a switching distance between 1 and 1.2 nm. The total potential energy in the system consisted of bonded energies and non-bonded pair interaction energies, described by:

$$\begin{aligned}
 U &= E_{bond} + E_{angle} + E_{dihedral} + E_{improper} + E_{elec} + E_{vdw} + E_{others} \\
 &= \sum k_b (b - b_0)^2 + \sum k_\theta (\theta - \theta_0)^2 + \sum k_\phi (1 + \cos(n(\phi - \delta))) \\
 &+ \sum k_\omega (\omega - \omega_0)^2 + \sum \frac{q_i q_j}{4\pi\epsilon_0 r_{ij}} + \sum_{i < j} \epsilon \left(\left(\frac{r_m}{r} \right)^{12} - 2 \left(\frac{r_m}{r} \right)^6 \right) + \sum U_{CMAP}(\phi, \psi)
 \end{aligned} \tag{1}$$

Here, the E_{bond} accounts for the bond stretches where k_b is the bond force constant and b_0 is the equilibrium bond length. The E_{angle} term stands for the bond angles where k_θ is the angle force constant and θ_0 is the equilibrium bond angle. The third term refers to the dihedral energy where k_ϕ is the dihedral force constant, n is the multiplicity factor, ϕ is the dihedral angle and δ is the phase shift. The $E_{improper}$ term stands for the improper energy where k_ω is the improper force constant and ω is the out of plane angle. The next two terms represent electrostatic and van der Waals energies, respectively. Here, the van der Waals (VDW) energy is calculated with a standard 12-6 Lennard-Jones potential and the electrostatic energy with a

Coulombic potential. U_{CMAP} represents dihedral energy correction term with backbone and torsional correction (CMAP, ϕ , ψ)

5.2.4 Simulation Details

For both the cases, the simulations were performed under constant-temperature, constant-volume (known as NVT) ensemble and conducted in two major steps. First, the systems were energy-optimized using conjugate gradient method [184]. After that, the temperature was raised and kept at 295 K using Langevin thermostat [143]. Long-range electrostatic interactions were calculated using particle-mesh Ewald (PME) method at time step of 1 fs [143]. Nonbonded forces were evaluated at every 2 time steps. The systems were later equilibrated without applying any external field.

5.2.5 Applied Forces and Electric Field

For evaluating the DNA stability, a uniform electric field comparable to experimental value was applied in the z-direction. The field was applied only during the simulation (16 ns). In experiments, a typical membrane with a nanopore is ~100 nm thick where the applied voltage across it is in the 0.5 V range. Considering most of the potential drop is across the nanopore, a typical electric field across the nanopore is in the range of 0.05 V/nm. However the profile inside the nanopore varies depending on the inner roughness. Usually nanopore is more constricted in the center due to the etching steps of the fabrication process. So, the field is higher in the central pore region. To verify that the DNA structure is not perturbed in the experimental voltage range, simulations were performed with gradually increasing applied electric field (Figure 5.3).

For the second case of protein translocation, the process of moving it through the nanopore using solely electric field (e-field) was slow. This was due to the fact that at physiological pH of 7.4, only a handful of protein residues are charged [185, 186]. Initially, after prepositioning the protein on the channel opening, increasingly higher voltage was applied to

facilitate faster translocation. However, it still took long for the protein to translocate through. In physical experiments, protein translocation normally occurs at the millisecond scale. A small force in z-direction was applied on the protein to guide it through the nanopore. This force would be akin to the forces stemming from the flow of cations, osmotic flow, salt concentration gradient etc in the experiment [185]. A word of caution here is necessary; A large force could potentially alter the 3-D conformation of protein. This could, in turn, affect the binding affinity with the DNA. The root-mean-square deviation (RMSD) of the protein was checked for different applied accelerations and an acceleration of 0.5 \AA/ps^2 was simulated. This was mild enough to not disturb the native 3-D structure. To further accelerate the process, a slightly higher applied voltage (0.2 V/nm) was used, which is comparable to values reported in experiments [146]. This approximated the electric potential applied on both ends of the nanopores in the experiments that establishes an ionic current through the nanopores. However, as can be seen from Figure 5.3(D), the RMSD deviation from the initial structure stayed within 0.5 for this field, i.e. this electric field did not affect the DNA structure.

5.3 Results

5.3.1 *Isolated DNA in Electric Field*

Figure 5.3 shows the changes in the DNA structure with applied voltage. The RMSD of each molecule of the DNA structure from the initial equilibrated position was calculated at the end of each simulation. It was observed that at lower electric fields, the RMSD of the nucleic acid sequence from the initial structure was minimal; indicating that the 3-D structure was stable at lower applied fields. As the field increased to 0.8 V/nm, it can be seen from Figure 5.3(D) that the RMSD had an upward slope for as long as 20 ns, indicating structural instability. Any higher field quickly elongates the negatively charged DNA. Figure 5.3(C) shows the elongation of the DNA strand in z-direction at higher applied voltage. As shown later, this elongation of DNA structure causes affinity to the protein to reduce.

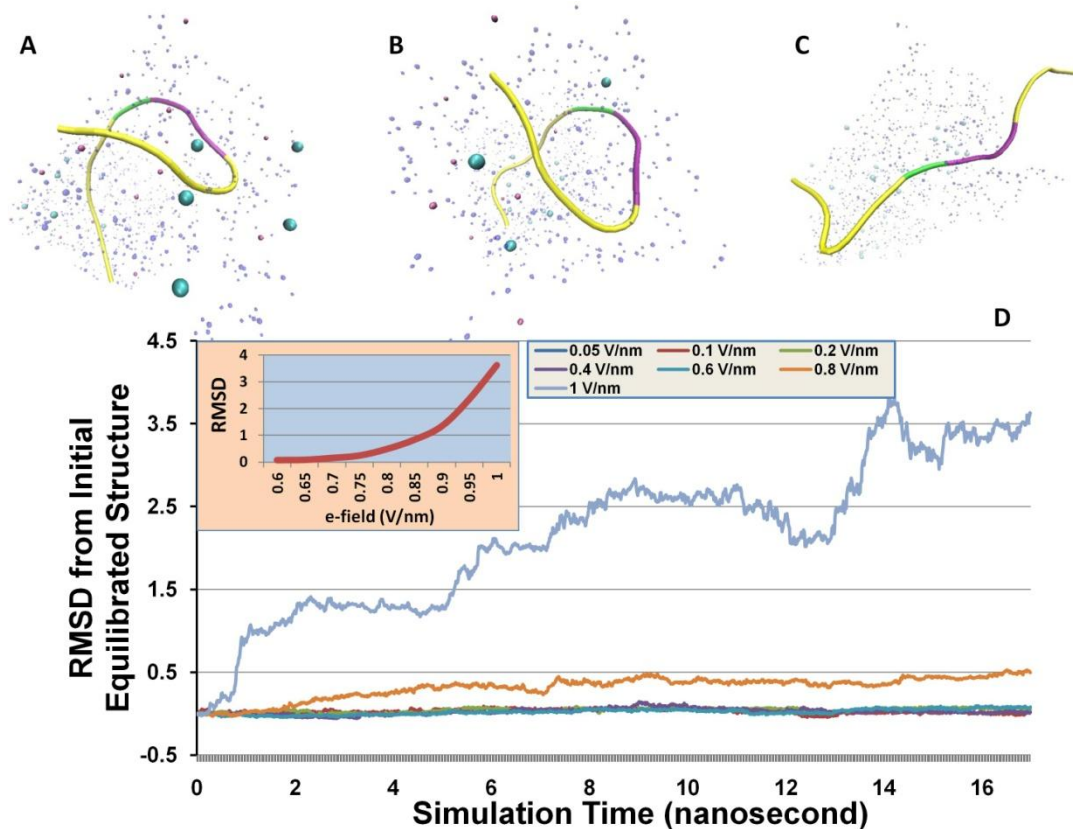


Figure 5.3: Stability of the 3-D DNA structure under applied bias. (A) and (B) show the initial structure and the structure after the simulation was run with an applied field of 0.1 V/nm, respectively. The structure is stable indicating that the functionality or affinity due to the 3-D conformation remains active. (C) Shows the same structure under applied field of 1 V/nm. The DNA elongates and loses its 3-D conformation. (D) RMSD calculated from the initial equilibrated structure. The 3-D conformation can hold up to a moderate field of 0.6 V/nm whereas higher voltage disintegrates the structure. The inset shows the dramatic change in RMSD within the short range of voltage change from 0.6 to 1 (V/nm).

5.3.2 Nanopore Protein Translocation

The x-ray resolved thrombin protein has maximum length of ~5 nm. The nanopore size was maintained at comparable but slightly larger diameter (7 nm). The length of the nanopore was also kept at 7 nm. Before running the actual protein translocation simulation, an electric field was applied for 2 ns. The RMSD of both protein and DNA indicated no disruption in their structures due to this applied field. In all cases, the translocation time was calculated from the

electrostatic and VDW energies between the molecules and the nanopore (Figure 5.4(A)). Three different scenarios were studied; (i) A single protein translocation through a bare nanopore (ii) Protein translocation through nanopore coated with ssDNA, and (iii) A complex of protein and ssDNA, translocating through the nanopore. For the first case, the DNA sequence was removed from the complex before the protein was allowed to translocate. The protein was pulled towards the nanopore using a small force on the molecule using Grid Molecular Dynamics. For the second case, DNA sequence was tethered inside the nanopore wall and the protein was separated from the complex. The protein was then pulled towards the nanopore and was allowed to come in contact with the DNA. The surface tethered probe DNA intercepted the protein through electrostatic and VDW interactions. For the third case, the DNA was not tethered to the surface and the protein-DNA complex was allowed to translocate instead.

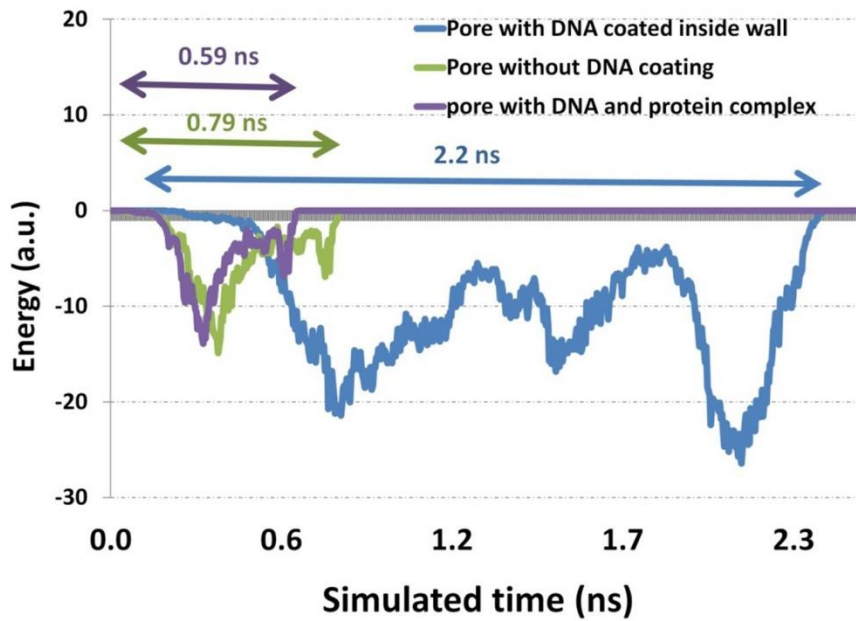
The study of translocation of DNA-protein complex has two important implications: First, the selective binding of the target protein in a solution with the aptamer can essentially result in changes in the physical dimensions and the pI of the molecule. The size and charge of the complex can change the translocation time much more profoundly. Secondly, the nanopore doesn't need to be functionalized. The complexity of the process can be reduced significantly and same framework can be used for detection of multiple target proteins.

In the absence of any surface friction, nanochannels would allow free translocation environment for protein molecules. However, molecular interactions with the confining walls of the nanopore can affect simple electrophoresis events. A bare nanopore allows faster translocation than the nanopore grafted with ssDNA. In other words, the translocation time for protein is significantly higher when nanopore is coated with tethered ssDNA (Figure 5.4). Protein with specific affinity to sequence of DNA strand can slow down more through a nanopore and hence give a distinct signature in the ionic current.

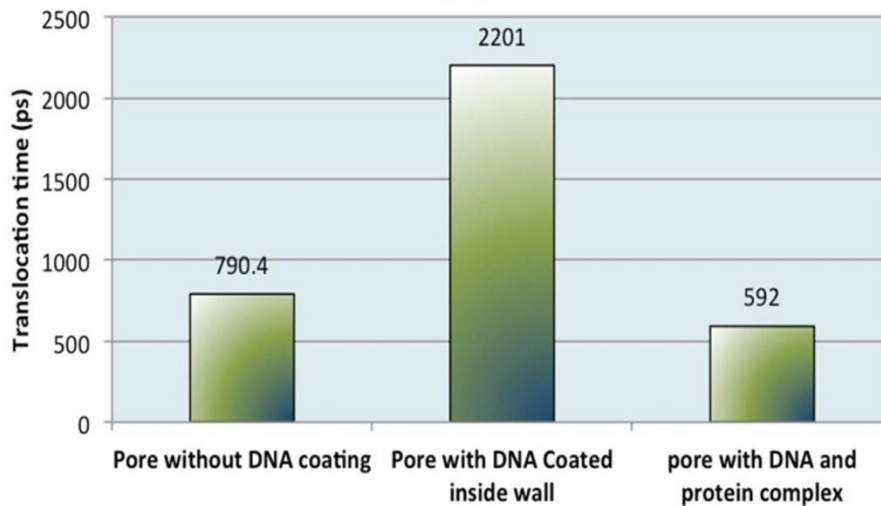
In case of protein-DNA complex, when a bias is applied to the electrolyte solution, the complex starts moving towards oppositely charged electrode. Force on a single protein is lower

than force on protein-DNA complex because the latter has additional charges of DNA. It should be noted that DNA binding may also change protein folding. The changes in protein folding can in turn change the surface charge distribution as well as the isoelectric point (pI) of the protein [187]. This force causes the protein-DNA complex to move faster within the electrolyte towards the nanopore (Figure 5.5). Also, the following competitive factors take place; (a) Protein-DNA complex has higher volume and surface area compared to the protein alone, hence causing higher interaction with the nanopore wall and thus slowing it down; (b) Due to the additional charges, the complex moves faster within the electrolyte before entering the nanopore (Figure 5.5(B)). The moment when protein and the complex just enter the nanopore, the latter has more mass, more inertia, and due to that, the complex should translocate faster through the nanopore in comparison to the case when protein alone is translocating. If the surface friction is not high enough, then the complex will translocate faster through the nanopore in comparison to the protein alone. As can be seen from Figure 5.4, in our scenario the dominating factor is the second one and that's why the complex translocates faster through the nanopore as compared to the protein alone.

Velocity of protein translocation was also calculated from the derivative of the translocation profile. Due to interaction with the tethered ssDNA, the protein slowed down significantly while translocating causing longer translocation times. Velocity dropped to as low as one-fourth inside the nanopore with DNA coating (Figure 5.5(A)). The interactions of the protein with the walls of a bare nanopore also slowed the protein down, but not as much. In larger nanopore, with more space to move around inside the nanopore such effect would be less noticeable, thus underlining the necessity of similar sized nanopores to impart selectivity. The velocity and nanopore-size relationship can help design nanopores for optimized signal.



(A)



(B)

Figure 5.4: (A) Plot of interaction energy (VDW and electrostatic) between nanopore and the protein molecule while translocating through. Translocation times for all three scenarios are shown for comparison. (B) A comparison of the translocation times of three cases. The translocation times for the three cases were calculated from the interaction energies between protein and the nanopore wall. Due to the binding of the protein to the DNA, the translocation time is significantly higher compared to the translocation time through a bare nanopore. A protein-DNA complex shows the fastest translocation.

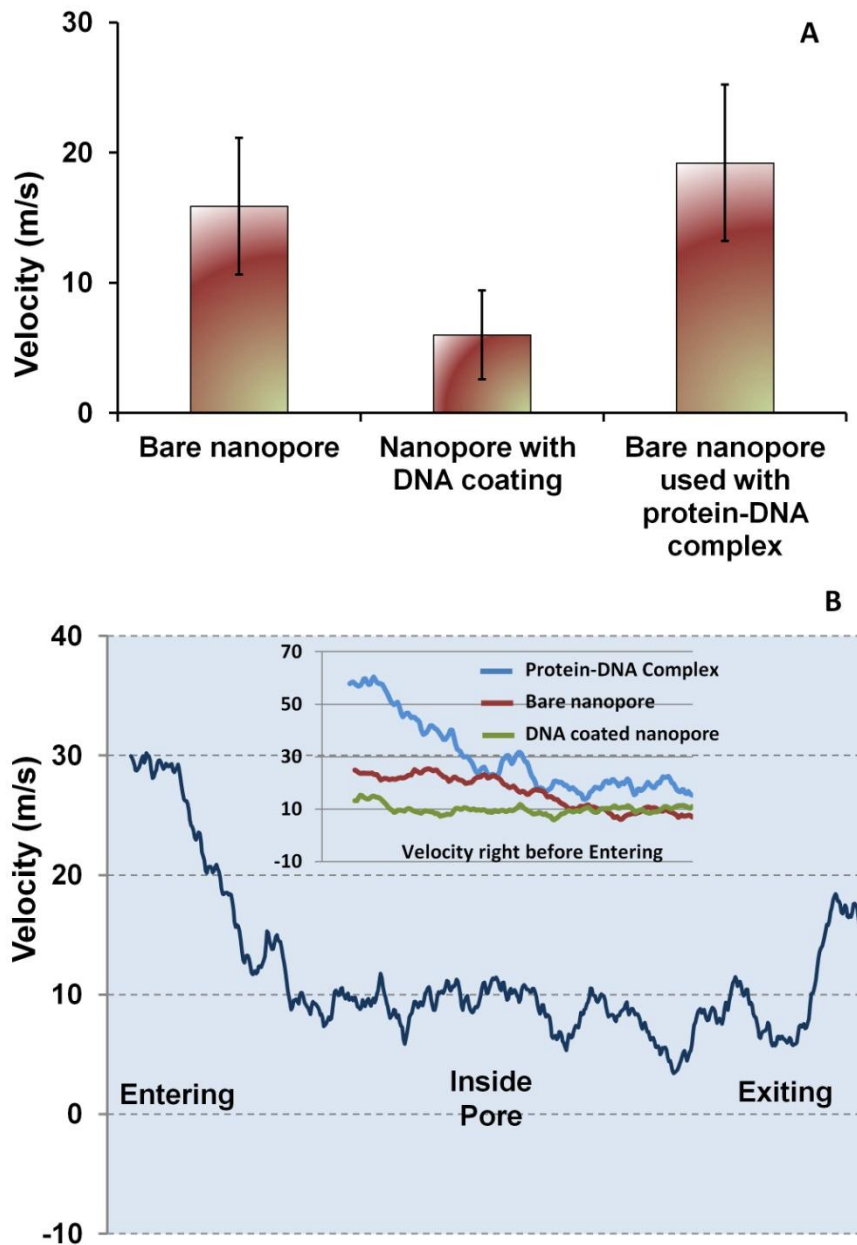


Figure 5.5: (A) Velocity comparison of three different scenarios of protein translocation inside the nanopore. (B) Shows the velocity of the protein when it passes through a bare nanopore. The magnified inset is presented to compare the entering velocity between three cases.

Velocity of protein translocation was also calculated from the derivative of the translocation profile. Due to binding with the tethered DNA, the protein slowed down

significantly causing longer translocation time. Velocity dropped to as low as one-fourth inside the nanopore with DNA coating (Figure 5.5(A)). On the other hand, the interactions of the protein with the walls of a bare nanopore do slow the protein down, but not significantly. In larger nanopore, with more space to move around inside the nanopore such effect would be less noticeable, thus underlining the necessity of similar sized nanopores to have selective detection modality. This velocity and nanopore-size relationship can help design nanopores for optimized signal.

Nanopore size also plays an important role for such detection modalities. To have better selectivity and sensitivity, it is important to have pore dimensions close to the target molecule size. Pores with larger dimensions have more area inside for proteins to move around. As a result, it is possible for the travelling molecules to pass through the nanopore without actually interacting with the surface-bound ligands. In such case, both the target and non-specific proteins will show similar translocation behavior. The thrombin protein is 5 nm on its largest axis. Translocation event of thrombin protein on both 6 nm and 8 nm nanopores were simulated. As can be seen from Table 5-1, increasing the nanopore size just by 25% increased the protein travel speed by more than 7 times. It is also important to note that the larger nanopore lost selectivity between specific and non-specific molecules. The translocation of thrombin through 8 nm functionalized and bare nanopore was not significantly different. One might argue that the selectivity stems from the nano-confinement itself where the two molecule have to come in intimate contact. But the selective binding of the two molecules is already established. The nano confinement may very well be enhancing the selective binding.

Table 5-1: Comparison of protein translocation time in nanopores of 6 nm and 8 nm.

Thrombin Travel	6 nm	8 nm
Nanopore without DNA coating	790 ps	274 ps
Nanopore with DNA coating	2201 ps	365 ps

5.3.3 Deviation in 3-D DNA Structure during Protein Translocation.

As the protein translocates through a nanopore, it comes in the vicinity of the DNA. The electrostatic and Van der Waals forces between the two molecules slow down the protein. However as protein passes through, the DNA strand stretches along the path losing its initial preferred loop structure (Figure 5.6). This indicates that after protein is released, the DNA will take some time to relapse back to its preferred structure. This latency places a theoretical boundary on the upper limit of the molecule detection frequency.

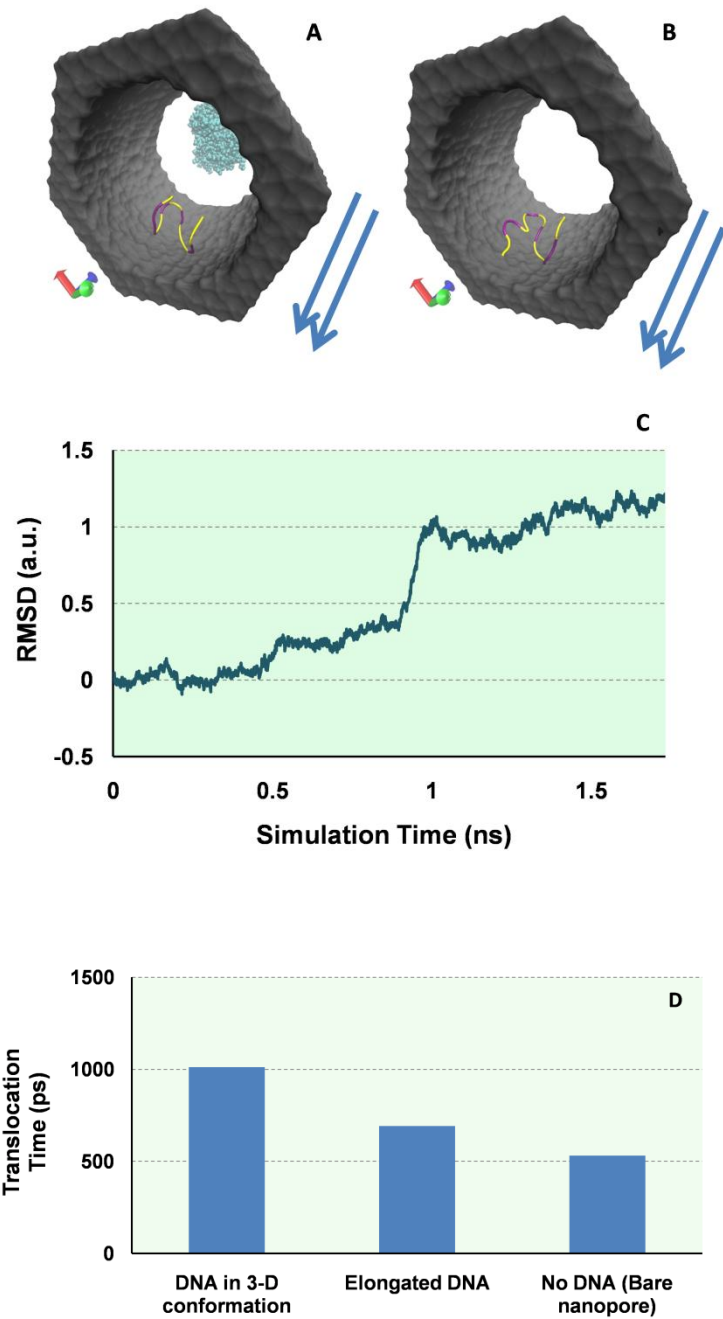


Figure 5.6 : Comparison of protein translocation time.(A) and (B) show the DNA inside the nanopore before and after translocation (arrows show the travel of protein). (C) Shows the RMSD deviation of the DNA while translocating. (D) Shows a comparison of the protein translocation times through a nanopore coated with DNA holding its 3-D conformation, a nanopore with the same DNA that lost its structure and a bare nanopore.

5.4 Conclusions

The close biological connections between DNA and protein dictate the energy interaction contributions of one molecule towards detection of the other. Nanopore is an emerging platform for such molecular sensing. Biophysical phenomena that take place between these biomolecules and also the inorganic substances are yet to be explored exhaustively, both in experimental setup as well as in simulations. Here, the feasibility of using DNA coated nanopore devices for protein detection was investigated using molecular dynamics simulations. Our results suggest that coating the nanopore wall with DNA molecules is indeed a feasible approach for such detection. One of the caveats in DNA coated nanopores is that whether these molecules can withstand the extreme electric fields inside the nanoscale dimensions of nanopore. In Brief, it was shown that, DNA strand can hold 3-D conformation with electric field applied in the experimental ranges and beyond. Although the specific affinity was not inspected, it was observed that proteins indeed slow down when passing through comparable sized nanopores coated with DNA-binding molecules. The difference in translocation time for protein was is significant between nanopore with DNA coating and bare nanopore with protein travelling through. The 3-D structure of the DNA was shown to be crucial to slow down the protein, which in turn gave the signature ionic currents due to translocation. Nanopore offers some significant advantages compared to the present methods of protein detection in terms of stability and reproducibility. The rational design of nanopore based point of care (POC) devices for bedside disease detection can promise early management of diseases to save many lives. Our results surely bolster the idea of such detection modalities.

Chapter 6

Future Work

6.1 Introduction

In this chapter, scopes and direction of future works are discussed which can complement/supplement the current research.

6.2 Integration and Automation of the System.

This research focused on two biomolecules, EGFR and thrombin. Several biomarkers have been established for many cancer types and other diseases. For example, PSA is overexpressed in prostate cancer and need to be targeted for detecting the cancer. For a generic device for cancer prediction/detection, multiple chip system has be developed, where each chip can be equipped with capture molecule targeting individual proteins. Finding capture molecules for various proteins is a daunting task. However, it is important for the effective use of the device. Building a multichip cartridge can also help in identification of the cancer affected organ.

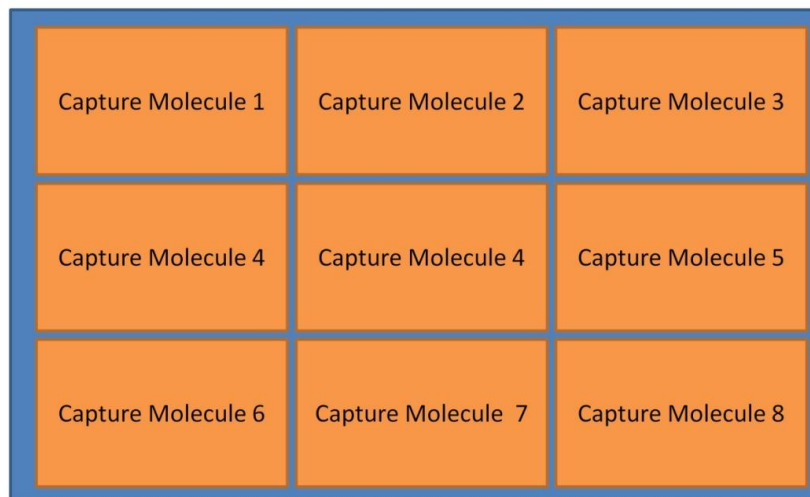


Figure 6.1: Schematics showing multi chip based cartridge towards a generic device that targets multiple types of cancer

Development of a better image acquisition system is important for this detection scheme. Speed and accuracy of the system critically depends on the initial raw images. Once developed, the total process can be integrated in a table top set up for quick diagnosis.

6.3 Optimization of Cell Response

The effect of surface texturing on the cell response and fine tuning of such texturing should be carried out to get the best possible response. Detailed work is necessary to determine the surface features which would be optimum for the cell movement. Again, whether this behavior is dependent on the cell types, needs to be investigated.

Cell response to the microenvironment, local temperature, electric and magnetic field and any enhancement in cell activity due to these needs to be investigated. This step will help to create more pronounced differences in the feature vectors between two types of the cells.

6.4 Simulation of the System with EGFR-specific RNA aptamer

The next work should be to simulate the same system with more relevant but larger protein and DNA. For example the EGFR and the complementary anti-EGFR aptamer pair can be investigated. Larger protein and DNA requires much more computational resource because of the significantly higher atom count. Protein-DNA interaction should be investigated more closely in terms of their complementary binding. This requires significantly longer simulation time and hence computing resources. Protein and DNA interact with each other with specific complementary binding sites. Inspection of such binding will also require strategic positioning of the protein relative to the RNA aptamer.

References

- [1] <http://www.cancer.org/>
- [2] Hanahan D, Weinberg RA. The hallmarks of cancer. *Cell*. 2000;100(1):57-70.
- [3] Hanahan D, Weinberg RA. Hallmarks of cancer: the next generation. *Cell*. 2011;144(5):646-74.
- [4] Mocellin S, Keilholz U, Rossi CR, Nitti D. Circulating tumor cells: the 'leukemic phase' of solid cancers. *Trends in Molecular Medicine*. 2006;12(3):130-9.
- [5] Ghossein RA, Bhattacharya S, Rosai J. Molecular detection of micrometastases and circulating tumor cells in solid tumors. *Clinical Cancer Research*. 1999;5(8):1950-60.
- [6] Sherry L. Murphy BSJX, M.D.; and Kenneth D. Kochanek, M.A. Deaths: Final Data for 2010 2013.
- [7] <http://www.ncbi.nlm.nih.gov/gene/>
- [8] Chaffer CL, Weinberg RA. A perspective on cancer cell metastasis. *Science*. 2011;331(6024):1559-64.
- [9] Kerr JFR, Winterford CM, Harmon BV. Apoptosis. Its significance in cancer and cancer therapy. *Cancer*. 1994;73(8):2013-26.
- [10] Weiss RA, Griffiths D, Takeuchi Y, Patience C, Venables PJW. Retroviruses: ancient and modern. *100 Years of Virology*: Springer 1999:171-7.
- [11] Gallis B, Linial M, Eisenman R. An avian oncovirus mutant deficient in genomic RNA: characterization of the packaged RNA as cellular messenger RNA. *Virology*. 1979;94(1):146-61.
- [12] Duncan IB. Evidence for an oncovirus in swimbladder fibrosarcoma of Atlantic salmon *Salmo salar* L. *Journal of Fish Diseases*. 1978;1(1):127-31.
- [13] Eisenman R, Shaikh R, Mason WS. Identification of an avian oncovirus polyprotein in uninfected chick cells. *Cell*. 1978;14(1):89-104.
- [14] Dudley J. *Retroviruses and Insights Into Cancer*: Springer 2011.
- [15] Miller JA. Carcinogenesis by chemicals: an overview-GHA Clowes Memorial Lecture. *Cancer Research*. 1970;30(3):559-76.
- [16] Knudson AG. Two genetic hits (more or less) to cancer. *Nature Reviews Cancer*. 2001;1(2):157-62.
- [17] Brenner DJ, Elliston CD, Hall EJ, Berdon WE. Estimated risks of radiation-induced fatal cancer from pediatric CT. *American Journal of Roentgenology*. 2001;176(2):289-96.
- [18] Wirtz D, Konstantopoulos K, Searson PC. The physics of cancer: the role of physical interactions and mechanical forces in metastasis. *Nature Reviews Cancer*. 2011;11(7):512-22.
- [19] Klein CA. The metastasis cascade. *Science*. 2008;321(5897):1785-7.
- [20] Saiki I. Cell adhesion molecules and cancer metastasis. *Japanese Journal of Pharmacology*. 1997;75(3):215-42.
- [21] Futreal PA, Coin L, Marshall M, Down T, Hubbard T, Wooster R, et al. A census of human cancer genes. *Nature Reviews Cancer*. 2004;4(3):177-83.
- [22] Fidler IJ. The pathogenesis of cancer metastasis: the 'seed and soil' hypothesis revisited. *Nature Reviews Cancer*. 2003;3(6):453-8.
- [23] Timpl R. Structure and biological activity of basement membrane proteins. *European Journal of Biochemistry*. 1989;180(3):487-502.
- [24] Kleinman HK, Martin GR. Matrigel: basement membrane matrix with biological activity. *Seminars in Cancer Biology*; 2005: Elsevier; 2005. p. 378-86.

- [25] Abrams GA, Goodman SL, Nealey PF, Franco M, Murphy CJ. Nanoscale topography of the basement membrane underlying the corneal epithelium of the rhesus macaque. *Cell and Tissue Research*. 2000;299(1):39-46.
- [26] Kalluri R. Basement membranes: structure, assembly and role in tumour angiogenesis. *Nature Reviews Cancer*. 2003;3(6):422-33.
- [27] Nagrath S, Sequist LV, Maheswaran S, Bell DW, Irimia D, Ulkus L, et al. Isolation of rare circulating tumour cells in cancer patients by microchip technology. *Nature*. 2007;450(7173):1235-9.
- [28] Saffran DC, Reiter RE, Jakobovits A, Witte ON. Target antigens for prostate cancer immunotherapy. *Cancer and Metastasis Reviews*. 1999;18(4):437-49.
- [29] Polanski M, Anderson NL. A list of candidate cancer biomarkers for targeted proteomics. *Biomarker Insights*. 2006;1:1.
- [30] Polanski M, Anderson NL. A list of candidate cancer biomarkers for targeted proteomics. *Biomark Insights*. 2007;1:1-48.
- [31] Stoscheck CM, King LE. Role of epidermal growth factor in carcinogenesis. *Cancer Research*. 1986;46(3):1030-7.
- [32] Carpenter G, Cohen S. Epidermal growth factor. *Annual review of biochemistry*. 1979;48(1):193-216.
- [33] Boonstra J, Rijken P, Humbel B, Cremers F, Verkleij A. The epidermal growth factor. *Cell Biology International*. 1995;19:413-30.
- [34] Rozengurt E, Brown KD, Pettican P. Vasopressin inhibition of epidermal growth factor binding to cultured mouse cells. *Journal of Biological Chemistry*. 1981;256(2):716-22.
- [35] Pérez R, Pascual M, Macías A, Lage A. Epidermal growth factor receptors in human breast cancer. *Breast Cancer Research and Treatment*. 1984;4(3):189-93.
- [36] Herbst RS. Review of epidermal growth factor receptor biology. *International Journal of Radiation Oncology* Biology* Physics*. 2004;59(2):S21-S6.
- [37] Nishikawa R, Ji X-D, Harmon RC, Lazar CS, Gill GN, Cavenee WK, et al. A mutant epidermal growth factor receptor common in human glioma confers enhanced tumorigenicity. *Proceedings of the National Academy of Sciences*. 1994;91(16):7727-31.
- [38] Ekstrand AJ, Longo N, Hamid ML, Olson JJ, Liu L, Collins VP, et al. Functional characterization of an EGF receptor with a truncated extracellular domain expressed in glioblastomas with EGFR gene amplification. *Oncogene*. 1994;9(8):2313-20.
- [39] Hynes NE, MacDonald G. ErbB receptors and signaling pathways in cancer. *Current opinion in cell biology*. 2009;21(2):177-84.
- [40] Mendelsohn J. The epidermal growth factor receptor as a target for cancer therapy. *Endocrine-Related Cancer*. 2001;8(1):3.
- [41] Nicholson RI, Gee JMW, Harper ME. EGFR and cancer prognosis. *European Journal of Cancer*. 2001;37:9-15.
- [42] McLendon RE, Wikstrand CJ, Matthews MR, Al-Baradei R, Bigner SH, Bigner DD. Glioma-associated antigen expression in oligodendroglial neoplasms: tenascin and epidermal growth factor receptor. *Journal of Histochemistry & Cytochemistry*. 2000;48(8):1103.
- [43] Hong WK, Ullrich A. The role of EGFR in solid tumors and implications for therapy. *Oncol Biother*. 2000;1(1).
- [44] Carpenter G. The biochemistry and physiology of the receptor-kinase for epidermal growth factor. *Molecular and Cellular Endocrinology*. 1983;31(1):1-19.
- [45] Wikstrand CJ, McLendon RE, Friedman AH, Bigner DD. Cell surface localization and density of the tumor-associated variant of the epidermal growth factor receptor, EGFRVIII. *Cancer research*. 1997;57(18):4130.
- [46] Baselga J. The EGFR as a target for anticancer therapy--focus on cetuximab. *European Journal of Cancer*. 2001;37:16-22.
- [47] Pao W, Chmielecki J. Rational, biologically based treatment of EGFR-mutant non-small-cell lung cancer. *Nature Reviews Cancer*. 2010;10(11):760-74.

- [48] Tang X, Shigematsu H, Bekele BN, Roth JA, Minna JD, Hong WK, et al. EGFR tyrosine kinase domain mutations are detected in histologically normal respiratory epithelium in lung cancer patients. *Cancer Research*. 2005;65(17):7568-72.
- [49] Marks JL, Broderick S, Zhou Q, Chitale D, Li AR, Zakowski MF, et al. Prognostic and therapeutic implications of EGFR and KRAS mutations in resected lung adenocarcinoma. *Journal of Thoracic Oncology*. 2008;3(2):111-6.
- [50] Lorimer IAJ. Mutant epidermal growth factor receptors as targets for cancer therapy. *Current Cancer Drug Targets*. 2002;2(2):91-102.
- [51] Saikali Sp, Avril T, Collet B, Hamlat A, Bansard J-Y, Drenou B, et al. Expression of nine tumour antigens in a series of human glioblastoma multiforme: interest of EGFRvIII, IL-13R α 2, gp100 and TRP-2 for immunotherapy. *Journal of Neuro-oncology*. 2007;81(2):139-48.
- [52] Rocha-Lima CM, Soares HP, Raez LE, Singal R. EGFR targeting of solid tumors. *Cancer Control*. 2007;14(3):295.
- [53] Gschwind A, Fischer OM, Ullrich A. The discovery of receptor tyrosine kinases: targets for cancer therapy. *Nature Reviews Cancer*. 2004;4(5):361-70.
- [54] Rowinsky EK. The pursuit of optimal outcomes in cancer therapy in a new age of rationally designed target-based anticancer agents. *Drugs*. 2000;60(Supplement 1):1-14.
- [55] Raymond E, Faivre S, Armand JP. Epidermal growth factor receptor tyrosine kinase as a target for anticancer therapy. *Drugs*. 2000;60(1):15-23.
- [56] Plaks V, Koopman CD, Werb Z. Circulating Tumor Cells. *Science (New York, NY)*. 2013;341(6151).
- [57] Hayes DF, Smerage JB. Circulating tumor cells. *Progress in Molecular Biology and Translational Science*. 2009;95:95-112.
- [58] Cristofanilli M, Budd GT, Ellis MJ, Stopeck A, Matera J, Miller MC, et al. Circulating tumor cells, disease progression, and survival in metastatic breast cancer. *New England Journal of Medicine*. 2004;351(8):781-91.
- [59] Liu MC, Shields PG, Warren RD, Cohen P, Wilkinson M, Ottaviano YL, et al. Circulating tumor cells: a useful predictor of treatment efficacy in metastatic breast cancer. *Journal of Clinical Oncology*. 2009;27(31):5153-9.
- [60] Pantel K, Alix-Panabières C. The clinical significance of circulating tumor cells. *Nature Clinical Practice Oncology*. 2007;4(2):62-3.
- [61] de Bono JS, Scher HI, Montgomery RB, Parker C, Miller MC, Tissing H, et al. Circulating tumor cells predict survival benefit from treatment in metastatic castration-resistant prostate cancer. *Clinical Cancer Research*. 2008;14(19):6302-9.
- [62] Barker li FG, Simmons ML, Chang SM, Prados MD, Larson DA, Sneed PK, et al. EGFR overexpression and radiation response in glioblastoma multiforme. *International Journal of Radiation Oncology* Biology* Physics*. 2001;51(2):410-8.
- [63] Sathornsumetee S, Rich JN, Reardon DA. Diagnosis and treatment of high-grade astrocytoma. *Neurologic clinics*. 2007;25(4):1111-39.
- [64] Ohgaki H, Kleihues P. Genetic pathways to primary and secondary glioblastoma. *The American Journal of Pathology*. 2007;170(5):1445-53.
- [65] Lokker NA, Sullivan CM, Hollenbach SJ, Israel MA, Giese NA. Platelet-derived Growth Factor (PDGF) Autocrine Signaling Regulates Survival and Mitogenic Pathways in Glioblastoma Cells Evidence That the Novel PDGF-C and PDGF-D Ligands May Play a Role in the Development of Brain Tumors. *Cancer Research*. 2002;62(13):3729-35.
- [66] Haas-Kogan DA, Prados MD, Tihan T, Eberhard DA, Jelluma N, Arvold ND, et al. Epidermal growth factor receptor, protein kinase B/Akt, and glioma response to erlotinib. *Journal of the National Cancer Institute*. 2005;97(12):880-7.
- [67] Heimberger AB, Suki D, Yang D, Shi W, Aldape K. The natural history of EGFR and EGFRvIII in glioblastoma patients. *Journal of Translational Medicine*. 2005;3(1):38.
- [68] Gan HK, Kaye AH, Luwor RB. The EGFRvIII variant in glioblastoma multiforme. *Journal of Clinical Neuroscience*. 2009;16(6):748-54.

- [69] Goldenberg DM. Radiolabeled antibodies. *Science & Medicine*. 1994;1(1):64.
- [70] Goldenberg DM. New developments in monoclonal antibodies for cancer detection and therapy. *CA: a Cancer Journal for Clinicians*. 1994;44(1):43-64.
- [71] Goldenberg DM. Monoclonal antibodies in cancer detection and therapy. *The American Journal of Medicine*. 1993;94(3):297-312.
- [72] Melero I, Hervas-Stubbs S, Glennie M, Pardoll DM, Chen L. Immunostimulatory monoclonal antibodies for cancer therapy. *Nature Reviews Cancer*. 2007;7(2):95-106.
- [73] Davies DR, Metzger H. Structural basis of antibody function. *Annual Review of Immunology*. 1983;1(1):87-115.
- [74] Heller MJ. DNA microarray technology: devices, systems, and applications. *Annual Review of Biomedical Engineering*. 2002;4(1):129-53.
- [75] Chen GY, Uttamchandani M, Lue RY, Lesaichere ML, Yao SQ. Array-based technologies and their applications in proteomics. *Current Topics in Medicinal Chemistry*. 2003;3(6):705-24.
- [76] MacBeath G. Protein microarrays and proteomics. *Nature Genetics*. 2002;32:526-32.
- [77] Schena M, Shalon D, Davis RW, Brown PO. Quantitative monitoring of gene expression patterns with a complementary DNA microarray. *Science*. 1995;270(5235):467-70.
- [78] Sassolas A, Leca-Bouvier BaD, Blum LcJ. DNA biosensors and microarrays. *Chemical Reviews*. 2008;108(1):109-39.
- [79] Liu RH, Yang J, Lenigk R, Bonanno J, Grodzinski P. Self-contained, fully integrated biochip for sample preparation, polymerase chain reaction amplification, and DNA microarray detection. *Analytical Chemistry*. 2004;76(7):1824-31.
- [80] Wang J. Survey and summary from DNA biosensors to gene chips. *Nucleic Acids Research*. 2000;28(16):3011-6.
- [81] Vercoutere W, Akeson M. Biosensors for DNA sequence detection. *Current Opinion in Chemical Biology*. 2002;6(6):816-22.
- [82] Sia SK, Kricka LJ. Microfluidics and point-of-care testing. *Lab on a Chip*. 2008;8(12):1982-3.
- [83] Schulze A, Downward J. Navigating gene expression using microarrays-a technology review. *Nature Cell Biology*. 2001;3(8):E190-E5.
- [84] Burge S, Parkinson GN, Hazel P, Todd AK, Neidle S. Quadruplex DNA: sequence, topology and structure. *Nucleic Acids Research*. 2006;34(19):5402-15.
- [85] Henderson E, Hardin CC, Walk SK, Tinoco Jr I, Blackburn EH. Telomeric DNA oligonucleotides form novel intramolecular structures containing guanine-guanine base pairs. *Cell*. 1987;51(6):899-908.
- [86] Zahler AM, Williamson JR, Cech TR, Prescott DM. Inhibition of telomerase by G-quartet DNA structures. *Nature*. 1991;350(6320):718-20.
- [87] Davis JT. G-Quartets 40 Years Later: From 5`-GMP to Molecular Biology and Supramolecular Chemistry. *Angewandte Chemie International Edition*. 2004;43(6):668-98.
- [88] Williamson JR. G-quartet structures in telomeric DNA. *Annual review of biophysics and biomolecular structure*. 1994;23(1):703-30.
- [89] Reed JE, Arnal AA, Neidle S, Vilar Rn. Stabilization of G-quadruplex DNA and inhibition of telomerase activity by square-planar nickel (II) complexes. *Journal of the American Chemical Society*. 2006;128(18):5992-3.
- [90] Bunka DHJ, Stockley PG. Aptamers come of age—at last. *Nature Reviews Microbiology*. 2006;4(8):588-96.
- [91] Weigand JE, Suess B. Aptamers and riboswitches: perspectives in biotechnology. *Applied microbiology and biotechnology*. 2009;85(2):229-36.
- [92] Kirby R, Cho EJ, Gehrke B, Bayer T, Park YS, Neikirk DP, et al. Aptamer-based sensor arrays for the detection and quantitation of proteins. *Analytical Chemistry*. 2004;76(14):4066-75.
- [93] Mairal T, Özalp VC, Sánchez PL, Mir M, Katakis I, O'Sullivan CK. Aptamers: molecular tools for analytical applications. *Analytical and Bioanalytical Chemistry*. 2008;390(4):989-1007.

- [94] Jayasena SD. Aptamers: an emerging class of molecules that rival antibodies in diagnostics. *Clinical Chemistry*. 1999;45(9):1628-50.
- [95] Hianik T, Ostatnı V, Sonlajtnerova M, Grman I. Influence of ionic strength, pH and aptamer configuration for binding affinity to thrombin. *Bioelectrochemistry*. 2007;70(1):127-33.
- [96] Di Giusto DA, King GC. Construction, stability, and activity of multivalent circular anticoagulant aptamers. *Journal of Biological Chemistry*. 2004;279(45):46483-9.
- [97] Brody EN, Gold L. Aptamers as therapeutic and diagnostic agents. *Reviews in Molecular Biotechnology*. 2000;74(1):5-13.
- [98] Chu TC, Shieh F, Lavery LA, Levy M, Richards-Kortum R, Korgel BA, et al. Labeling tumor cells with fluorescent nanocrystalaptamer bioconjugates. *Biosensors and Bioelectronics*. 2006;21(10):1859-66.
- [99] Downward J. Targeting RAS signalling pathways in cancer therapy. *Nature Reviews Cancer*. 2003;3(1):11-22.
- [100] Wan Y, Kim Y-t, Li N, Cho SK, Bachoo R, Ellington AD, et al. Surface-immobilized aptamers for cancer cell isolation and microscopic cytology. *Cancer research*. 70(22):9371-80.
- [101] Paterlini-Brechot P, Benali NL. Circulating tumor cells (CTC) detection: clinical impact and future directions. *Cancer Letters*. 2007;253(2):180-204.
- [102] Olapade-Olaopa EO, Moscatello DK, MacKay EH, Horsburgh T, Sandhu DPS, Terry TR, et al. Evidence for the differential expression of a variant EGF receptor protein in human prostate cancer. *British Journal of Cancer*. 2000;82(1):186.
- [103] Pinzani P, Salvadori B, Simi L, Bianchi S, Distante V, Cataliotti L, et al. Isolation by size of epithelial tumor cells in peripheral blood of patients with breast cancer: correlation with real-time reverse transcriptasepolymerase chain reaction results and feasibility of molecular analysis by laser microdissection. *Human Pathology*. 2006;37(6):711-8.
- [104] Lin HK, Zheng S, Williams AJ, Balic M, Groshen S, Scher HI, et al. Portable filter-based microdevice for detection and characterization of circulating tumor cells. *Clinical Cancer Research*. 2010;16(20):5011-8.
- [105] Pereira P, Grandne Vr, Forel JM, Gabriele S, Camara M, Theodoly O. Passive circulating cell sorting by deformability using a microfluidic gradual filter. *Lab on a Chip*. 2013;13(1):161-70.
- [106] Wang JHC, Goldschmidt-Clermont P, Wille J, Yin FCP. Specificity of endothelial cell reorientation in response to cyclic mechanical stretching. *Journal of Biomechanics*. 2001;34(12):1563-72.
- [107] Stott SL, Hsu C-H, Tsukrov DI, Yu M, Miyamoto DT, Waltman BA, et al. Isolation of circulating tumor cells using a microvortex-generating herringbone-chip. *Proceedings of the National Academy of Sciences*. 2010;107(43):18392-7.
- [108] Dharmasiri U, Balamurugan S, Adams AA, Okagbare PI, Obubuafo A, Soper SA. Highly efficient capture and enumeration of low abundance prostate cancer cells using prostate-specific membrane antigen aptamers immobilized to a polymeric microfluidic device. *Electrophoresis*. 2009;30:3289-300.
- [109] Hunt TP, Westervelt RM. Dielectrophoresis tweezers for single cell manipulation. *Biomedical microdevices*. 2006;8(3):227-30.
- [110] Chiou PY, Chang Z, Wu MC. A novel optoelectronic tweezer using light induced dielectrophoresis. 2003: IEEE; 2003. p. 8-9.
- [111] Han KH, Frazier AB. Paramagnetic capture mode magnetophoretic microseparator for high efficiency blood cell separations. *Lab Chip*. 2006;6(2):265-73.
- [112] Radbruch A, Grutzkau A, Mechtold B, Thiel A, Miltenyi S, Pfluger E, et al. High-gradient magnetic cell sorting. *Essential Cytometry Methods*. 2009:143.
- [113] Thiel A, Scheffold A, Radbruch A. Immunomagnetic cell sorting-pushing the limits. *Immunotechnology*. 1998;4(2):89-96.
- [114] Timonen T, Saksela E. Isolation of human NK cells by density gradient centrifugation. *Journal of Immunological Methods*. 1980;36(3):285-91.

- [115] Gertler R, Rosenberg R, Fuehrer K, Dahm M, Nekarda H, Siewert JR. Detection of circulating tumor cells in blood using an optimized density gradient centrifugation. *Molecular Staging of Cancer*. Springer 2003:149-55.
- [116] Barlogie B, Raber MN, Schumann J, Johnson TS, Drewinko B, Swartzendruber DE, et al. Flow cytometry in clinical cancer research. *Cancer Research*. 1983;43(9):3982-97.
- [117] Jahan-Tigh RR, Ryan C, Obermoser G, Schwarzenberger K. Flow cytometry. *Journal of Investigative Dermatology*. 2012;132(10):e1.
- [118] Gazi E, Ward AD, Clarke NW, Harvey TJ, Snook RD, Gardner P, et al. Spectral discrimination of live prostate and bladder cancer cell lines using Raman optical tweezers. *Journal of Biomedical Optics*. 2008;13(6):064004--12.
- [119] Niemeyer CM, Adler M, Wacker R. Immuno-PCR: high sensitivity detection of proteins by nucleic acid amplification. *Trends in Biotechnology*. 2005;23(4):208-16.
- [120] Bamrungsap S, Chen T, Shukoor MI, Chen Z, Sefah K, Chen Y, et al. Pattern recognition of cancer cells using aptamer-conjugated magnetic nanoparticles. *ACS Nano*. 2012;6(5):3974-81.
- [121] Lai RY, Plaxco KW, Heeger AJ. Aptamer-based electrochemical detection of picomolar platelet-derived growth factor directly in blood serum. *Analytical Chemistry*. 2007;79(1):229-33.
- [122] Medley CD, Smith JE, Tang Z, Wu Y, Bamrungsap S, Tan W. Gold nanoparticle-based colorimetric assay for the direct detection of cancerous cells. *Analytical Chemistry*. 2008;80(4):1067-72.
- [123] Ireson CR, Kelland LR. Discovery and development of anticancer aptamers. *Molecular Cancer Therapeutics*. 2006;5(12):2957-62.
- [124] Zhao W, Cui CH, Bose S, Guo D, Shen C, Wong WP, et al. Bioinspired multivalent DNA network for capture and release of cells. *Proceedings of the National Academy of Sciences*. 2012;109(48):19626-31.
- [125] Smith IO, Liu XH, Smith LA, Ma PX. Nanostructured polymer scaffolds for tissue engineering and regenerative medicine. *Wiley Interdisciplinary Reviews: Nanomedicine and Nanobiotechnology*. 2009;1(2):226-36.
- [126] Han W, Allio BA, Foster DG, King MR. Nanoparticle coatings for enhanced capture of flowing cells in microtubes. *ACS Nano*. 2009;4(1):174-80.
- [127] Chen W, Weng S, Zhang F, Allen S, Li X, Bao L, et al. Nanoroughened Surfaces for Efficient Capture of Circulating Tumor Cells without Using Capture Antibodies. *ACS nano*. 2012;7(1):566-75.
- [128] den Toonder J. Circulating tumor cells: the Grand Challenge. *Lab on a Chip*. 2011;11(3):375-7.
- [129] Weeraratna AT, Jiang Y, Hostetter G, Rosenblatt K, Duray P, Bittner M, et al. Wnt5a signaling directly affects cell motility and invasion of metastatic melanoma. *Cancer Cell*. 2002;1(3):279-88.
- [130] Sahai E. Mechanisms of cancer cell invasion. *Current opinion in genetics & development*. 2005;15(1):87-96.
- [131] Lauffenburger DA, Horwitz AF. Cell migration: a physically integrated molecular process. *Cell*. 1996;84(3):359-69.
- [132] Mitchison TJ, Cramer LP. Actin-based cell motility and cell locomotion. *Cell*. 1996;84(3):371-9.
- [133] Branton D, Deamer DW, Marziali A, Bayley H, Benner SA, Butler T, et al. The potential and challenges of nanopore sequencing. *Nature biotechnology*. 2008;26(10):1146-53.
- [134] Clarke J, Wu H-C, Jayasinghe L, Patel A, Reid S, Bayley H. Continuous base identification for single-molecule nanopore DNA sequencing. *Nature Nanotechnology*. 2009;4(4):265-70.
- [135] Rotem D, Jayasinghe L, Salichou M, Bayley H. Protein detection by nanopores equipped with aptamers. *Journal of the American Chemical Society*. 2012;134(5):2781-7.

- [136] Murray RW. Nanoelectrochemistry: metal nanoparticles, nanoelectrodes, and nanopores. *Chemical Reviews*. 2008;108(7):2688-720.
- [137] Dekker C. Solid-state nanopores. *Nature Nanotechnology*. 2007;2(4):209-15.
- [138] Nivala J, Marks DB, Akeson M. Unfoldase-mediated protein translocation through an [alpha]-hemolysin nanopore. *Nature biotechnology*. 2013.
- [139] Han A, Creus M, Schulzmann G, Linder V, Ward TR, de Rooij NF, et al. Label-free detection of single protein molecules and protein-protein interactions using synthetic nanopores. *Analytical Chemistry*. 2008;80(12):4651-8.
- [140] Iqbal SM, Bashir R. *Nanopores: sensing and fundamental biological interactions*: Springer 2011.
- [141] Haile JM. *Molecular dynamics simulation: elementary methods*: John Wiley & Sons, Inc. 1992.
- [142] Humphrey W, Dalke A, Schulten K. VMD: visual molecular dynamics. *Journal of molecular graphics*. 1996;14(1):33-8.
- [143] Phillips JC, Braun R, Wang W, Gumbart J, Tajkhorshid E, Villa E, et al. Scalable molecular dynamics with NAMD. *Journal of computational chemistry*. 2005;26(16):1781-802.
- [144] Wan Y, Kim Y, Li N, Cho SK, Bachoo R, Ellington AD, et al. Surface-immobilized aptamers for cancer cell isolation and microscopic cytology. *Cancer research*. 2010;70(22):9371-80.
- [145] Piro B, Reisberg S, Noel V, Pham MC. Investigations of the steric effect on electrochemical transduction in a quinone-based DNA sensor. *Biosensors and Bioelectronics*. 2007;22(12):3126-31.
- [146] Iqbal SM, Akin D, Bashir R. Solid-state nanopore channels with DNA selectivity. *Nature Nanotechnology*. 2007;2(4):243-8.
- [147] Sethian JA. A fast marching level set method for monotonically advancing fronts. *Proceedings of the National Academy of Sciences*. 1996;93(4):1591.
- [148] Huttenlocher DP, Klanderman GA, Rucklidge WJ. Comparing images using the Hausdorff distance. *Pattern Analysis and Machine Intelligence, IEEE Transactions on*. 1993;15(9):850-63.
- [149] Zhang W, Choi DS, Nguyen YH, Chang J, Qin L. Studying Cancer Stem Cell Dynamics on PDMS Surfaces for Microfluidics Device Design. *Scientific Reports*. 2013;3.
- [150] Byun S, Son S, Amodei D, Cermak N, Shaw J, Kang JH, et al. Characterizing deformability and surface friction of cancer cells. *Proceedings of the National Academy of Sciences*. 2013;110(19):7580-5.
- [151] Zhao G, Schwartz Z, Wieland M, Rupp F, Geisler Gerstorfer J, Cochran DL, et al. High surface energy enhances cell response to titanium substrate microstructure. *Journal of Biomedical Materials Research Part A*. 2005;74(1):49-58.
- [152] Low SP, Williams KA, Canham LT, Voelcker NH. Evaluation of mammalian cell adhesion on surface-modified porous silicon. *Biomaterials*. 2006;27(26):4538-46.
- [153] Curtis ASG, Casey B, Gallagher JO, Pasqui D, Wood MA, Wilkinson CDW. Substratum nanotopography and the adhesion of biological cells. Are symmetry or regularity of nanotopography important? *Biophysical Chemistry*. 2001;94(3):275-83.
- [154] Craighead HG, James CD, Turner AMP. Chemical and topographical patterning for directed cell attachment. *Current Opinion in Solid State and Materials Science*. 2001;5(2):177-84.
- [155] Cheng MM-C, Cuda G, Bunimovich YL, Gaspari M, Heath JR, Hill HD, et al. Nanotechnologies for biomolecular detection and medical diagnostics. *Current Opinion in Chemical Biology*. 2006;10(1):11-9.
- [156] Sajay BNG, Chang C-P, Ahmad H, Chung WC, Puiu PD, Rahman ARA. Towards an optimal and unbiased approach for tumor cell isolation. *Biomedical Microdevices*. 2013:1-11.

- [157] Hossainy S, Trollsas M, Cardinal K, Foley M, Consigny P. Surface modification of medical devices to enhance endothelial adhesion and coverage. US Patent 20,130,103,138 2012.
- [158] Chen W, Weng S, Zhang F, Allen S, Li X, Bao L, et al. Nanoroughened Surfaces for Efficient Capture of Circulating Tumor Cells without Using Capture Antibodies. *ACS nano*. 7(1):566-75.
- [159] Gadegaard N, Martines E, Riehle MO, Seunarine K, Wilkinson CDW. Applications of nano-patterning to tissue engineering. *Microelectronic Engineering*. 2006;83(4):1577-81.
- [160] Im SG, Yoo PJ, Hammond PT, Gleason KK. Grafted Conducting Polymer Films for Nano-patterning onto Various Organic and Inorganic Substrates by Oxidative Chemical Vapor Deposition. *Advanced Materials*. 2007;19(19):2863-7.
- [161] Kim DH, Lee H, Lee YK, Nam J-M, Levchenko A. Biomimetic nanopatterns as enabling tools for analysis and control of live cells. *Advanced Materials*. 2010;22(41):4551-66.
- [162] Kim D-J, Seol J-K, Wu Y, Ji S, Kim G-S, Hyung J-H, et al. A quartz nanopillar hemocytometer for high-yield separation and counting of CD4+ T lymphocytes. *Nanoscale*. 2012;4(7):2500-7.
- [163] Singh SK, Hawkins C, Clarke ID, Squire JA, Bayani J, Hide T, et al. Identification of human brain tumour initiating cells. *nature*. 2004;432(7015):396-401.
- [164] Wan Y, Kim Y-t, Li N, Cho SK, Bachoo R, Ellington AD, et al. Surface Immobilized Aptamers for Cancer Cell Isolation and Microscopic Cytology. *Cancer Research*. 2010;70(22):11.
- [165] Wan Y, Liu Y, Allen PB, Asghar W, Mahmood MAI, Tan J, et al. Capture, isolation and release of cancer cells with aptamer-functionalized glass bead array. *Lab on a Chip*. 2012;12(22):4693-701.
- [166] Nosonovsky M, Bhushan B. Biologically Inspired Surfaces: Broadening the Scope of Roughness**. *Advanced Functional Materials*. 2008;18(6):843-55.
- [167] Wan Y, Mahmood M, Li N, Allen PB, Kim Yt, Bachoo R, et al. Nanotextured substrates with immobilized aptamers for cancer cell isolation and cytology. *Cancer*. 2012;118(4):1145-54.
- [168] Fologea D, Ledden B, McNabb DS, Li J. Electrical characterization of protein molecules by a solid-state nanopore. *Applied physics letters*. 2007;91:053901.
- [169] Bunka DHJ, Stockley PG. Aptamers come of age-at last. *Nature Reviews Microbiology*. 2006;4(8):588-96.
- [170] Song S, Wang L, Li J, Fan C, Zhao J. Aptamer-based biosensors. *TrAC Trends in Analytical Chemistry*. 2008;27(2):108-17.
- [171] Zalfa F, Giorgi M, Primerano B, Moro A, Di Penta A, Reis S, et al. The Fragile X Syndrome Protein FMRP Associates with *BC1* RNA and Regulates the Translation of Specific mRNAs at Synapses. *Cell*. 2003;112(3):317-27.
- [172] Lomholt MA, van den Broek B, Kalisch S-MJ, Wuite GJL, Metzler R. Facilitated diffusion with DNA coiling. *Proceedings of the National Academy of Sciences*. 2009;106(20):8204-8.
- [173] Lockhart C, Berlin JD. The epidermal growth factor receptor as a target for colorectal cancer therapy. *Seminars in oncology*; 2005: Elsevier; 2005. p. 52-60.
- [174] Haber DA, Bell DW, Sordella R, Kwak EL, Godin-Heymann N, Sharma SV, et al. Molecular targeted therapy of lung cancer: EGFR mutations and response to EGFR inhibitors. *Cold Spring Harbor Symposia on Quantitative Biology*; 2005: Cold Spring Harbor Laboratory Press; 2005. p. 419-26.
- [175] Wan Y, Tan J, Asghar W, Kim Y-t, Liu Y, Iqbal SM. Velocity effect on aptamer-based circulating tumor cell isolation in microfluidic devices. *The Journal of Physical Chemistry B*. 115(47):13891-6.
- [176] Javed A, Iqbal SM, Jain A. Microheater platform for selective detachment of DNA. *Applied Physics Letters*. 101:093707.
- [177] Ramachandran A, Liu Y, Asghar W, Iqbal SM. Characterization of DNA-nanopore interactions by molecular dynamics. *Am J Biomed Sci*. 2009;1:344-51.

- [178] Hazel P, Parkinson GN, Neidle S. Topology variation and loop structural homology in crystal and simulated structures of a bimolecular DNA quadruplex. *Journal of the American Chemical Society*. 2006;128(16):5480-7.
- [179] Padmanabhan K, Tulinsky A. An ambiguous structure of a DNA 15-mer thrombin complex. *Acta Crystallographica Section D: Biological Crystallography*. 1996;52(2):272-82.
- [180] Aksimentiev A. Deciphering ionic current signatures of DNA transport through a nanopore. *Nanoscale*. 2010;2(4):468-83.
- [181] MacKerell AD, Brooks B, Brooks CL, Nilsson L, Roux B, Won Y, et al. CHARMM: The energy function and its parameterization. *Encyclopedia of Computational Chemistry*. 2002.
- [182] Brooks BR, Brooks CL, Mackerell AD, Nilsson L, Petrella RJ, Roux Bt, et al. CHARMM: the biomolecular simulation program. *Journal of Computational Chemistry*. 2009;30(10):1545-614.
- [183] MacKerell AD, Feig M, Brooks CL. Extending the treatment of backbone energetics in protein force fields: Limitations of gas-phase quantum mechanics in reproducing protein conformational distributions in molecular dynamics simulations. *Journal of Computational Chemistry*. 2004;25(11):1400-15.
- [184] Shewchuk JR. An introduction to the conjugate gradient method without the agonizing pain. Carnegie Mellon University, Pittsburgh, PA 1994.
- [185] He Y, Tsutsui M, Scheicher RH, Fan C, Taniguchi M, Kawai T. Mechanism of How Salt-Gradient-Induced Charges Affect the Translocation of DNA Molecules through a Nanopore. *Biophysical journal*. 2013;105(3):776-82.
- [186] Geoffrey MC, Robert HE. *The cell: a molecular approach*. Harvard Medical School. 1997:1-673.
- [187] Goldenberg DP, Creighton TE. Gel electrophoresis in studies of protein conformation and folding. *Analytical Biochemistry*. 1984;138(1):1-18.

Biographical Information

Mohammed Arif I. Mahmood received his B.Sc. degree from Bangladesh University of Engineering and Technology in 2004. He worked as Lecturer and then as Assistant Professor in the Department of Applied Physics at University of Chittagong till August 2009. He joined University of Texas at Arlington in August 2009 in BS to PhD program in Electrical Engineering Department. While working under supervision of Dr. Samir M. Iqbal during these years, he obtained several awards and scholarship for academic and research excellence which includes, **Best Oral Presentation Award** at Sigma Xi Southwest Region Research Conference, 2013, Award for **Excellence in Abstract Writing**, ACES 2012, **NSF Travel Scholarship for Petra** 2012, **I-Engage Mentoring Fellowship** 2012, 2013, **CONTACT** Research Grant in 2010 and **Spring 2014 Dissertation Fellowship**.